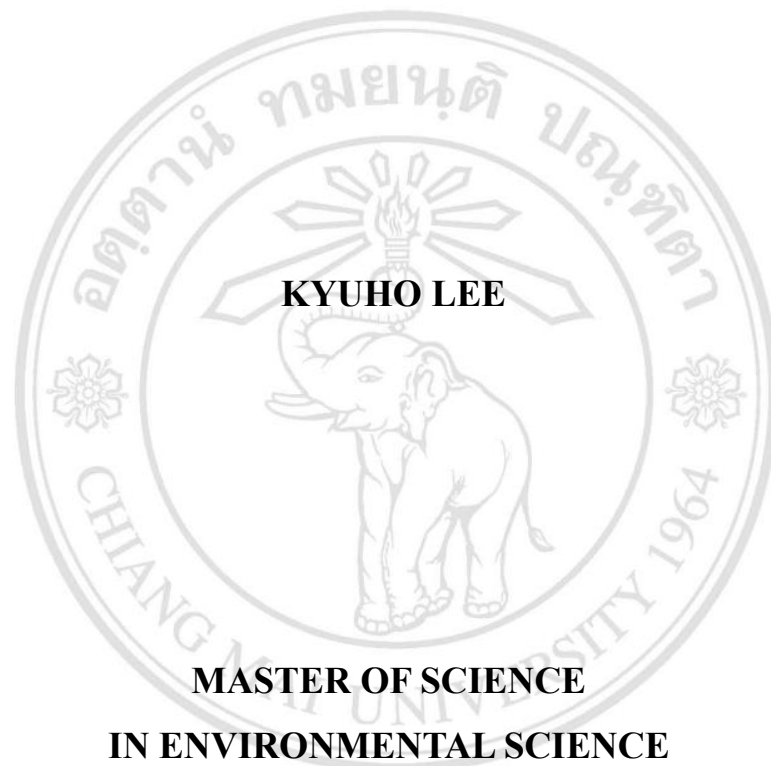


**DEVELOPING A FOREST-DEGRADATION INDEX
FOR FOREST ECOSYSTEM RESTORATION
USING UAV-BASED RGB PHOTOGRAPHY**



ลิขสิทธิ์มหาวิทยาลัยเชียงใหม่
Copyright© by Chiang Mai University
All rights reserved

**GRADUATE SCHOOL
CHIANG MAI UNIVERSITY
JULY 2021**

**DEVELOPING A FOREST-DEGRADATION INDEX
FOR FOREST ECOSYSTEM RESTORATION
USING UAV-BASED RGB PHOTOGRAPHY**

KYUHO LEE

**A THESIS SUBMITTED TO CHIANG MAI UNIVERSITY IN PARTIAL
FULFILLMENT OF THE REQUIREMENTS FOR THE DEGREE OF
MASTER OF SCIENCE**

IN ENVIRONMENTAL SCIENCE

ลิขสิทธิ์มหาวิทยาลัยเชียงใหม่
Copyright© by Chiang Mai University
All rights reserved

GRADUATE SCHOOL, CHIANG MAI UNIVERSITY

JULY 2021

**DEVELOPING A FOREST-DEGRADATION INDEX
FOR FOREST ECOSYSTEM RESTORATION
USING UAV-BASED RGB PHOTOGRAPHY**

KYUHO LEE

THIS THESIS HAS BEEN APPROVED TO BE A PARTIAL FULFILLMENT
OF THE REQUIREMENTS FOR THE DEGREE OF
MASTER OF SCIENCE
IN ENVIRONMENTAL SCIENCE

Examination Committee :

Sasaki Nophea
.....Chairman
(Prof. Dr. Nophea Sasaki)

S. Elliott
.....Member
(Assoc. Prof. Dr. Stephen Elliott)

Pimonrat Tiansawat
.....Member
(Asst. Prof. Dr. Pimonrat Tiansawat)

Advisory Committee :

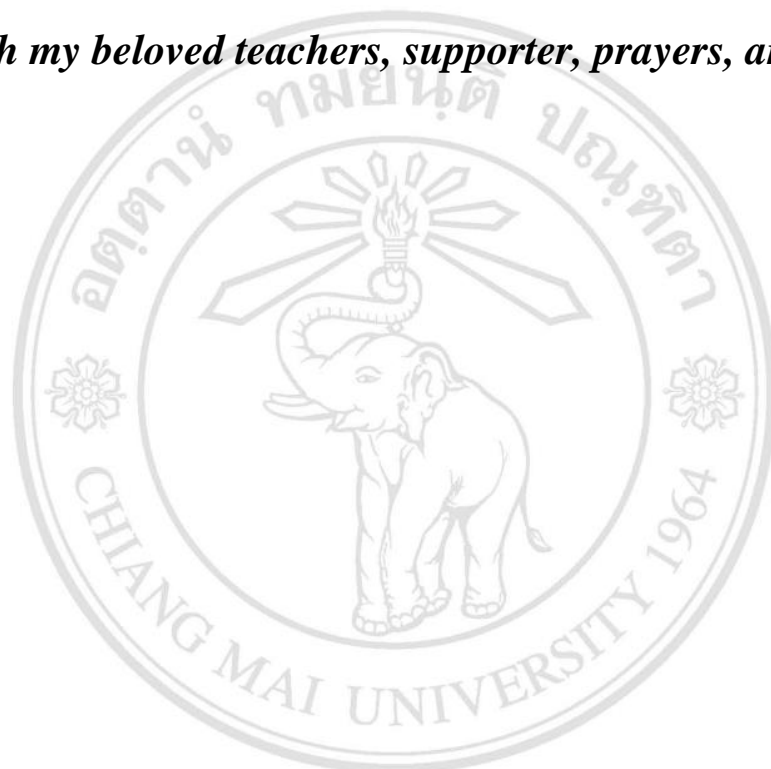
S. Elliott
.....Advisor
(Assoc. Prof. Dr. Stephen Elliott)

Pimonrat Tiansawat
.....Co-advisor
(Asst. Prof. Dr. Pimonrat Tiansawat)

9 July 2021

Copyright © by Chiang Mai University

*This study is dedicated to my family, Jae, Hyun, Kang & Ha,
who have been backing and patient in this late journey,
along with my beloved teachers, supporter, prayers, and artists.*



ลิขสิทธิ์มหาวิทยาลัยเชียงใหม่
Copyright© by Chiang Mai University
All rights reserved

ACKNOWLEDGEMENT

I thank Chiang Mai University for fully supporting this academic opportunity, studying tropical forests in Northern Thailand, under the CMU Presidential Scholarship. Also, I thank the Forest Restoration Research Unit of Chiang Mai University (FORRU-CMU) for supporting a small project research grant and instrument, which were the main budget and tools for conducting this research.

I greatly appreciate Dr. Stephen Elliott for showing diverse and urgent needs for forest ecosystem restoration and advising this study, along with my countless delays and tenacious questions. Despite of these, you have been kind and passionate to teach me all the time. In addition, I also appreciate my co-advisor, Assoc.Prof.Dr. Pimonrat Tiansawat for opening my eyes to the statistics and the strong tool, which we call R. Those became fundamental knowledge to design this research.

I cannot forget the dedicated help from Assoc.Prof.Dr. Puttipol Dumrongchai, and his students, from Department of Civil Engineering. They generously trained me, an alien, studying in another Faculty, for applying land surveying technique, which was a big solution to one of the biggest barriers in this research. I'd like to express my gratitude to all the nine experts in the field of forest ecology and restoration from various nations, who showed their supports to this young scientist by responding to the questionnaire.

Finally, I want to represent my appreciation to all members in FORRU, who volunteered their hands and knowledge for this study. As the representative of them, I specially thank Ms. Khuanphirom Naruangsri, who helped and joined in every single field works with her great expertise, experiences, and kindness.

Kyuhoo Lee

หัวข้อวิทยานิพนธ์	การพัฒนาดัชนีความเสื่อมโทรมของป่าเพื่อการฟื้นฟูระบบนิเวศป่าไม้ โดยใช้ภาพถ่ายอาร์จีบีจากอากาศยานไร้คนขับ	
ผู้เขียน	นายเลียว โฮ ลี	
ปริญญา	วิทยาศาสตร์สิ่งแวดล้อม	
คณะกรรมการที่ปรึกษา	รศ.ดร. สตีเฟน เอลเลียต	อาจารย์ที่ปรึกษาหลัก
	ผศ.ดร. พิมลรัตน์ เทียนสวัสดิ์	อาจารย์ที่ปรึกษาร่วม

บทคัดย่อ

การประเมินความเสื่อมโทรมของป่ามีความสำคัญต่อการวางแผนการฟื้นฟู การศึกษานี้เป็นการศึกษาแรกที่สร้างดัชนีความเสื่อมโทรมของป่า (forest-degradation index: FDI) โดยอาศัยข้อมูลจากอากาศยานไร้คนขับ (UAV) โดยมีวัตถุประสงค์เพื่อหาแนวปฏิบัติที่จะทดแทนการสำรวจภาคพื้นดินแบบเดิมที่ใช้กำลังคนมากในการเก็บข้อมูลที่ซับซ้อน การศึกษาประกอบด้วยการศึกษาความสัมพันธ์ระหว่างข้อมูลที่ได้จาก UAV และข้อมูลภาคพื้นดิน และการสร้าง FDI วิธีศึกษาเริ่มจากการถ่ายภาพพื้นที่โดยใช้ UAV คู่ไปกับการเก็บข้อมูลภาคพื้นดินในแปลงฟื้นฟูป่า 5 แปลง ซึ่งมีความเสื่อมโทรมแตกต่างกัน ภาพถ่ายถูกประมวลผลเพื่อสร้างโมเดลความสูงของเรือนยอดและสร้างภาพถ่ายออร์โธที่ใช้ในการวัดตัวแปร 6 ตัวของการวัดระดับความเสื่อมโทรม การศึกษาพบว่าตัวแปร 4 ตัวที่แสดงความสัมพันธ์อย่างมีนัยสำคัญระหว่างข้อมูลจาก UAV และภาคพื้นดิน คือ ความหนาแน่นของต้นไม้ ($r = 0.84$) ร้อยละการปกคลุมของเรือนยอด ($r = 0.91$) ร้อยละการปกคลุมของพืชพื้นล่าง ($r = 0.84$) และร้อยละของพื้นดินที่เปิดโล่ง ($r = 0.75$) ในการสร้าง FDI ค่าร้อยละการปกคลุมของเรือนยอดมีความสัมพันธ์อย่างมากกับตัวแปรอื่นจึงถูกตัดออกเพื่อป้องกันการถ่วงน้ำหนักที่มากเกินไป ตัวแปร 3 ตัวที่เหลือถูกล่วงน้ำหนักโดยผู้เชี่ยวชาญและปรับค่าตัวแปรให้เป็นปกติ (นอร์มัลไลเซชัน) ค่า FDI ที่คำนวณได้สามารถประเมินความเสื่อมโทรมและจัดอันดับพื้นที่ตามสภาพความเสื่อมโทรมได้ แต่ FDI มีข้อจำกัด คือ 1) ไม่สามารถแสดงถึงจุดเปลี่ยนระหว่างระดับความเสื่อมโทรมได้ชัดเจนเหมือนเกณฑ์จากข้อมูลภาคพื้นดิน 2) FDI เป็นค่าต่อเนื่อง การแบ่งค่าระดับไม่จำเพาะเจาะจง และ 3) FDI ขาดองค์ประกอบด้านภูมิทัศน์ของพื้นที่ ด้วยข้อจำกัดดังกล่าว การใช้ FDI ร่วมกับการพิจารณาข้อมูลภาคพื้นดินอาจเป็นทางเลือกที่ดีที่สุดสำหรับการวางแผนการฟื้นฟูป่า

Thesis Title	Developing a Forest-Degradation Index for Forest Ecosystem Restoration Using UAV-based RGB Photography	
Author	Mr. Kyuho Lee	
Degree	Master of Science (Environmental Science)	
Advisory Committee	Assoc. Prof. Dr. Stephen Elliott	Advisor
	Asst. Prof. Dr. Pimonrat Tiansawat	Co-advisor

ABSTRACT

Forest degradation assessment is essential to plan restoration. This study was a first attempt to develop a forest-degradation index (FDI), based on data from unmanned aerial vehicles (UAVs). It aimed to find a practical solution to replace labor-intensive conventional ground surveys with complex multiple variables, to plan restoration projects. It explored correlations between UAV and ground data, to construct a FDI. Five forest-restoration trial plots, representing a wide range of degradation level, were surveyed, with ground sample plots and a UAV. Aerial photos were processed, to produce canopy-height models (CHMs) and orthophotos, used to measure six variables, related to degradation. Four were highly correlated between ground and UAV-derived measurements: tree stocking-density (TD, $r = 0.84$), per cent canopy cover (CC, $r = 0.91$), per cent ground vegetation (VEG, $r = 0.84$), and per cent exposed soil + rock (SOIL, $r = 0.75$). To construct the FDI, a highly intercorrelated variable (CC) was rejected, to prevent over-weighting of related factors. The three remaining criteria were weighted by experts and applied to the normalized values. The resultant FDI quantified degradation levels reasonably intuitively and ranked the sites in logical order of degradation. However, limitations of the technique included i) obscurement of tipping points, which define conventional degradation stages ii) use of 5 arbitrary categories in the FDI, and iii) exclusion of landscape criteria. Until these issues are resolved, a hybrid system, combining individual variables, with the UAV-derived FDI system, may be the best solution for planning restoration strategies.

CONTENTS

	Page
Acknowledgement	d
Abstract in Thai	e
Abstract in English	f
List of Tables	j
List of Figures	k
List of Abbreviations	n
List of Glossary	p
Chapter 1 Introduction	1
1.1 Background	1
1.2 Problem statement and rationale	2
1.3 Objectives	4
1.4 Conceptual framework	5
Chapter 2 Literature Review	6
2.1 Forest-degradation assessment as the basis for restoration planning	6
2.2 Remote sensing as the platform for effective forest survey	10
2.3 UAVs as optimal remote-sensing platforms for small-scale restoration planning	12
Chapter 3 Methodology	15
3.1 Study sites	15
3.2 Ground surveys	18
3.2.1 Data collection	18
3.3 Aerial survey (UAV Flight)	20
3.3.1 UAV flight	20
3.3.2 Image processing for producing DEMs and orthophotos	23

3.3.3	Detecting tree-top points from CHMs	26
3.3.4	Delineating tree-crown boundaries from CHMs	27
3.4	Measuring variables from ground and UAV-derived data	29
3.4.1	Tree stocking-density	29
3.4.2	Tree height	29
3.4.3	Per cent canopy cover accounting for overlap	29
3.4.4	Ratio of three elements of the ground	30
3.4.5	Aboveground Carbon Density (ACD)	31
3.5	Forest-Degradation Index (FDI)	32
3.5.1	Selecting criteria to be integrated into the index	32
3.5.2	Determining weight of each criterion using AHP method	32
3.5.3	Data normalization and data aggregation	35
Chapter 4	Results and Discussion	36
4.1	Forest-degradation assessment by ground survey in study sites	36
4.2	UAV flight and image processing	38
4.2.1	Collected images by UAV flight	38
4.2.2	Processed DEMs and orthophotos	39
4.2.3	Accuracy of positioning circular plots using stadia method	40
4.3	Tree-top points detected by <i>variable window filter</i> algorithm	42
4.3.1	Variable window-size functions	42
1)	Arbitrary window-size function presented by package developers	42
2)	Empirically developed window-size functions	42
4.3.2	The best setting of the various functions and minimum tree heights	43
4.4	Tree-crown boundaries detected by <i>watershed</i> algorithm	45
4.4.1	The best setting of minimum crown-boundary height	45
4.5	Correlation between the variables from ground and UAV surveys	47
4.5.1	Tree stocking-density	47
4.5.2	Tree height	48
4.5.3	Per cent canopy cover, ground vegetation, and exposed soil + rock	49
4.5.4	Aboveground Carbon Density (ACD)	50

4.6 Estimated measurements of overall sites	51
4.7 Forest-Degradation Index (FDI)	55
4.7.1 Selected criteria to be integrated into the index	55
4.7.2 Weighting each criterion using the AHP method	56
4.7.3 Data normalization and resultant FDI	57
4.8 Limitations and challenges	61
4.8.1 Weather, time of day and seasonality	61
4.8.2 Absence of ground control points (GCPs)	62
4.8.3 Limited visibility of understory in UAV imagery	63
4.8.4 Non-inclusion of landscape criteria	64
4.8.5 Application of the FDI in more or less degraded sites	65
4.8.6 Labor, time and costs for UAV-derived FDI	66
Chapter 5 Conclusion	67
References	69
Appendices	78
Appendix A Experts' evaluation of weighting drone-derived indicators for Forest-Degradation Index	78
Appendix B Orthophotos presented with DEMs	80
Appendix C Estimating plot points using stadia method and comparisons with GPS detected points in orthophotos	85
Curriculum Vitae	88

LIST OF TABLES

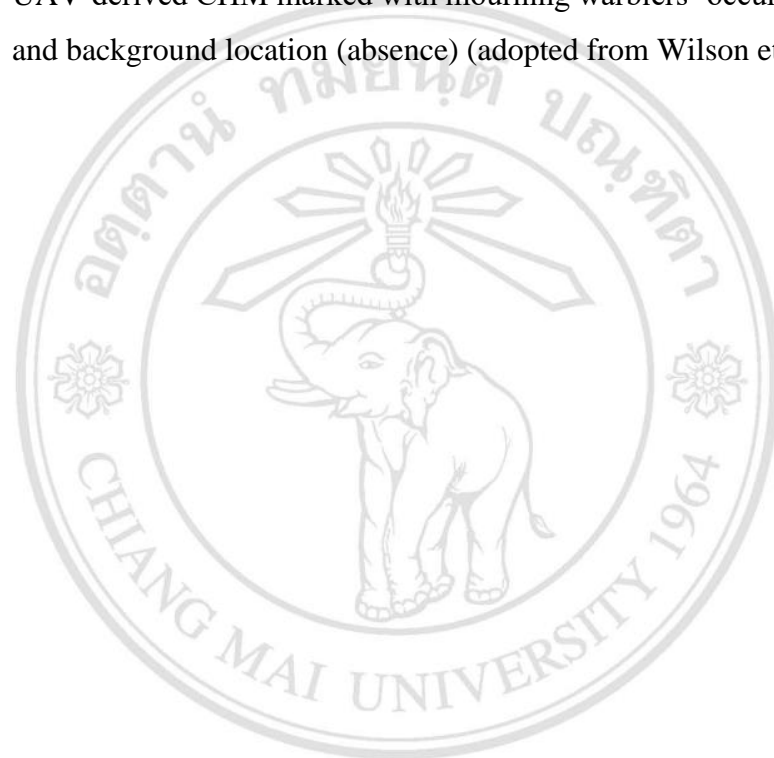
	Page
Table 2.1 Six thresholds to classify and describe forest-degradation stages and restoration strategies (adopted from Elliott et al., 2013)	9
Table 3.1 Five study sites in a range of restoration progress	16
Table 4.1 Ground survey results of five selected sites	36
Table 4.2 UAV flight records, weather conditions and flight-mission settings when capturing aerial RGB images (50 m above ground)	38
Table 4.3 Distance to reference (visible) center point of 11 plots (in meters)	41
Table 4.4 R-Squared and correlation coefficients with reference (ground surveyed data), highly correlated coefficients are in bold	55
Table 4.5 Data min-max normalization	57
Table 4.6 Calculated FDI and comparison between five stages and FDI categories	58
Table 4.7 Consumption comparison between ground survey and UAV-derived FDI	66

LIST OF FIGURES

		Page
Figure 1.1	Conceptual framework of this study	5
Figure 2.1	A stocking chart determining per cent of stock from number of trees and basal area. (adopted from Bahamondez & Thompson, 2016)	8
Figure 3.1	Location of five study sites, located in Chiangmai, and Lampang provinces, northern Thailand.	15
Figure 3.2	View and expected degradation level of each study site	17
Figure 3.3	Measurements from ground survey	19
Figure 3.4	(L) DJI Phantom 4 Pro, (R) flight mission plan in LITCHI application	20
Figure 3.5	(L) red-black ground marker set at the center of circular plots, (R) red-black ground marker, detected by UAV image sensing	21
Figure 3.6	Wild Heerbrugg T1 theodolite	21
Figure 3.7	Principle of stadia method (Benton & Taetz, 1991; Brinker & Wolf, 1984)	22
Figure 3.8	Comparison two types of DEM (i.e., DSM and DTM), and CHM derived from the difference between DSM and DTM	24
Figure 3.9	(Top) RGB single image, taken from a UAV, (Down) Referenced orthophotos derived from the multiple overlapped RGB images	25
Figure 3.10	Concept diagram of <i>variable window filter</i> algorithm for detecting tree-top points	26
Figure 3.11	Principle of <i>marker-controlled watershed segmentation</i> (mcws) algorithm, delineating crown boundaries (adopted from Fisher, 2013)	28
Figure 3.12	Example of separating three elements of the ground. (A) Canopy cover, merged tree-crown boundaries, delineated from CHM, (B) Canopy cover, pre-removed orthophoto, exposed soil + rock detection using color threshold, (C) Per cent three ground elements	30

Figure 4.1	Tipping points in degradation levels determining different forest-restoration strategies (adopted with permission from Stephen Elliott)	37
Figure 4.2	Orthophotos from five sites in unified scale. Comparisons with DEMs (i.e., DSM, DTM, and CHM) are presented in Appendix B.	39
Figure 4.3	Examples of stadia method and comparisons with GPS detected points in orthophoto of BPK site. Results of stadia method at the three sites are presented in Appendix C.	40
Figure 4.4	Empirically developed window-size functions	42
Figure 4.5	Comparison of settings, for detecting tree-top points by <i>variable window filter</i> algorithm, with different window-size functions and minimum tree heights	43
Figure 4.6	Example result of detected tree-crown boundaries comprising canopy cover, with different minimum crown boundary heights	45
Figure 4.7	Comparison of setting, for delineating tree-crown boundaries by <i>watershed</i> algorithm, with different minimum crown boundary heights	46
Figure 4.8	Scatter plot of tree stocking-density	47
Figure 4.9	Scatter plots of tree height descriptive statistic values	48
Figure 4.10	Scatter plots of per cent of three ground-elements	49
Figure 4.11	Scatter plots of ACD	50
Figure 4.12	Mean stocking-density estimates from sample plots: i) sampled ground survey, ii) sampled UAV survey, and iii) overall-detected UAV survey (each whole site)	51
Figure 4.13	Per cent three ground elements, averaged from sample plots: i) sampled ground survey, ii) sampled UAV survey, and iii) overall-detected UAV survey (each whole site)	52
Figure 4.14	Per cent frequency of tree size class from ground surveys in sample plots for each site	54
Figure 4.15	Intercorrelations among the four variables that were closely correlated between UAV and ground surveys	56
Figure 4.16	(Top) BMSM re-planting day in 2012: small previously planted trees; (Down) ML planting day in 2014: scattered remnant mature trees	59

Figure 4.17	(Top) Ground survey in BPK: large and dense trees; (Down) Ground survey in BMM: dense weed, low tree stocking-density	60
Figure 4.18	Examples of different quality of UAV-derived RGB images from various weather condition in ML site (1,290 m a.s.l.)	61
Figure 4.19	Examples of UAV derived point clouds in the same forest by (A) LiDAR and (B) SfM point cloud (adopted from Sankey et al., 2017)	63
Figure 4.20	UAV-derived CHM marked with mourning warblers' occurrence and background location (absence) (adopted from Wilson et al., 2021)	65



ลิขสิทธิ์มหาวิทยาลัยเชียงใหม่
 Copyright© by Chiang Mai University
 All rights reserved

LIST OF ABBREVIATIONS

ACD	Above-ground Carbon Density
AFR100	The African Forest Landscape Restoration Initiative
AGB	Above Ground Biomass
AHP	Analytic Hierarchy Process
ANR	Assisted Natural regeneration
APEC	Asia-Pacific Economic Cooperation
APFNet	Asia-Pacific Network for Sustainable Forest Management and Rehabilitation
BEF	Biodiversity-Ecosystem Functioning
BMM	Ban Meh Me
BMSM	Ban Mae Sa Mai
BPK	Ban Pong Krai
CBD	Convention on Biodiversity
CHM	Canopy Height Model
CPA	Crown Projected Area (m ²)
CSR	Corporate Social Responsibility
DBH	Diameter at Breast Height
DEM	Digital Elevation Model
DSM	Digital Surface Model
DTM	Digital Terrain Model
FAO	Food and Agriculture Organization of the United Nations
FDI	Forest-Degradation Index
GBH	Girth at Breast Height

HMLS	Hand-held, Mobile, Laser Scanners
HSB	Hue, Saturation, and Brightness
IPCC	Intergovernmental Panel on Climate Change
ITTO	The International Tropical Timber Organization
IUCN	The International Union for Conservation of Nature
LAI	Leaf Area Index
Lidar	Light Detection and Ranging
LP	Lam Pang
MCDA	Multi-Criteria Decision Analysis
ML	Mon Long
NYDF	New York Declaration on Forest
PCM	Pairwise Comparison Matrix
PV	Photosynthetic Vegetation
RADAR	Radio Detection and Ranging
REDD+	Reducing Emission from Deforestation and Forest Degradation in developing countries
RGB	Red, Green, and Blue
RS	Remote Sensing
RSAP	Rapid Site Assessment Protocol
SfM	Structure from Motion
TLS	Terrestrial Laser Scanners
UAVs	Unmanned Aerial Vehicles
UNEP	United Nations Environment Programme
UNFCCC	United Nations Framework Convention on Climate Change

GLOSSARY

3D mesh	A model consists of triangle-shaped meshes, polygonised with major points from point clouds. It presents more distinct boundaries over objects compared to raster formats.
AHP	Analytic Hierarchy Process: Descriptive approach to decision-making. A theory of prioritization that derives relative scales of absolute numbers known as priorities from judgments expressed numerically on an absolute fundamental scale.
ANR	Assisted Natural Regeneration: A forest ecosystem restoration strategy, enhancing the natural processes of forest regeneration, rather than planting new trees, by i) removing barriers to natural forest, ii) helping the growth of established natural, and iii) encouraging seed dispersal.
BMM	Ban Meh Me: One of five study sites, where was expected as the 2nd most degraded site according to the ground survey.
BMSM	Ban Mae Sa Mai: One of five study sites, where was expected as the 1st least degraded site according to the ground survey.
BPK	Ban Pong Krai: One of five study sites, where was expected as the middle level of degraded site according to the ground survey.
CHM	Canopy Height Model: A type of DEM, presenting the features of upper canopy in the forest.

DEM	Digital Elevation Model: A grid of pixels identified with their 3D coordinates (x, y, and z), presenting topographical features on the ground, generated from elevation data. DSM, DTM, and CHM are type of DEM.
DSM	Digital Surface Models: A type of DEM, presenting ground features.
DTM	Digital Terrain Models: A type of DEM, presenting upper surface of objects on the ground.
Framework tree species method	A forest ecosystem restoration strategy, the least intensive of the tree planting options. It exploits natural seed dispersal mechanisms to number of trees necessary to shade out weeds and attract seed-dispersing animals.
HSB	Hue, Saturation, and Brightness: A color model, identifying colors with three elements—Hue: a particular wavelength in visible ray; Saturation: percentage of purity of color (0% is pale and 100% is pure and strong); Brightness: percentage of whiteness (0% is black and 100% is white).
Hyperspectral imagery	Remotely sensed image consists of various bands, not only multispectral level, but higher level of spectral details, i.e., hundreds or thousands of bands, generally unnamed, with narrower bands (10-20 nm)
LP	Lam Pang: One of five study sites, where was expected as the 1st most degraded site according to the ground survey.

Maximum diversity planting	A forest ecosystem restoration strategy, recreating the tree species composition near to the original diversity by intensive planting. It is recommended when seed-dispersal is limited from remnant forest (e.g., by far distance with seed trees, and lack of seed-dispersing animals).
MCDA	Multi-Criteria Decision Analysis: general term for explicit and formal techniques to aid decision making using multiple criteria.
ML	Mon Long: One of five study sites, where was expected as the 2nd least degraded site according to the ground survey.
Multispectral imagery	Remotely sensed image consists of various bands, not only visible rays (i.e., RGB: Red, Green, and Blue bands), but generally 3-10 bands (e.g., near infrared, thermal infrared, etc.), which can be described with titles.
Nurse tree plantation	A forest ecosystem restoration strategy, plating highly resilient tree species to improve the soil and modify the micro-climate.
Orthophoto	A referenced image compiled by aggregating multiple-overlapping images, so that radial distortion of each raw image is removed, and the overall area can be projected as a completely vertical image map. Also called, ortho-mosaic photo, ortho-mosaic map
PCM	Pairwise Comparison Matrix: A matrix consists of judges, comparing entities in pairs, to evaluate which of each entity is preferred.
Point cloud	A set of data points, each associated with its spatial coordinates, representing a 3D shape or object.

RGB	Red, Green, and Blue lights are added together in various proportions to reproduce a broad array of colors. Conversely each color can be decomposed in and coded using these three components.
RS	Remote Sensing: Collecting information without physical contact to the object. It can be grouped into three platforms on the basis of spatial scale, i) spaceborne, ii) airborne, and iii) ground-based platforms.
SfM	Structure from Motion: A digital aerial photogrammetry (DAP) technique, based on parallax—the fact that from a moving platform, close objects appear to move past faster than distant objects—thus distance of points from the camera can be calculated from overlapping photographs.

ลิขสิทธิ์มหาวิทยาลัยเชียงใหม่
 Copyright© by Chiang Mai University
 All rights reserved

CHAPTER 1

Introduction

1.1 Background

All over the world, forest restoration is being promoted as a major contribution towards the mitigation of global climate change and to address socio-economic issues, such as food security, poverty alleviation and economic growth. This trend is supported by several international organizations, such as the Convention on Biodiversity (CBD), Aichi Target 15 and the UN Framework Convention on Climate Change (UNFCCC), through their initiative: Reducing Emission from Deforestation and Forest Degradation (REDD+) program. Such global programs are major drivers of forest restoration (SCBD, 2002; 2010; UNFCCC, 2008). The Bonn Challenge was launched by the German government and the International Union for Conservation of Nature (IUCN) in 2011. It targeted restoration of 150 million hectares of deforested and degraded lands by 2020. Subsequently, the New York declaration on Forest (NYDF), proposed at the UN Climate Summit in 2014, added a further 200 million hectares to the target and extended the time frame to 2030 (UN Climate Summit, 2014; Dave *et al.*, 2019). In March 2019, the UN Decade on Ecosystem Restoration was declared by UN General Assembly (UNGA). The UN's Environment Programme (UNEP) and the Food and Agricultural Organization of the United Nations (FAO) are co-ordinating the initiative, which includes global restoration activities towards the Bonn Challenge (UNEP & FAO, 2019; 2020). This means that ecosystem restoration, including forest ecosystems, has achieved global recognition, as an urgent goal for the coming decades.

Accordingly, various organizations are implementing initiatives to contribute towards these ambitious goals, at both regional and national levels. The African Forest Landscape Restoration Initiative (AFR100) aims to restore 100 million hectare of degraded and deforested land in sub-Saharan Africa by 2030 (AFR100 Governance, 2017), whilst Initiative 20×20 seeks to restore 20 million hectares of degraded land by

2020 in Latin America and the Caribbean (IUCN, 2017). Also, Asia-Pacific Economic Cooperation (APEC) launched APEC 2020 Forest Cover Goal from the Sydney APEC Leader's Declaration on Climate Change, Energy Security and Clean Development in 2007, aiming to increase forest cover to 20 million hectares by 2020 in the Asia-Pacific region (APEC Economic Leaders, 2007; FAO, 2019) and, the Asia-Pacific Regional Strategy and Action Plan for Forest Landscape Restoration to 2030 has been developed by FAO and Asia-Pacific Network for Sustainable Forest Management and Rehabilitation (APFNet). It suggests strategic priorities and action plans, to support attaining international and national goals, related to boosting forest restoration and strengthening ecological functionality (FAO & APFNet, 2018).

1.2 Problem statement and rationale

Participants in such initiatives should focus on the *ecological impacts* of the restoration as much as the quantity. According to the five-year assessment report of NYDF in 2019, most restoration projects are outside of natural forestland. Increased tree cover has been detected on non-forest areas (e.g., croplands and shrublands), three times more than inside natural forest (NYDF Assessment Partners, 2019). Furthermore, only one third of the restoration areas, pledged under the Bonn Challenge, is in natural forest; the rest is plantations and agroforests (Lewis *et al.*, 2019), whilst natural forest cover decreases more rapidly, from 18.3 Mha, to 26.1 Mha in annual average before and after NYDF launched (NYDF Assessment Partners, 2019). This is problematic because forest destruction brings about losses of biomass, biodiversity and ecosystem functioning, particularly carbon sequestration (NYDF Assessment Partners, 2019). The carbon sequestration capacity of forest ecosystem restoration is 6 times and 40 times higher than that of agroforestry and plantations respectively (Lewis *et al.*, 2019). Forest ecosystem restoration is not simply revegetation. It includes re-instating biodiversity-ecosystem functioning (BEF). Multiple (various) and stable (sustainable) forest functioning requires multiple species, genetic diversity and above- & below-ground linkage of plants, which are highly developed in natural forest. Forest ecosystem restoration means returning levels of biomass (and carbon) accumulation, structural complexity, biodiversity, and ecological functioning to those of the reference forest type (Elliott *et al.*, 2013). It is not a single intervention, but rather a process of adaptive management in response to a series

of interdependent interventions, aimed at reversing the process of forest degradation. (Aerts *et al.*, 2011; Stanturf *et al.*, 2014).

Consequently, it is important that forest restoration is prioritized in degraded forests or recently deforested lands. Furthermore, identifying and assessing different levels of forest degradation are necessary, to devise effective restoration strategies for each level (Sasaki *et al.*, 2011). Numerous reforestation projects have failed, due to inadequate planning and execution. For example, a 13-year restoration program in Hainan, China, failed because of inadequate identification and assessment of forest condition. This allowed expansion of deforestation and plantations even into remaining natural forest remnants (Zhai *et al.*, 2014). Failure was also due to inappropriate species choices and low genetic diversity of planting stock, leading to poor reproduction (i.e. low seed germination and seedling survival rate) (Thomas *et al.*, 2015). Although some forest restoration projects fail due to fire and drought, most failures occur because of technical factors, such as lack of weed control, poor species selection and seed sourcing, low planting stock and inadequate nutrients (FAO Regional Office for Asia and the Pacific, 2005). To prevent further technical failures, informed restoration plans, based on clear recognition of prevailing environmental constraints are needed. The process of planning begins with identifying degradation levels, as a basis for deriving restoration strategies.

However, the current ways of measuring forest degradation are labor-intensive, and teams of field workers can generally cover very small sample plots. For example, in northern Thailand, Chiang Mai University's Forest Restoration Research Unit (FORRU-CMU) conducts rapid site assessment for planning restoration projects. Generally, it takes a whole day for each project (approximately 0.5 – 3.0 hectare), with 3 - 4 teams, each of 2 - 4 members. Remote sensing has advantages in terms of convenient data collection from remote, requiring less labor, and availability of advanced data analysis and overall survey, whilst conventional ground surveys are limited by sampling. It can also be applied for measuring and analyzing forest structure. Especially, Unmanned Aerial Vehicles (UAVs) are able to closely approach trees and detect detailed structure.

Furthermore, forest degradation has been presented conventionally in terms of discrete 'stages'. For example, FORRU-CMU published a 5-stages view of degradation based on six critical thresholds (criteria), with tipping points indicating the transition from

one degradation to the next. However, each of the tipping points were mostly based on only one each of the six criteria. This makes it difficult to integrate multiple criteria to classify forest degradation stages. It limits understanding of degradation processes subject to various interconnected criteria and may result in bias in determining restorative interventions. Also, discrete categorizing systems are limited for comparing degradation levels among sites and for monitoring the effectiveness of strategies. On the other hand, a continuous index system can distinguish detailed differences, among sites even within the same conventional degradation stage. As indices are generated by combining multiple criteria, bias due to dependency on single criteria can be prevented.

Resolving these issues fulfills one of the recommendations of the UN Decade on Ecosystem Restoration 2021–2030, i.e., to overcome the barrier of the limited technical knowledge and capacity, which currently limits the success of restoration projects and initiatives, at both national and local levels. The UN Decade specifically emphasizes provision of and sharing methods and tools, including baseline studies, site-specific restoration protocols, and monitoring (UNEP & FAO, 2019). Ultimately, this research, presented here, supports successful restoration projects, to achieve climate change mitigation in line with global initiatives.

1.3 Objectives

Consequently, this research project explored the use of RGB images, from a consumer UAV, to define stages of forest degradation/regeneration for the development of forest restoration (or conservation) strategies. The aim of this study was to develop an advanced UAV-based forest-survey methodology, which is more effective, in terms of time and labor consumption, and with more accurate results, compared with other current techniques. It is intended that the methods, developed by this project, will be applicable for assessing forest-degradation levels and for developing effective restoration plans.

The detailed objectives were:

1. To identify correlations between variables of forest degradation, currently measured on the ground, with equivalent indicators derivable from UAV-based imagery.
2. To develop an advanced forest degradation assessment system, leading to degradation index, using RGB data collected by consumer UAVs.

1.4 Conceptual framework

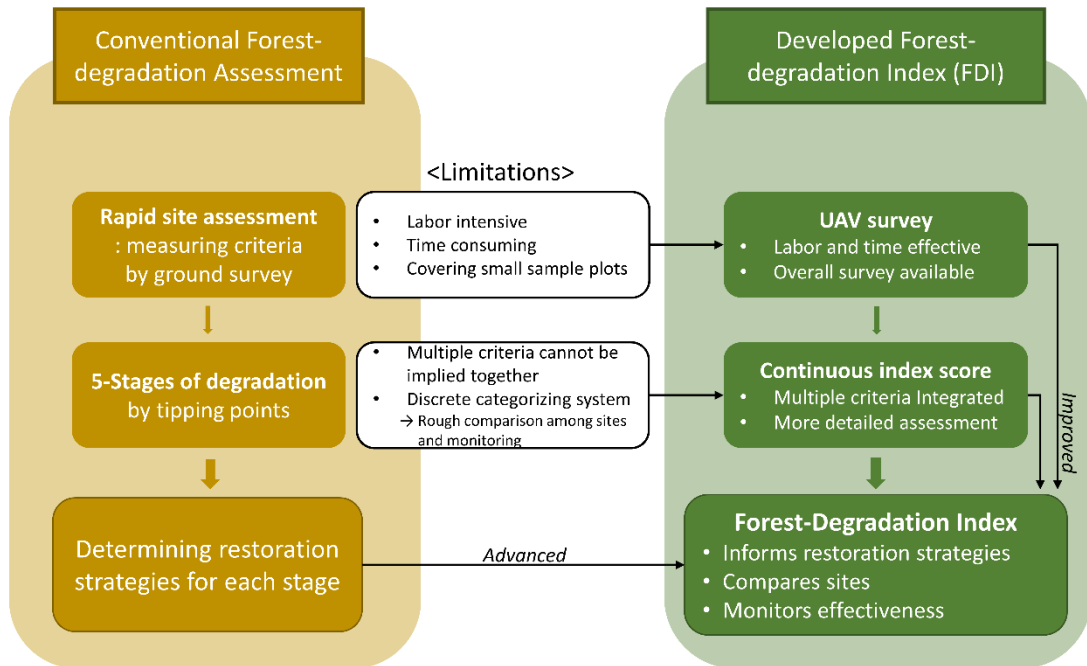


Figure 1.1 Conceptual framework of this study

CHAPTER 2

Literature Review

2.1 Forest-degradation assessment as the basis for restoration planning

Forest degradation is defined differently by different organizations, but there are two main perspectives of definition: one based on ecological criteria (biophysical definitions); the other based on the impact of degradation on human livelihoods (anthropocentric definitions). For example, the Convention on Biodiversity (CBD) focuses on the availability of habitat for forest-dependent species and considers forest degradation as one of the leading causes of biodiversity loss. The organization describes forest degradation as any combination of loss of soil fertility, compaction and salinization and reduced forest cover and ecological functioning that impedes or retards unassisted forest recovery, through secondary succession (SCBD, 2002). Also, IPCC (2003) focuses on the loss of forest values (particularly carbon), likely to be characterized by a reduction of tree cover. Focusing more on the socio-economic impacts of forest degradation, the FAO and ITTO define it in terms reduced capacity of forests to provide goods and services (to humans) (FAO, 2002; ITTO, 2002). Temporal change, spatial scale and causes of degradation (human or nature) have also been proposed as components of the definition of forest degradation by various researchers (FAO, 2011). In reality, anthropocentric definitions are a consequence of degradation of biophysical factors, since, if forest degradation reduces biomass and biodiversity etc. ecological services that support agriculture are reduced, along with the productivity and variety of forest and products to meet varied human needs. Consequently, in this study, forest degradation was assessed on based on biophysical factors such as relative cover of tree-crowns, vegetation, and bare ground, and number and height of remaining trees. Conversely, the effectiveness of restoration was evaluated in terms of reversing these variables.

A wide variety of forest-degradation indicators have been put forward. For example, Thompson et al. (2013) proposed a scoring system, based on comparing the percent value of current 5 criteria and 7 indicators relative to target levels. However, they did not provide threshold levels for each indicator. Vásquez-Grandón et al. (2018) proposed 3 key elements, to evaluate forest degradation: i) a reference forest, ii) degradation indicators and iii) threshold values of those indicators. The FAO reported that different countries define or assess forest degradation, in terms of reduced productivity, biomass, and biodiversity (FAO, 2011; Simula, 2009). Such reports imply the necessity of effective and systematic programs to assess degree of degradation. Specifically, Vásquez-Grandón et al. (2018) concluded their review by identifying a fundamental and urgent need for implementing suitable practices, against ongoing degradation of forests, where they have not been totally degraded beyond thresholds, rather than simply finding degraded forests in landscape.

Bahamóndez et al. (2009) modeled a stocking chart, whose concept was adopted from Ginrich (1967), and tested the availability of applying the stocking chart for assessing forest degradation with respect to sustainable productivity, but also expected it to be used for monitoring carbon stock. Subsequently the stocking chart was applied for quantitatively assessing and predicting forest degradation, resilience, and stability of stands, according to the intensity of harvesting (Figure 2.1) (Bahamondez & Thompson, 2016). These approaches suggested tools for quantitatively assessing forest degradation and deciding on practical solutions. However, these studies focused on sustained yield, considering only productivity, rather than forest ecosystem restoration.

Sasaki et al. (2011) stated that restoration interventions should match different degrees of degradation. They proposed strategies, which were based on different degradation levels from a minimum (e.g., reducing harvest and avoiding logging vulnerable area) to a maximum (e.g., assisted natural regeneration and replanting). However, this concept only considered harvesting and logging, as the main drivers of degradation. Other disturbances were not considered (e.g., agricultural activities, grazing, forest fire, etc.). Also, only observed inventories were described as carbon stock. Practical boundaries or standards, categorizing each level of degradation, were not mentioned

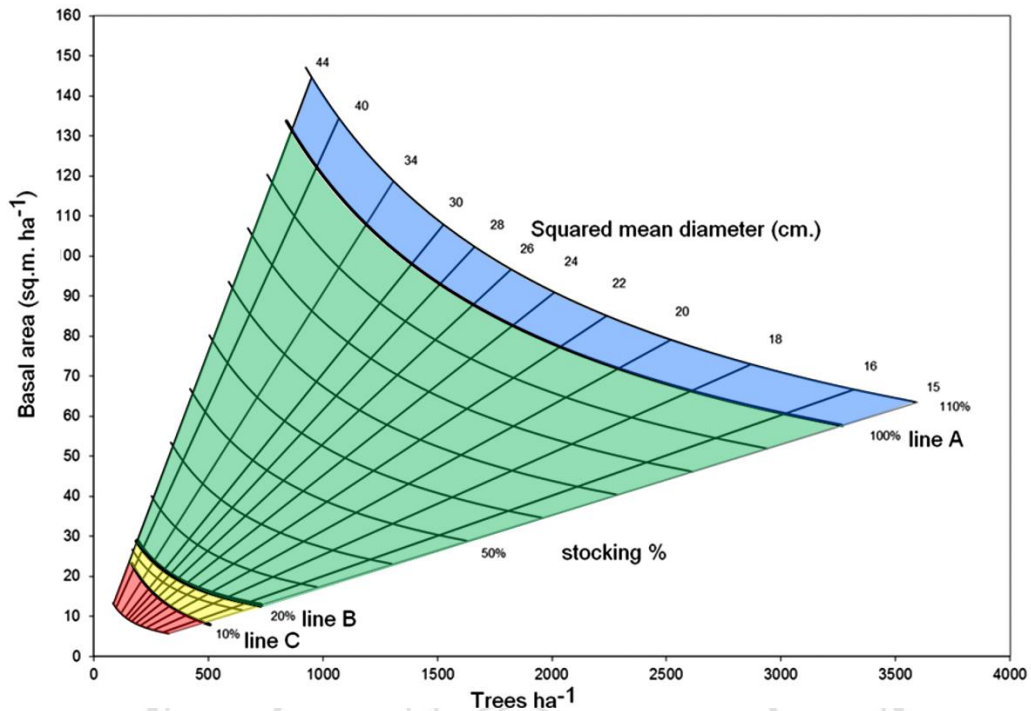


Figure 2.1 A stocking chart determining per cent of stock from number of trees and basal area. It shows gradual changes of stock and discrete categories, marked in different colors, separated by line A, B, and C. (adopted from Bahamondez & Thompson, 2016)

Chiang Mai University's Forest Restoration Research Unit (FORRU-CMU) proposed 5 stages of forest ecosystem degradation, on the basis of 6 critical thresholds, which, once crossed, necessitate a substantial change in restoration methodology. A rapid-site-assessment protocol (RSAP) was developed, to identify degradation stages and provide essential inputs into developing effective restoration strategies for each stage. Five levels of degradation were distinguished by tipping points based on the critical thresholds, resulting in 5 different restoration responses (see Table 2.1) (Elliott *et al.*, 2013).

Modica *et al.* (2015) proposed a gradual index system, to describe forest-degradation. Individual indicators were applied, to represent not only the biophysical characteristics, but also biodiversity and ecological functionality. Combining these criteria into a forest-degradation index (FDI) was done using Multi-Criteria Decision Analysis (MCDA), weighting each variable using an Analytic Hierarchy Process (AHP), to process expert opinions. Modica *et al.*, (2015) stated that the AHP approach provides simplicity, flexibility, and transparency to aid decision-making and conflict-resolution.

Table 2.1 Six thresholds to classify and describe forest-degradation stages and restoration strategies (adopted from Elliott *et al.*, 2013).

Degradation stage Suggested restoration strategies	Landscape-critical Threshold			Site-critical Threshold		
	Forest in landscape	Seed-dispersal mechanisms	Fire risk	Vegetation cover	Natural regenerants	Soil
Stage 1 Protection	Remnant forest remains within a few km of the site	Mostly intact, limiting the recovery of tree species richness	Low to medium	Tree-canopy cover exceeds herbaceous weed cover	Natural regenerants exceeds 3,100/ha with more than 30 common tree species represented	Soil does not limit tree seedling establishment
Stage 2 Protection + ANR			Medium to high	Tree-canopy cover insufficient to shade out herbaceous weeds		
Stage 3 Protection + ANR + Planting Framework tree sp.			High	Herbaceous weed cover greatly exceeds tree-crown		
Stage 4 Protection + ANR + maximum diversity planting	Remnant forest patches very sparse or absent from the surrounding landscape	Seed-dispersing animals rare or absent such that the recruitment of tree species to the restoration site will be limited	Initially low (soil conditions limit plant growth) higher as the vegetation recovers	Herbaceous weed cover limited by poor soil conditions	Natural regenerants sparser than 3,100 trees/ha with fewer than 30 common tree species represented	Soil degradation limits seedling establishment
Stage 5 Soil amelioration + Nurse tree plantation, followed by thinning and gradual replacement of maximum diversity tree planting						

All rights reserved

2.2 Remote sensing as the platform for effective forest survey

Due to the limitations of direct ground surveys for forest inventory and degradation assessments, various trials have explored using data derived from remote sensing (RS)—collecting information without physical contact to the object. RS technologies can be grouped into three platforms on the basis of spatial scale, i) spaceborne, e.g., satellites, ii) airborne, e.g., airplanes, helicopters, and unmanned aerial vehicles (UAVs), and iii) ground-based, e.g., terrestrial laser scanners (TLS), and hand-held, mobile, laser scanners (HMSL). Sensors mounted on such platforms can be i) passive, sensing naturally generated or reflected radiation from objects (e.g., visible, heat radiation, multispectral, and hyperspectral types), or ii) active, emitting radiation and sensing its reflection back from objects, e.g., Radio Detection And Ranging (RADAR), and Light Detection and Ranging (LiDAR) (Camarretta et al., 2019).

Interest in spaceborne systems has grown since 1999, because of its usefulness to determine changes over time, since data are collected regularly and relatively frequently and the various sensors cover very large areas (Alonzo et al., 2018; Camarretta et al., 2020). Surveys of various forest attributes, using different satellite data and ancillary data have been published as follows.

Zhuravleva et al. (2013) assessed forest degradation in the Democratic Republic of the Congo from 2000 to 2010. Data from Landsat satellite imagery were used to generate maps of forest cover, extent, and loss. Data from GLAS (Geoscience Laser Altimeter System) sensors were used, to determine tree-canopy heights and for calibration. They recorded 1.02 % of primary forest was cleared over 10 years and 2 % degraded, due to land-use change and fragmentation. Hansen et al., (2016) also detected tree-height information in Sub-Saharan Africa, between 2013 and 2014, from Landsat and GLAS data, to describe tree-height distribution and canopy discontinuity. Heights of tall trees (> 20 m height) were significantly underestimated by about 4 and half meter on average, whilst those of small trees (< 5 m height) were overestimated by about 1 and half meter on average.

Rapinel et al., (2014) classified vegetation cover into three types, i) non-vegetation area, ii) artificial vegetation (i.e., crops, garden and parks, and plantation), iii) natural and semi-natural vegetation (i.e., forests and thickets) from Worldview-2 satellite images applied with thematic ancillary data. This classification was reasonably accurate with Kappa index of 0.74. (Kappa index quantifies the accuracy of categorical maps. With value of one indicating 100 % accuracy). Shimabukuro et al. (2014) and Da Ponte et al., (2017) assessed temporal changes in forest cover. Shimabukuro et al. (2014) used fraction images, extracted from Landsat. Soil fraction images were derived from high-reflectance areas, distinguishing clear-cut deforestation sites and bare soil, whilst shade fraction images were from low reflectance areas, quantifying areas of water, shadow and burnt forest. With these two fraction images, they were able to distinguish between degraded forests by selective logging and forest fire from June to October in 2002. Da Ponte et al., (2017) also used Landsat data to identify five classes of forest cover (i.e., forest, croplands, grasslands, urban areas, and water) and detect the change for 17 years, from 1999 to 2016. They reported a 7,500 km² loss in forest cover, which was 27 % of the original area in 1999. They also included landowners' perceptions as socio-economic data to identify those factors affecting forest dynamics: farm type, level of dependency and use of forest products and ecological services, and the level of education of forest owners. The use of satellite data for assessing forest attributes has expanded the research spectrum, enabling exploration of wider temporal and spatial scales, especially identification of land cover and detection of accelerated land use changes with greater accuracy at the landscape level (Miranda et al., 2020).

However, challenges and limitations when using satellite data remain. Calibration and validation of site information from satellite images is not extensive enough (Alonzo et al., 2018), and the frequency of temporal scale is not always that required by project goals (Rapinel et al., 2014). Moreover, satellite images have limited resolution, which is not high enough to be useful at the site level (Da Ponte et al., 2017; Alonzo et al., 2018). In particular, use of satellite data to quantify forest-degradation severity, from qualitative changes in forest attributes and composition, is complicated and limited (Miranda et al., 2020).

2.3 UAVs as optimal remote-sensing platforms for small-scale restoration planning

Unlike satellites, airborne platforms can fly close to vegetation canopies, such that data resolution is exceptionally high and geographical information is precise (although much smaller areas can be covered, compared with satellite data). In particular, unmanned aerial vehicles (UAVs) can fly very close to forest canopies more cheaply and safely compared to the conventional airborne platforms (e.g., airplanes and helicopters), leading to higher spatial and temporal resolutions (Alonzo et al., 2018; Camarretta et al., 2019).

So, UAV-derived data can be more effectively used to complement or replace satellite data, when surveying forest attributes and determining strategies particularly for small-scale restoration projects, which are mostly organized by local practitioners and Corporate Social Responsibility (CSR) donors. Getzin et al., (2012) used high-resolution airborne photographs from a UAV to detect canopy gaps to assess plant diversity in the forest understory. They reported that disturbance patterns of canopy gaps were highly correlated ($R^2 = 0.74$) with plant diversity under the canopy layer.

Active sensors are also mounted on airborne platforms for forest survey purposes. Mutwiri et al. (2017) used a light detection and ranging (LiDAR) sensor on an aircraft to estimate tree height and biomass in different forests types (e.g., natural, plantation, and other scattered forests) to correlate the results with ground-survey data. For tree height, correlation coefficients averaged 0.92 (from 0.79 in natural forest to 0.95 in plantations) and for above-ground-biomass (AGB), the average correlation coefficient was 0.86 (from 0.51 in scattered forests to 0.84 for plantations). De Almeida et al., (2020) also detected canopy structural attributes (i.e., canopy height, rugosity, gap fraction, canopy Shannon index, leaf area index (LAI), and understory LAI) from LiDAR on a UAV and analyzed their relationships with AGB and species diversity, to monitor tropical forest succession. Canopy gap fraction, rugosity, and understory LAI were correlated with forest age, and canopy height was correlated with AGB.

Various data from different sensors and platforms have been integrated to maximize the effectiveness of remote sensing. Caughlin et al., (2016) used fraction of photosynthetic vegetation (PV) from Landsat satellite data and detected a correlation with tree height ($R^2 = 0.51$) and canopy cover ($R^2 = 0.56$) from LiDAR data. Sankey et al.

(2017) merged high-resolution LiDAR data with hyperspectral and multispectral data from a UAV. Multispectral data were used to classify the vegetation and detect bare soil (76 % of accuracy), by generating 3D point clouds, but the technique was not successfully applied to measure tree height ($R^2 = 0.64$) and tree density ($R^2 = 0.53$) in dense forest. Therefore, they used LiDAR data to successfully estimate tree height ($R^2 = 0.90$), crown diameter ($R^2 = 0.72$), tree-canopy cover ($R^2 = 0.87$) and tree density ($R^2 = 0.77$). Furthermore, combined LiDAR-hyperspectral imagery was more accurate (88 %) for classifying vegetation species, compared with hyperspectral data alone.

However, LiDAR and hyperspectral cameras are expensive, whereas RGB cameras, which come as standard on consumer UAVs, are more cost-effective. To generate three-dimensional point clouds model using RGB imagery, structure-from-motion (SfM) techniques have been applied and is incorporated into many drone imaging software packages (e.g., Ecosynth, Agisoft Metashape, Pix4D, DroneDeploy, and OpenDroneMap (ODM), etc.) This technique is based on parallax—the fact that from a moving platform, close objects appear to move past faster than distant objects—thus the magnitude of shifts in position of the same point between 2 or more photographs can be used to calculate the distance of that point from the UAV (Ullman, 1979; Stockman & Shapiro, 2001).

Zahawi et al. (2015) used the SfM technique on images taken with a consumer-grade camera on a small multicopter drone, analyzed by the open-source ‘Ecosynth’ software, to measure canopy structure of 7–9 years tropical forest restoration plots, compared with ground-based measurements. Correlations between field-based measurements and the Ecosynth 3D model were high for canopy height ($R^2 \geq 0.85$), AGB ($R^2 \geq 0.81$) and canopy openness ($R^2 = 0.82$). Only canopy roughness ($R^2 = 0.53$) was not highly correlated. Since Zahawi et al.’s landmark paper, the SfM technique has been widely applied to assess forest attributes. Fujimoto et al., (2019) generated canopy height models (CHMs) from SfM point clouds. Then, they detected tree-top points (92.3 % accuracy) and tree-crown boundaries to distinguish two tree species (83.6 % accuracy). These variables were used to estimate DBH, and carbon stock. Khokthong et al., (2019) compared estimated canopy cover derived from SfM point cloud with hemispherical photography captured on the ground, in mixed-species planted oil palm agroforest, and found strong correlation ($R^2 = 0.84$) between them. Furthermore, they separated crown

cover into oil palm and mixed-species interplanted trees and found higher level of oil palm cover increases the mortality of interplanted trees. Swinfield et al., (2019) proved that SfM is just as effective as LiDAR for generating 3D point clouds to investigate forest structure by comparing canopy height and AGB detected from both of the techniques.

As LiDAR has been integrated with other types of data sources for better synergized accuracy, point clouds from SfM were also applied with other types of RS data. Alonzo et al. (2018) and Riihimäki et al. (2019) collected data at the plot scale, using a UAV and bridged the gap between the coarse scale of satellite data and field measurement. Baena et al., (2017) flew a UAV to collect RGB and near-infrared imagery to generate SfM 3D point clouds and object-based image analysis. 95.32 % of overall accuracy was analyzed for identifying three tree species using the integrated method.



ลิขสิทธิ์มหาวิทยาลัยเชียงใหม่
Copyright© by Chiang Mai University
All rights reserved

CHAPTER 3

Methodology

3.1 Study sites

This study was performed on sites at various stages of progress after restorative interventions in Chiang Mai and Lampang Provinces, northern Thailand (Figure 3.1).

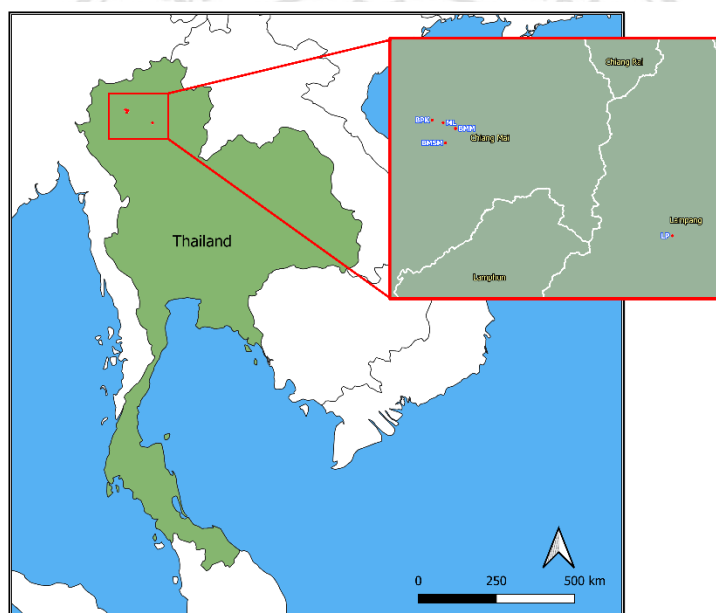


Figure 3.1 Location of five study sites, located in Chiangmai, and Lampang provinces, northern Thailand.

Five sites, covering a wide range of restoration progress were selected. All were FORRU-CMU experimental plots of known history, undergoing restoration, ranging in age since tree planting from 0 to 8 years. Prior disturbances before restoration ranged from severe: quarry site after mining, to abandoned agricultural sites and fire-damaged sites (Table 3.1). Therefore, these five sites represented a range of degradation levels. This was because all sites were undergoing restoration. i.e., reversing forest degradation. Details of each plot are provided in Table 3.1, whilst views of each plot are provided in Figure 3.2.

Table 3.1 Five study sites in a range of restoration progress

No.	Site	Restored year	Land cover Before restoration	Longitude	Latitude	Altitude (m a.s.l.)	Area, Sampling Circles
1	Ban Mae Sa Mai (BMSM)	2012	- restored in 2007 (5 years before) - burnt in 2010 (2 years before) - remained as an abandoned site, with dense and strong weed	98° 50' 57"	18° 51' 22"	1,247 m	1.07 ha (6.69 rai) 10 plots
2	Mon Long (ML)	2014	- severely impacted evergreen forest by forest fire - enrichment planting amongst scattered remnant mature trees - with dense and strong weed	98° 50' 28"	18° 55' 20"	1,290 m	1.03 ha (6.44 rai) 10 plots
3	Ban Pong Krai (BPK)	2016	- agriculture - natural regeneration continued - planting trees few years ago, but not successful.	98° 48' 19"	18° 55' 52"	1,408 m	2.69 ha (16.81 rai) 10 plots
4	Ban Meh Me (BMM)	2020	- used to be deforested for agriculture activity (until 3–4 years ago) - beginning of recovery from surrounding remnant forest	98° 52' 53"	18° 54' 13"	601 m	0.41 ha (2.56 rai) 8 plots
5	Lampang (LP)	2019	- 1 year after restoration on quarry area - structured for bench planting with nurse tree species.	99° 35' 23"	18° 33' 12"	419 m	0.66 ha (4.13 rai) 8 plots

Meteorological data of each site for five years (2010–2015) were from three stations in northern Thailand. BMSM, ML, and BPK, were higher, wetter sites. The nearest meteorological station was Station No.3, Doi Ang Kang station (1,530 m a.s.l.): recorded mean annual precipitation of 1,897.6 mm, and temperature range 3.9–32.1 °C. Climatic data for the BMM site came from Station No.4, Chiang Mai station (313 m a.s.l.): with less rainfall (mean 1,119.2 mm) and higher temperatures (11.0–41.0 °C). Climatic data for the LP site, also lowland, came from Station No.13, Lampang A station (319 m a.s.l.): mean rainfall, 1,196 mm, and temperature ranged from 8.2 °C to 43.0 °C.

Copyright© by Chiang Mai University
All rights reserved

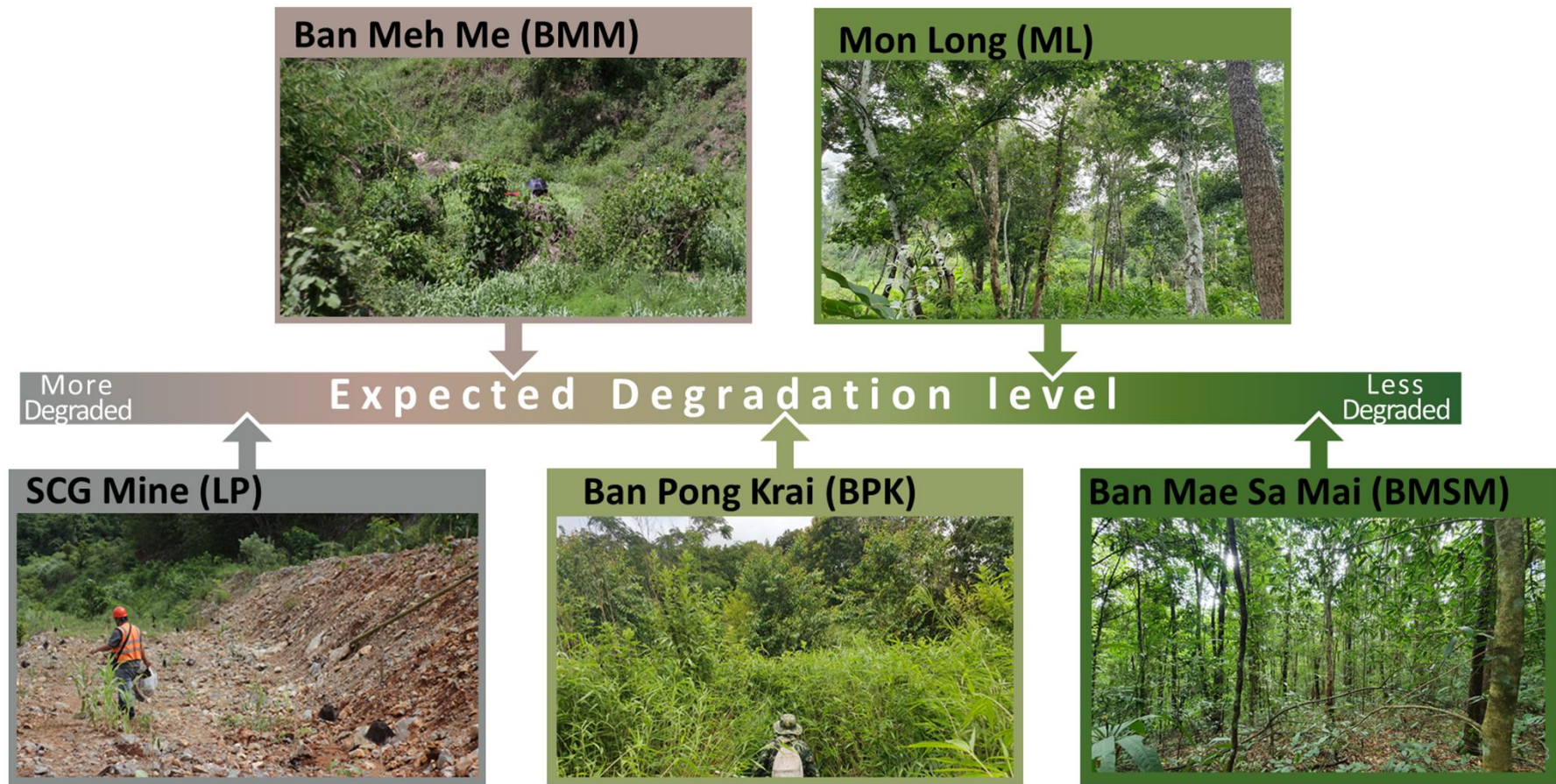


Figure 3.2 View and expected degradation level of each study site

Copyright © by Chiang Mai University
All rights reserved

3.2 Ground surveys

3.2.1 Data collection

Ground surveys were conducted by adopting the rapid-site-assessment protocol (RSAP) of FORRU-CMU (Elliott et al., 2013, Chapter 3) to be compatible with UAV-derived data. Ten circular plots (5 m radius) were laid out randomly across each study site except for the two smaller sites where eight plots were installed (i.e., BMM, and LP, < 1 ha) to keep the distances among the circular plots consistent. The RSAP involves counting and measuring 3 categories of regenerants, i) trees larger than 30 cm GBH, ii) smaller than 30 cm GBH (but longer than 50 cm tall), iii) and live tree stumps. In this study, however, 1 m tall was used as the minimum regenerant size, and live tree stumps were not separately recorded, since very small saplings and coppices would not be detectable by UAVs.

Height, and girth at breast height (GBH, 1.3 m above the ground) were measured for the counted trees. To measure various heights of trees in different degraded forests, various measurements were applied according to the conditions. Direct measurement using tape measure mounted on an extension pole (8 m maximum extension), and indirect measurement for the taller trees, using laser range finder (where applicable, with sparse density of trees and avoidable obstacles in the plot) and optical estimation from the top of the extension pole (where laser range finder cannot be applied due to the dense obstacles in the plot), were used. GBH was measured using a tape measure. For trees that branched below 1.3 m the largest stem was recorded as the main trunk. Tree-crown size (the most distinctive variable in UAV imagery) were measured by tape measure from below: length (longest distance) \times width (perpendicular to length) (Figure 3.3).

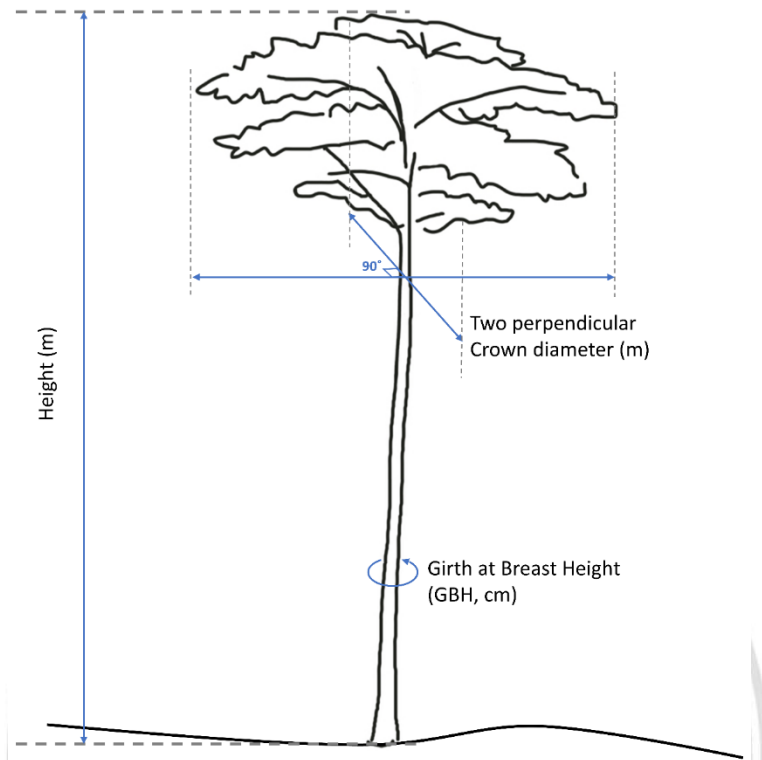


Figure 3.3 Measurements from ground survey

In each sampling plot, per cent ground cover was estimated into two categories, i) ground vegetation and weed cover, ii) and exposed rocks and bare soil cover, with optical estimation by observers. Signs of livestock and fire were recorded respectively, without quantitative measurement.

ลิขสิทธิ์มหาวิทยาลัยเชียงใหม่
 Copyright© by Chiang Mai University
 All rights reserved

3.3 Aerial surveys (UAV Flight)

3.3.1 UAV flight

A DJI Phantom 4 Pro drone, a quadcopter type of unmanned aerial vehicle (UAV) was used to collect RGB photographs by the on-board camera with 1 inch 20-megapixel CMOS sensor (Figure 3.4, Left).

To apply SfM, photographs must overlap (and side-lap) by at least 70–80 %. The LITCHI application was used to design flight missions with this degree of overlap, using grids of parallel flight lines. According to the different sizes and shapes of the plots and limited battery time (c.a. 25 minute per flight), distances between flight paths (15–20 m), and flight speed (12–13 m/s) were adjusted to achieve the required overlap and flight height was set constantly to 50m above ground (Figure 3.4, Right).

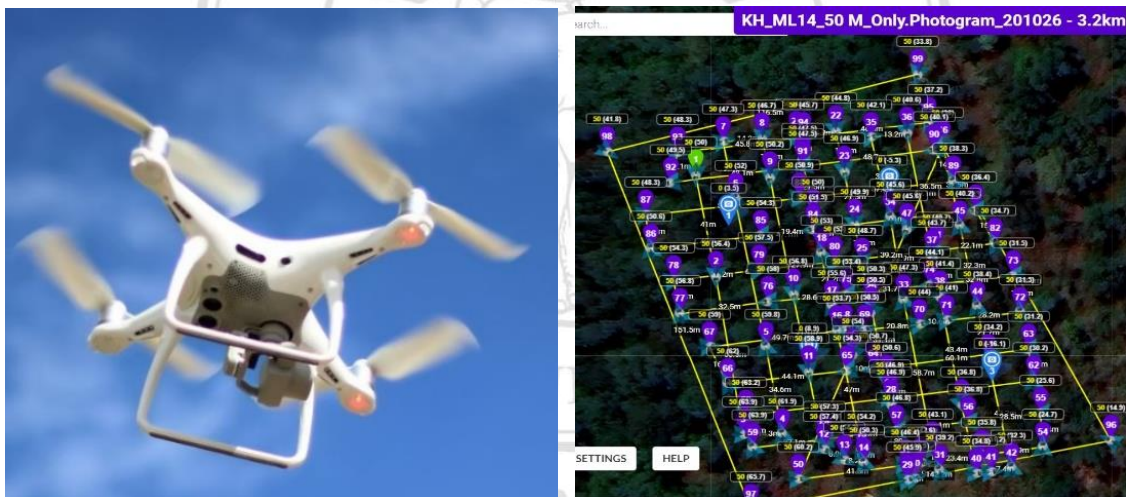


Figure 3.4 (Left) DJI Phantom 4 Pro, (Right) flight mission plan in LITCHI application

To compare the variables from each plot between UAV-derived images and ground surveys, the central points of each plot were marked with checkboard designed plates colored red-black, which could easily be detected from aerial photographs (Figure 3.5).



Figure 3.5. (Left) red-black ground marker set at the center of circular plots,
(Right) red-black ground marker, detected by UAV image sensing

However, in less degraded sites with dense canopy cover (e.g., more closed canopy), these markers were covered by tree-canopy and not visible from the UAV camera. To solve this problem, additional visible points were set at the forest gaps and centers of circular plots were surveyed by theodolite (Figure 3.6), so that azimuth and distance among the points could be calculated using stadia method (Benton & Taetz, 1991; Brinker & Wolf, 1984) and the centers of circular plots could be detected on orthomosaic maps (orthophotos) derived from the UAV imagery.



Figure 3.6 Wild Heerbrugg T1 theodolite

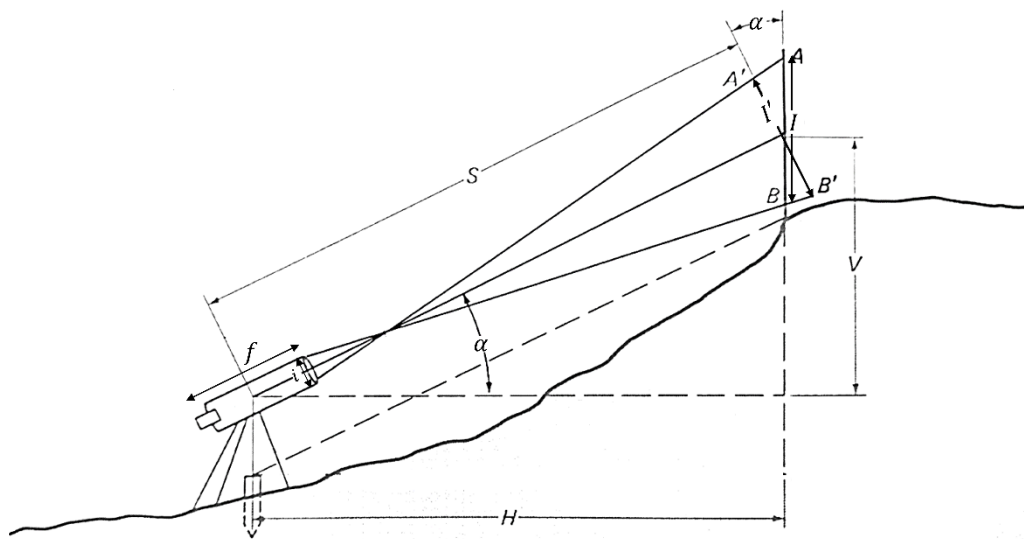


Figure 3.7 Principle of stadia method (Benton & Taetz, 1991; Brinker & Wolf, 1984)

In Figure 3.7, H (horizontal distance) is the value to be calculated and applied on the ortho-mosaic map. I is the measurement, we read on theodolite to the rod, set on the targeted point. By using trigonometric ratio, S (slope distance) can be calculated with following equations. This process was applied to prevent the data collection being biased by setting circular plots at the visible forest gaps intentionally.

$$\frac{S}{I'} = \frac{f}{i}$$

$$S = \left(\frac{f}{i}\right) I'$$

Where,

$$I' = I \times \cos \alpha,$$

$\left(\frac{f}{i}\right) = 100$, is stadia interval factor, fixed value of the theodolite.

Therefore, H (horizontal distance) can be calculated with following equations.

$$H = S \times \cos \alpha$$

$$H = \left(\frac{f}{i}\right) \times I \times \cos^2 \alpha$$

3.3.2 Image processing for producing DEMs and orthophotos

Using Open Drone Map (ODM) software, overlapping photographs from each site were processed into 3D point clouds and meshes by the SfM technique, to generate a Digital Terrain Model (DTM), a Digital Surface Model (DSM) and a 2D orthophoto. DTM and DSM are in a raster format, a grid of pixels identified with their 3D coordinates (x, y, and z), presenting ground features (DTM), and the upper surface of objects (DSM) respectively. Consequently, a Canopy Height Model (CHM) was derived by subtracting DSM from DTM (Figure 3.8). The orthophoto is a referenced image compiled by aggregating multiple-overlapping images, so that radial distortion of each raw image is removed, and the overall area can be projected as a completely vertical image map (Figure 3.9). ODM is an open-source tool, with a user-friendly interface (WebODM), working on local devices and cloud processing services (WebODM Lightning), accessing powerful servers, to process large datasets more rapidly compared to WebODM. It is more affordable than most other commercial drone-mapping software offering similar functions and features.

Between 250 and 400 pictures, generated at each site (depending on site size) were processed. DSMs and DTMs were generated at 2 cm resolution, and orthophotos were generated at 1 cm resolution—the most precise that could be generated with the image sets produced by the Phantom 4 Pro camera. The texturing data term for the 3D mesh, which affects orthophoto quality, was set to *area* mode, prioritizing images covering the largest area, which the tool's developers recommend for forest surveys.

ลิขสิทธิ์มหาวิทยาลัยเชียงใหม่
Copyright © by Chiang Mai University
All rights reserved

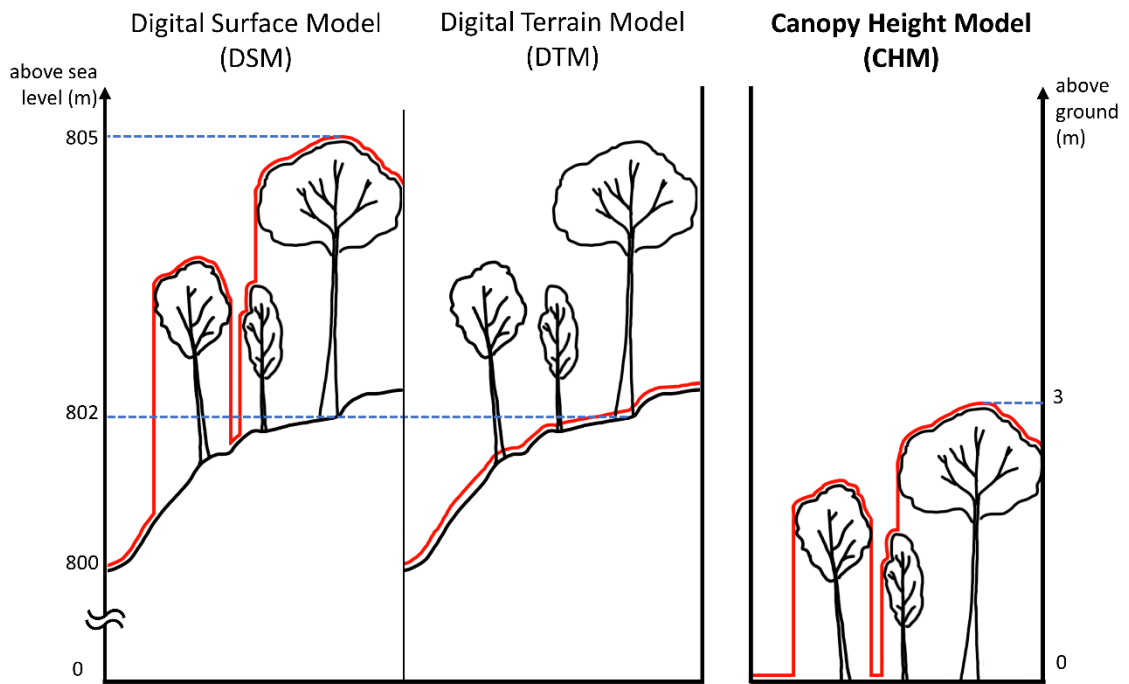


Figure 3.8 Comparison two types of DEM (i.e., DSM and DTM), and CHM derived from the difference between DSM and DTM

ลิขสิทธิ์มหาวิทยาลัยเชียงใหม่
 Copyright© by Chiang Mai University
 All rights reserved

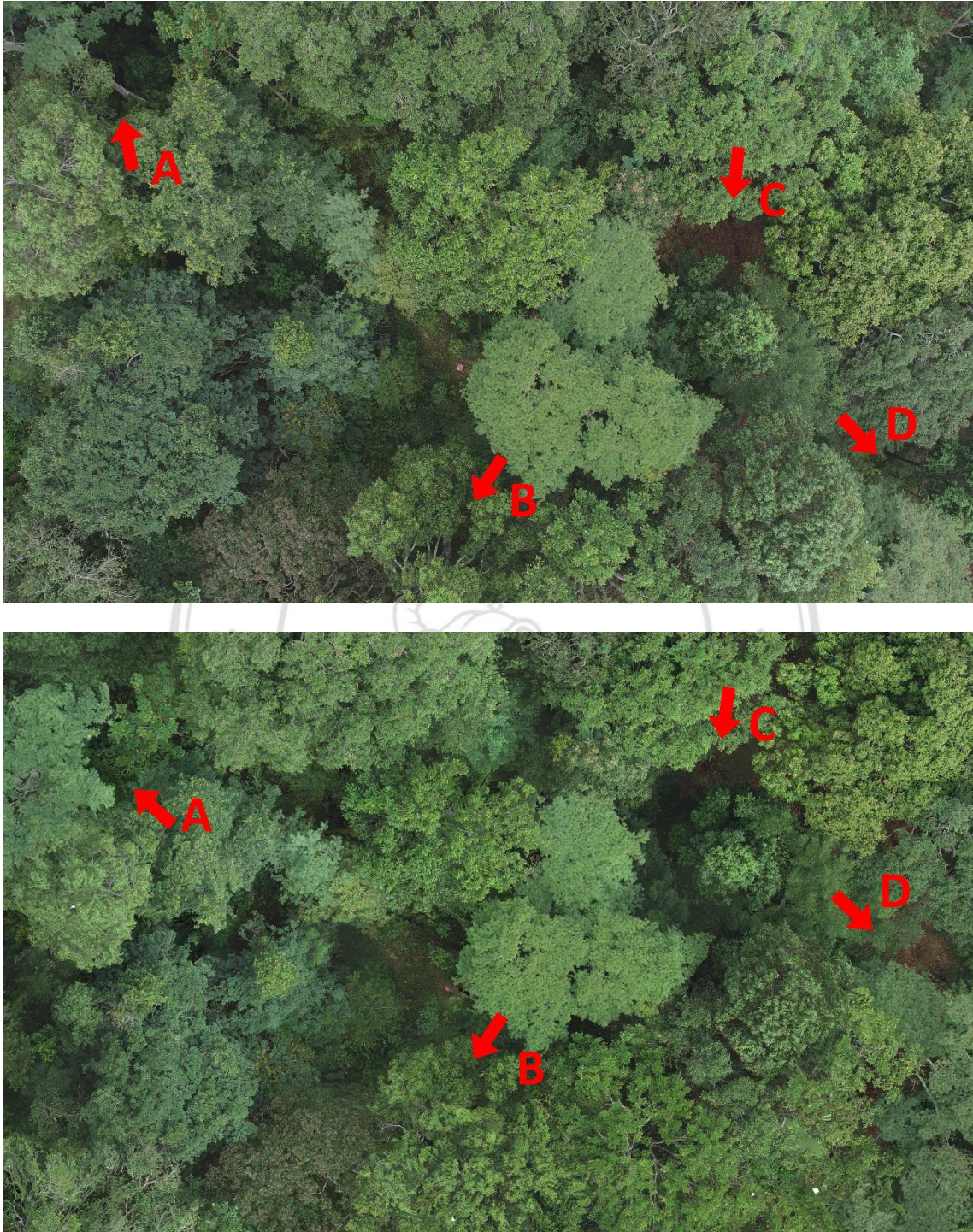


Figure 3.9 (Top) RGB single image, taken from a UAV, (Down) Referenced orthophotos derived from the multiple overlapped RGB images. A and B point to tree trunks and branches visible due to radial distortion in RGB image (Top), replaced by completely vertical tree-crowns in the lower orthophoto (Down). C and D point out different shape and area of gaps between RGB image and orthophoto.

3.3.3 Detecting tree-top points from CHMs

Canopy Height Models (CHMs) were generated by subtracting DTMs from DSMs in R (Figure 3.8) using the package ‘rgdal’ to import spatial raster files (DTM and DSM) in R, and ‘raster’ for raster calculations (Roger et al., 2020; Etten et al., 2020). Generated CHMs were used to detect tree-top points and tree-crown boundaries, using the package ‘ForestTools’ (Plowright & Roussel, 2020). This package detects tree-top points using a *variable window filter* algorithm, which assumes that higher trees have wider crowns, so the relationship of tree-height and crown-radius is given for the function of window radius from the center point. One by one, every pixel of the CHM is checked as the center point of a circular window (Plowright, 2020; Plowright & Roussel, 2020) (Figure 3.10). If the center point is the highest within each circular window, the algorithm defines the center point as a tree-top point.

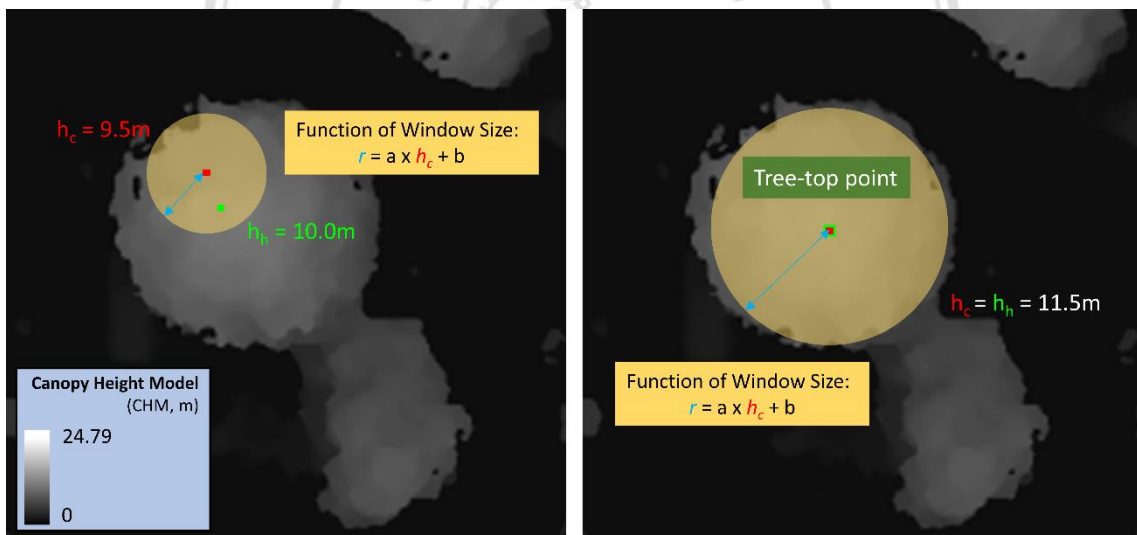


Figure 3.10 Concept diagram of *variable window filter* algorithm for detecting tree-top points. Where, h_c is the height of the center point which the algorithm is currently inspecting, h_h is the highest point in the crown window (transparent yellow circle in the figure), r is the radius determined based on the given function. When there is another point higher than the center point ($h_h > h_c$) in the crown window, the center point is rejected as the tree-top point. When the center point is the highest point ($h_c = h_h$) in the crown window, the point is determined as the tree-top point.

In this study, different window size equations and minimum tree height settings were applied, to find the best-fit setting for detecting tree-top points. The possible window size functions were adopted from arbitrary function, presented by package developers (Plowright, 2020), and developed empirically from the ground survey data. Individually matching detected tree-top points with the actual trees on the ground was not performed in this research. The circular sample plots were the units for correlation analysis between ground and UAV data.

3.3.4 Delineating tree-crown boundaries from CHMs

As each tree-top point was detected, boundaries of individual trees were drawn using the ‘mcws’ function in the same package, ‘ForestTools’ (Plowright & Roussel, 2020). This function is generated from the *maker-controlled watershed* algorithm, which was originally developed to delineate drainage basins (Beucher & Meyer, 1993). It simulates flooding until the inserted threshold level and the filled water in basins segments features of each watershed. Depends on the set threshold levels, several basins are merged and segmented as a large watershed (Figure 3.11 B). To prevent this problem, *marker-controlled watershed* algorithm sets markers at the lowest point of each basin, and builds walls where water, from two basins, touches each other (Figure 3.11 A). CHM is similar with inverted profile of topography. The markers are not the lowest points in the basins, but the highest points on trees (tree-top points). Also, the walls are not built at the highest point of hills between basins, but at the lowest points between tree-crowns or at the edge of crowns (Plowright, 2020; Plowright & Roussel, 2020).

ลิขสิทธิ์ © โดย Chiang Mai University
All rights reserved

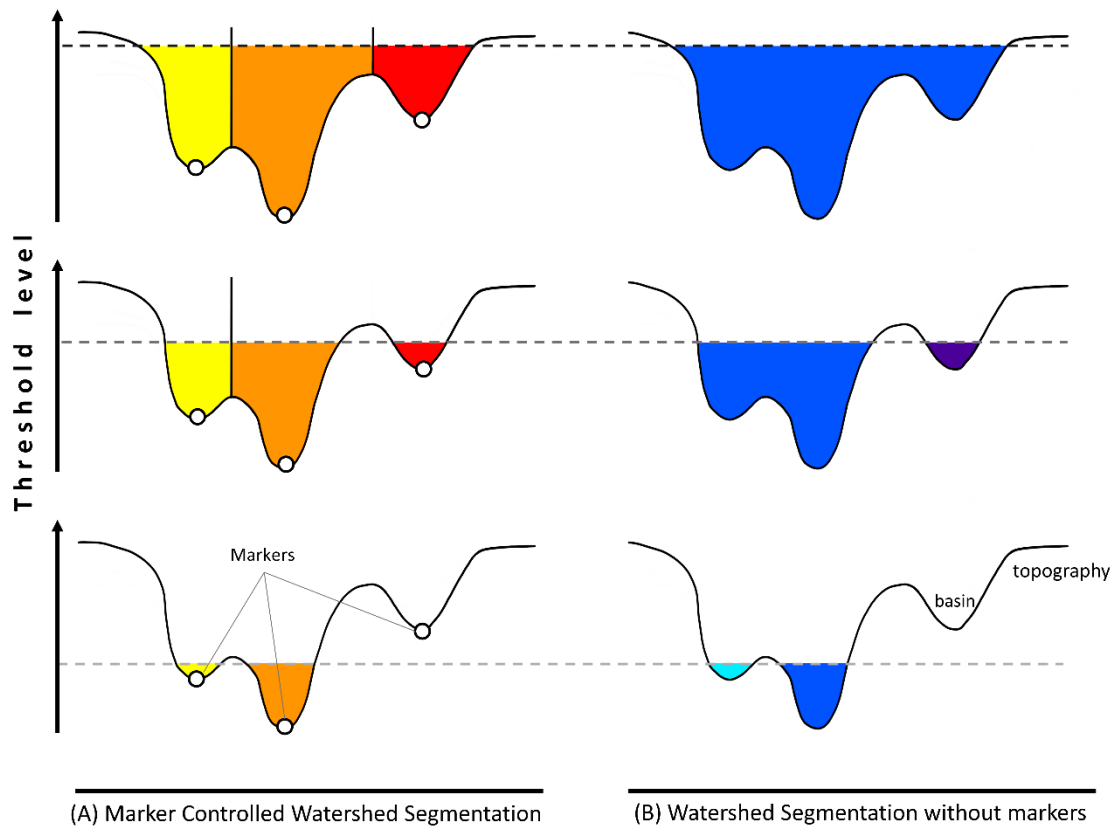


Figure 3.11 Principle of *marker-controlled watershed segmentation* (mews) algorithm, delineating crown boundaries (adopted from Fisher, 2013).

ลิขสิทธิ์มหาวิทยาลัยเชียงใหม่
 Copyright© by Chiang Mai University
 All rights reserved

3.4 Measuring variables from ground and UAV-derived data

3.4.1 Tree stocking-density

Tree-top points were counted in each circular plot and compared with the number of trees recorded in the ground surveys in each plot. Since tall trees obscured small trees when view from the air (but not in ground surveys) tree-top point counts were lower than ground tree counts, particularly for less degraded sites with high stocking-densities of larger trees. Therefore, per cent tree-canopy cover was also applied as an additional predictor variable in the multiple regression model. It was based on the assumption that higher per cent tree-canopy cover more obscures the view of UAV-camera to the small trees beneath larger trees.

3.4.2 Tree height

From the ground survey, the top 25 % of the highest trees in each plot, were compared with the height of tree-top points detected from CHM. Only top 25 % highest trees were compared because small trees, obscured by larger trees, were not detectable above the canopy. Descriptive statistic values were compared (e.g., max, mean, median).

3.4.3 Per cent canopy cover accounting for overlap

Tree-crown boundaries were detected from the CHM and the area of total canopy cover in each plot was converted to the per cent. On the ground, the crown projected area (CPA, m²) of individual trees were calculated with perpendicularly crossed two diameters of tree-crowns. In each plot, all the CPAs were summed and converted to a per cent of the plot. To deal with overestimated canopy cover, due to the overlapping crowns, an exponential equation was applied (Adesoye & Akinwunmi, 2016)

$$C' = 100 \left(\sum_{i=1}^n (CPA_i) \right) A^{-1} \quad (\text{eq 3.1})$$

$$C = 100[1 - \exp(-0.01C')] \quad (\text{eq 3.2})$$

Where,

C' is the per cent canopy cover without accounting for overlap,

CPA_i is crown projected area if individual trees (m²),

A is the given area of the site (m²).

C is the per cent canopy cover accounting for overlap.

3.4.4 Ratio of three elements of the ground

2D orthophoto images were processed to separate pixels of exposed soil + rock from weed and vegetative cover. Canopy cover consists of tree-crown boundaries, detected from the CHM, were overlaid on the orthophotos. Canopy cover were then removed, to prevent their being misclassified as ground vegetation. Height differences were used from the CHM, to completely separate tree-crowns and ground vegetation in advance. Remaining pixels were classified as exposed soil or weedy vegetation using the function 'color threshold' tool of Image-J to vary filters for pixel hue, saturation, and brightness (HSB). Finally, all the pixels were classified into tree-canopy, ground vegetation, and exposed soil + rock, the relative cover of three elements of the ground could be determined (Figure 3.12).

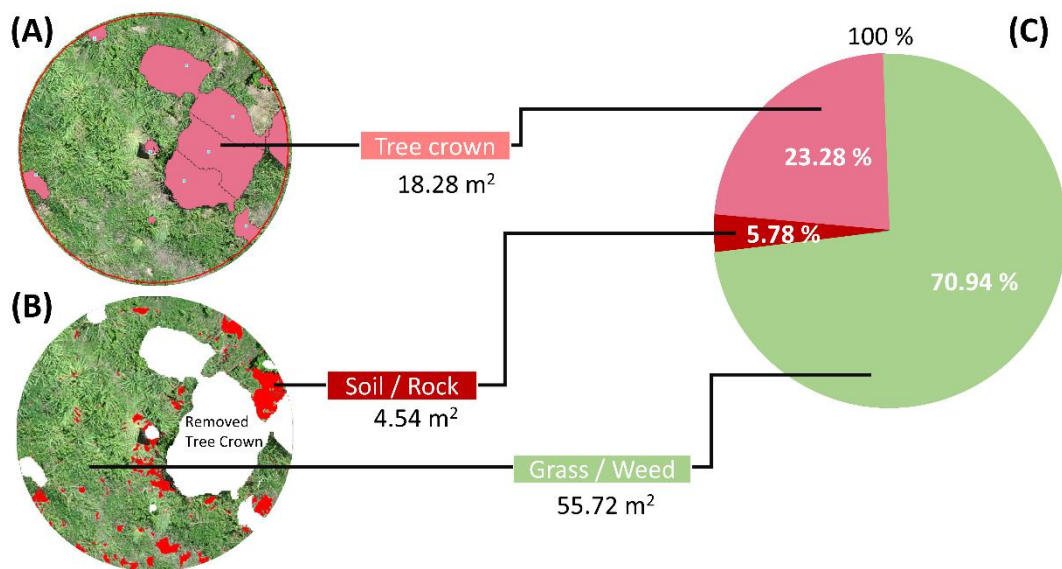


Figure 3.12 Example of separating three elements of the ground. (A) Canopy cover, merged tree-crown boundaries, delineated from CHM, (B) Canopy cover pre-removed orthophoto, exposed soil + rock detection using color threshold, (C) Per cent three ground elements

3.4.5 Aboveground Carbon Density (ACD)

ACD was estimated from CHM data using Jucker et al.'s, (2018) regional allometric model for Asian tropical forests (eq 3.3).

$$ACD(MgC/ha)_{Regional} = 0.567 \times TCH^{0.554} \times BA^{1.081} \times WD^{0.186} \quad (eq\ 3.3)$$

Where,

TCH is the mean top-of-canopy height (m),

WD is wood density = 0.52 g/cm², local average, studied by Pothong et al., (2021),

BA is stand basal area (m²/ha) = 1.112 × TCH , modeled by Jucker et al., (2018).

Corresponding ground-based ACD values were converted by following equations (eq 3.5, 3.6), where AGB was calculated using a regional AGB allometric model of northern Thailand (eq 3.4), recently developed by destructive sample analysis (Pothong et al., 2021). Trees whose GBH are larger than 15 cm, approximately DBH 5 cm, were applies for estimating AGB from ground measurement.

$$AGB(kg) = 0.134 \times (D^2 \cdot H \cdot WD)^{0.847} \quad (eq\ 3.4)$$

Where,

D is diameter at breast height of individual tree trunks,

H is height of individual trees,

WD is wood density = 0.52 g/cm², local average, studied by Pothong et al., (2021),

$$AGB(kg/ha) = AGB(kg/78.54m^2) \div 78.54m^2 \times 10,000m^2 \quad (eq\ 3.5)$$

$$ACD(MgC/ha) = AGB(kg/ha) \times \rho \div 1,000kg \quad (eq\ 3.6)$$

Where,

ρ is carbon content = 0.44, local average, studied by Pothong et al., (2021).

3.5 Forest-Degradation Index (FDI)

Not all the variables were incorporated into forest-degradation index (FDI). Variables were selected to be criteria into FDI by considering their correlation with ground-derived data, and their intercorrelations with each other. Methods for constructing the forest-degradation index were adopted from Modica et al., (2015); namely i) determining weight of each criterion, ii) data normalization, to offset the different sizes of units, and iii) data aggregation.

3.5.1 Selecting criteria to be integrated into the index

First of all, among the six UAV-derived variables, tested for correlation with ground survey results, only highly correlated variables were considered (correlation coefficient ≥ 0.70). Second, considered variables were screened for intercorrelation with each other, to prevent over-weighting certain characteristics in the overall degradation assessment. Strongly intercorrelated variables were eliminated according to the following principles: i) if two variables were negatively correlated, they were not considered as intercorrelated, because they affected degradation in different ways, ii) when we found one intercorrelated variable was used for estimating another one (e.g., as a variable into a regression model or an equation, etc.), the integrated one is taken into FDI. For example, if we find ACD and height are intercorrelated, we take ACD because height is used as TCH in the equation for calculating ACD. Selected variables are criteria to be integrated into the index.

3.5.2 Determining weight of each criterion using AHP method

As definitions of forest degradation are inconsistent, the main factors and the weighted importance of each factor differ among observers. Determining the weighting of each criterion is therefore somewhat subjective and should be done by combining the opinions of various likely users of a degradation index. Therefore, the weight of each criteria was determined by an Analytic Hierarchy Process (AHP): a method of multi-criteria decision analysis (MCDA). MCDA combines explicit and formal techniques to aid decision making using multiple criteria. (Figueira et al., 2005; Ananda & Herath, 2009; de Castro & Urios, 2016). AHP has been widely used to integrate different levels of importance and weights of criteria for forest management (Modica et al., 2015). The

process uses experts' judgement, in the form of pairwise comparisons, to gain relative preference or importance information, not only ordinal judgement, but also quantitative difference, among heterogenous criteria. Therefore it minimizes bias from decision makers. (Figueira et al., 2005; Modica et al., 2015; de Castro & Urios, 2016)

Experts in the field of forest ecology and restoration were asked to perform a pairwise comparison. They were asked to select which criterion, in each pair, they considered to be most sensitive to changes in degradation levels and then to score how much more important on a scale from 1 to 9 i.e., score 1 (both criteria are equal or cannot be decided), score 2 (selected criterion is slightly more important), score 9 (selected criterion is much more important). See evaluation form in Appendix A. The scored pairwise comparisons were expressed as matrices, namely pairwise comparison matrix (PCM), which is the positive reciprocal matrix. In other words, when a_{ij} refers the comparative importance of criterion i over criterion j , the comparative importance of criterion j over criterion i is $a_{ji} = 1/a_{ij}$.

$$PCM_{Expert\ 1} : \begin{bmatrix} a_{111} & a_{112} & \dots & a_{11j} \\ a_{121} & a_{122} & \dots & a_{12j} \\ \vdots & \dots & \ddots & \dots \\ a_{1i1} & a_{1i2} & \dots & a_{1ij} \end{bmatrix}, PCM_{Expert\ 2} : \begin{bmatrix} a_{211} & a_{212} & \dots & a_{21j} \\ a_{221} & a_{222} & \dots & a_{22j} \\ \vdots & \dots & \ddots & \dots \\ a_{2i1} & a_{2i2} & \dots & a_{2ij} \end{bmatrix},$$

$$\dots, PCM_{Expert\ k} : \begin{bmatrix} a_{k11} & a_{k12} & \dots & a_{k1j} \\ a_{k21} & a_{k22} & \dots & a_{k2j} \\ \vdots & \dots & \ddots & \dots \\ a_{ki1} & a_{ki2} & \dots & a_{kij} \end{bmatrix}$$

Where,

k is the number of experts evaluating of pairwise comparisons,

$i, j = 1, 2, 3, \dots, n$, and n is the number of criteria,

a_{kij} is the scored importance of criterion i compared to j , evaluated by expert k .

It is natural that PCMs, evaluated by humans, may be inconsistent ordinally (i.e., if A is more important than B, and B is more important than C, totally consistent evaluation must imply A is more important than C) and cardinally (i.e., if A is two times more important than B, and B is three times more than C, the totally consistent evaluation must imply A is six times more important than C) (R. W. Saaty, 1987; T. L. Saaty, 2003). AHP deals with acceptable inconsistency, by checking for consistency level (eq 3.7, 3.8).

$$CI = \frac{\lambda_{max} - n}{n - 1} \quad (\text{eq 3.7})$$

$$CR = \frac{CI}{RI} \quad (\text{eq 3.8})$$

Where,

CI is the consistency index,

λ_{max} is the principal eigenvalue (perron vector) of the given $PCM_{expert k}$,

CR is the consistency ratio,

RI is the random consistency index determined by the number of criteria.

$PCM_{expert k}$, whose CR is less than 0.1 (10 %), were considered acceptable and were included in PCM_{total} . The geometric mean of each pairwise comparison of total PCM_{total} was calculated by eq 3.9. (T. L. Saaty & Shang, 2011)

$$PCM_{total} = \begin{bmatrix} a_{11} & a_{12} & \dots & a_{1j} \\ a_{21} & a_{22} & \dots & a_{2j} \\ \vdots & \dots & \ddots & \dots \\ a_{i1} & a_{i2} & \dots & a_{ij} \end{bmatrix}$$

$$a_{ij} = (a_{1ij} \times a_{2ij} \times \dots \times a_{kij})^{\frac{1}{k}} \quad (\text{eq 3.9})$$

Where,

a_{ij} is the geometric mean of the scored importance of criterion i compared to j from all experts (1, 2, ..., k)

k is the number of experts evaluating of pairwise comparisons,

$i, j = 1, 2, 3, \dots, n$, and n is the number of criteria,

a_{kij} is the scored importance of criterion i compared to j , evaluated by expert k .

Weights of criteria were derived by the eigenvector method (R. W. Saaty, 1987), specifically represented with principal eigenvector, satisfying $Aw = \lambda_{max}w$. (Modica et al., 2015; T. L. Saaty, 2003). Where A refers PCM_{total} ; w is the local priority vector, represented with principal eigenvector, implementing the weight of each criterion ($w = w_1, w_2, \dots, w_n$); λ_{max} is the principal eigenvalue (perron vector) of PCM_{total} (Goepel, 2018).

3.5.3 Data normalization and data aggregation

Before computing all measured criteria with determined weight applied, the data were normalized (eq 3.10). This was because multiple criteria had different sizes of measured values, ranges, and units. Without normalization, any criterion represented by big numbers would add bias to the results. After normalization, the criteria were all converted into ranges of 0 to 1.

$$S' = \frac{s - \min\{s_n\}}{\max\{s_n\} - \min\{s_n\}} \quad (\text{eq 3.10})$$

Where,

S' is the normalized score,

s is the measured score,

$\max\{s_n\}, \min\{s_n\}$ are the maximum and minimum score of the n_{th} criterion in the overall range.

The calculated weightings were then applied to the normalized criteria, and the results were aggregated into the forest-degradation index, using weighted linear combination (WLC) (eq 3.11).

$$FDI = 10 \sum_{i=1}^n w_i \cdot s'_i \quad (\text{eq 3.11})$$

Where,

FDI is Forest-Degradation Index of the given site,

i is the each of criteria applied into the FDI ,

w_i is the determined weight of the i_{th} criterion,

s'_i is the normalized score of the i_{th} criterion.

CHAPTER 4

Results and Discussion

4.1 Forest-degradation assessment by ground survey in study sites

Table 4.1 describes selected sites based on the ground survey data. It shows characteristic of each study site, comparison among sites, and wideness of a degradation and/or restoration raga in five study sites.

Table 4.1 Ground survey results of five selected sites

Site (Years after restoration)	Survey Date YY-MM-DD	No. of Sample plots	Mean no. of trees per circle, 78.51 m ² (Height >= 1.0 m)	Tree stocking- density (no.)		% Canopy Cover	% Ground Vegetation	% Exposed Soil + Rock	Stage
				ha ⁻¹	rai ^{1*}				
BMSM (8Y)	20-11-02	10	29.9 ^a	3,833.3 ^a	613.3 ^a	86.50 ^a	3.88 ^c	9.62 ^b	Stage 1
ML (6Y)	20-09-04	10	22.5 ^a	2,884.6 ^a	461.5 ^a	74.78 ^a	22.66 ^{bc}	2.56 ^b	Stage 3
BPK (4Y)	20-07-03	10	10.3 ^b	1,320.5 ^b	211.3 ^b	67.66 ^a	32.11 ^b	0.23 ^b	Stage 3
BMM (0Y)	20-06-13	8	4.5 ^b	576.9 ^b	92.3 ^b	4.97 ^b	91.21 ^a	3.82 ^b	Stage 3
LP (1Y)	20-09-25	8	1.4 ^b	176.3 ^b	28.2 ^b	5.51 ^b	69.48 ^a	25.01 ^a	Stage 5

Note: *6.25 rai = 1 ha, ^{a-c} within each column, comparing sites, means without a common superscript significantly differ ($P < 0.05$).

Generally, both tree stocking-density and per cent canopy cover increased with plot age, but LP site was ranked as more degraded, compared with the BMM site despite order plot age. Differences in per cent canopy cover between the BMM and LP sites were insignificant, but significantly higher per cent exposed soil + rock in the LP site led it as more degraded site.

According to FORRU-CMU's system of five forest-degradation stages (Elliott et al., 2013), LP was categorized as Stage-5, because poor soil conditions limited herbaceous weed growth, whilst BMM was classified as Stage-3 degradation, because ground vegetation cover (92.21 %) was larger than canopy cover (4.97 %). LP was a bench terrace in a limestone-quarry, ameliorated with loosened substrate and planted with saplings in 2019. BMM was an abandoned agricultural site, planted with saplings of framework tree species in 2020, dominated by grasses and bamboos, with sparse tall trees and shrubs, i.e., better preliminary conditions than at the LP site.

BMSM was the only site where tree stocking-density exceeded 3,100 trees/ha, which is the tipping point between Stage-2 and Stage-3 degradation. Moreover, per cent canopy cover at the BMSM site was sufficiently high to effectively exclude herbaceous weeds, so that site was categorized as Stage-1 degradation. In contrast, tree stocking-densities on the ML and BPK sites were less than 3,100 trees/ha, and herbaceous weed growth was sufficient to inhibit performance of tree seedlings and saplings in large gaps. However, because the soil remained intact and potential seed sources of forest trees remained nearby, they were categorized as Stage-3 degradation and were undergoing restoration by the framework species method.

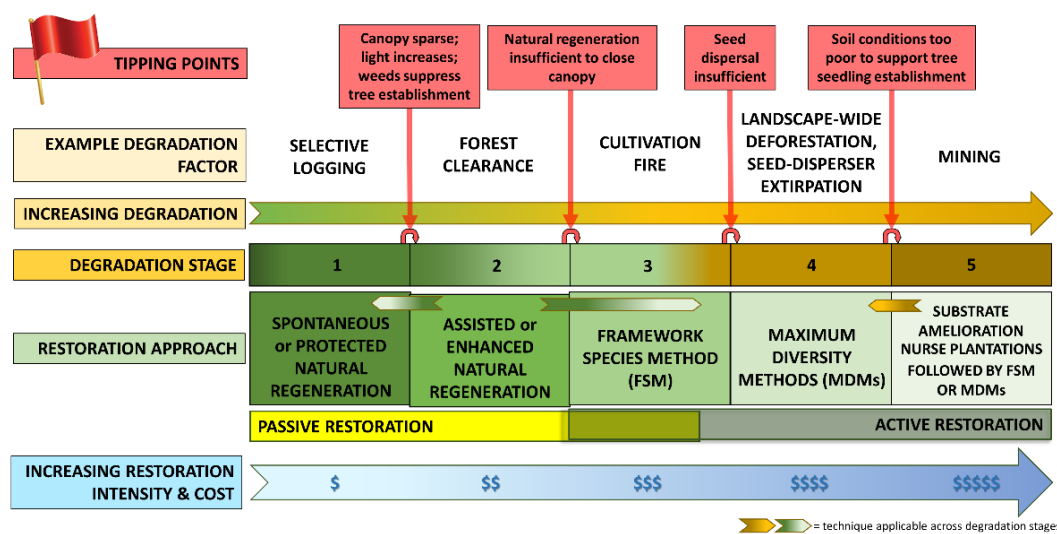


Figure 4.1 Tipping points in degradation levels determining different forest-restoration strategies (adopted with permission from Stephen Elliott)

The five selected study sites exhibited degradation stages 1, 3 and 5 (Figure 4.1). Despite missing degradation stages 2 and 4, the sites captured degradation intensity over a wide range, from Stage-1 to Stage-5 with medium degradation (Stage-3) represented at 3 sublevels, differing markedly in per cent cover of the three quantified ground elements and tree stocking-density. The range of degradation levels was considered to be wide enough for development of a forest-degradation index. Furthermore, the variation among the three Stage-3 sites emphasized the need for a more quantifiable forest-degradation index with higher acuity than that achieved by FORRU-CMU's qualitative degradation classification system (Elliott et al., 2013).

4.2 UAV flight and image processing

4.2.1 Collected images by UAV flight

Table 4.2 UAV flight records, weather conditions and flight-mission settings when capturing aerial RGB images (50 m above ground)

Site	Flight Date YY-MM-DD	Flight Time	Weather Condition	Plot locations referencing	No. of pictures	Flight mission setting		
						Overlap (%)	Average Distance Between Flight Grid Lines	UAV Speed
BMSM	20-11-04	11:37 - 11:51	Heavy clouds under strong sunlight, strong windy (c. 9.6 km/h).	Ground marker + Stadia method	283	75 %	19.0 m	12 km/h
ML	20-11-09	10:13 - 10:32	Moderate cloudy, weak wind.	Ground marker + Stadia method	335	76 %	18.2 m	12 km/h
BPK	20-10-24	15:48 - 16:10	Sunny with low solar altitude, weak wind.	Ground marker + Stadia method	335	75 %	19.0 m	13 km/h
BMM	20-06-13	11:38 - 11:51	Sunny with high solar altitude, weak wind	Ground marker	205	80 %	15.2 m	10 km/h
LP	20-09-26	13:07 - 13:21	Sunny with high solar altitude, weak wind	Ground marker	228	80 %	15.2 m	10 km/h

4.2.2 Processed DEMs and orthophotos



Figure 4.2 Orthophotos from five sites in unified scale. Comparisons with DEMs (i.e., DSM, DTM, and CHM) are presented in Appendix B.

4.2.3 Accuracy of positioning circular plots using stadia method

Application of the stadia method, using a theodolite, was necessary at three sites, i.e., BMSM, ML, and BPK, where ground markers were sometimes obscured beneath tall tree-crowns. All of 10 ground markers in BMSM were not detectable on UAV-derived images, but 11 plots out of 20 plots from ML and BPK were visible in the RGB images and in the orthophotos. Therefore, these were applied to achieve accuracy of the stadia method compared with GPS coordinates. (Figure 4.3).



Figure 4.3 Examples of stadia method and comparisons with GPS detected points in orthophoto of BPK site. (Left) Plot point was visible on UAV-derived image (actual plot point; red square) and estimated using stadia method (red point) from visible subpoint (pink square). Two points were closer than the distance between GPS detection (grey triangle) and actual plot point. (Right) ground marker was not visible, and plot point was estimated using stadia method. Results of stadia method at the three sites, where it was necessary, are presented in Appendix C.

High accuracy in matching UAV-derived images with the ground circular sample plots was achieved by using the stadia method, compared with GPS receiver (Figure 4.3 and Table 4.3).

Table 4.3 Distance to reference (visible) center point of 11 plots (in meters)

Distance to reference	Methods	
	GPS coordinates	Stadia Method
Mean \pm SD	3.71 \pm 1.45	0.79 \pm 0.77
Min	2.00	0.11
Max	6.28	2.83



ลิขสิทธิ์มหาวิทยาลัยเชียงใหม่
Copyright© by Chiang Mai University
All rights reserved

4.3 Tree-top points detected by *variable window filter* algorithm

4.3.1 Variable window-size functions

1) Arbitrary window-size function presented by package developers

In the R package ‘ForestTools’, the developers presented an arbitrary function (Plowright, 2020).

$$r_s = 0.05 \cdot h + 0.6$$

2) Empirically developed window-size functions

From the ground-measured data of individual trees ($n = 393$), the relationship between tree height (m), and average tree-crown radius (m) (from the two crossed diameters, measured perpendicularly) was developed into functions based on various regression models (Figure 4.4) as follows:

Simple linear: $r_d = 0.213287 \cdot h + 0.324948$, ($R^2 = 0.6001$)

Quadratic linear: $r_e = 0.001009 \cdot h^2 + 0.196022 \cdot h + 0.380694$, ($R^2 = 0.6004$)

Logarithmic: $r_l = 1.26080 \cdot \log(h) - 0.45780$, ($R^2 = 0.5282$)

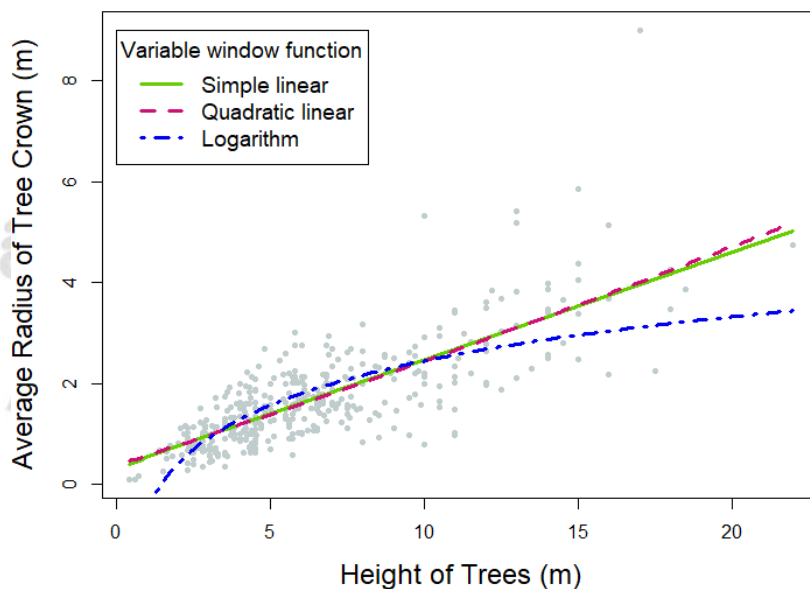


Figure 4.4 Empirically developed window-size functions

4.3.2 The best setting of the various functions and minimum tree heights

All the equations, except one (logarithm model), showed that setting minimum tree-top point height to 1.0 m resulted in a more accurate tree count (compared with ground survey data) than when it was set to 1.5 m (Figure 4.5).

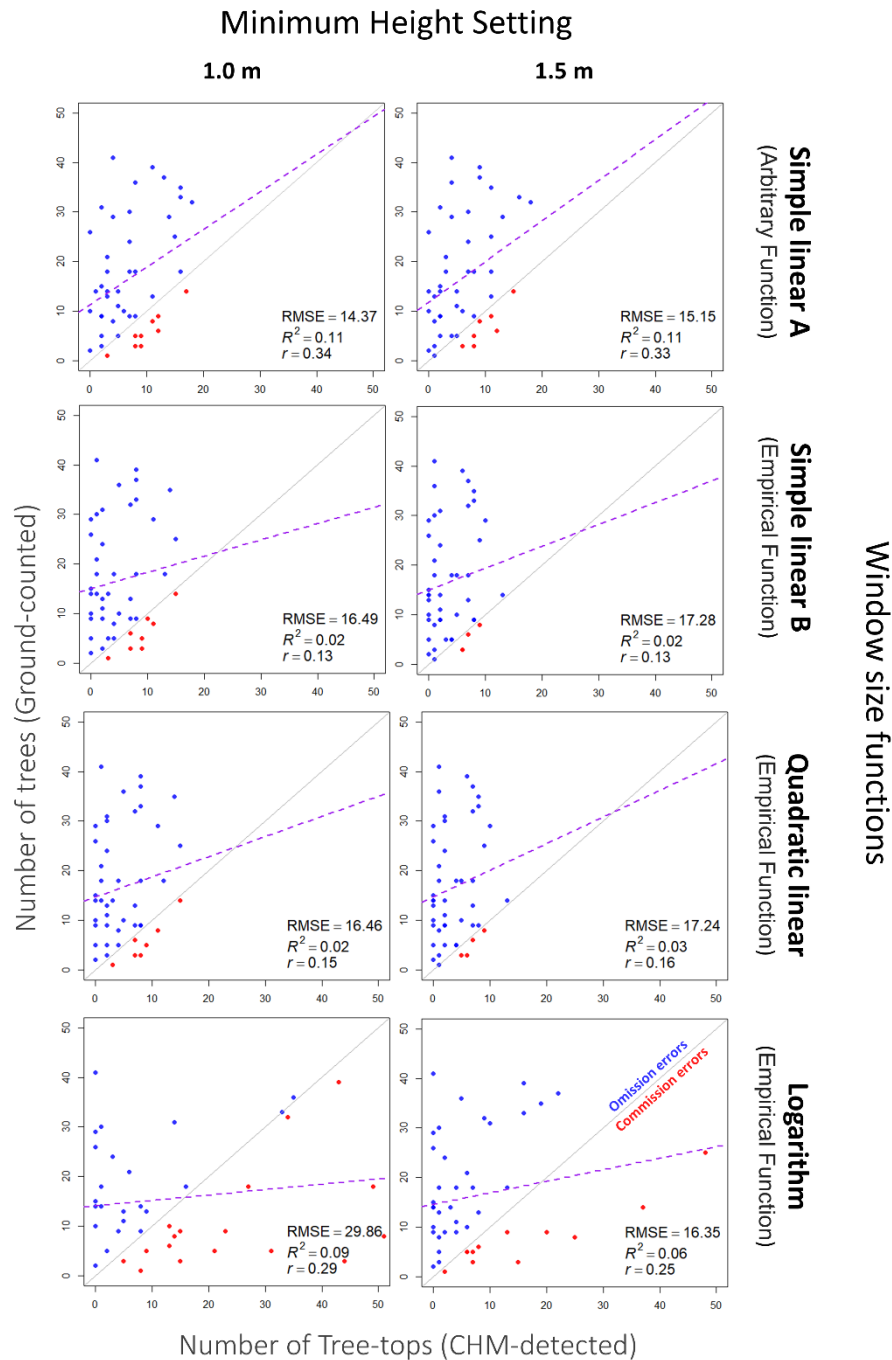


Figure 4.5 Comparison of settings, for detecting tree-top points by *variable window filter* algorithm, with different window-size functions and minimum tree heights

The empirically developed logarithm model resulted in a different pattern compared with the other linear models (greater scattering, comparing number of trees), particularly with the 1.0 m min-height setting, so RMSE was exceptionally high (29.86) compared with all other settings. The distribution of commission and omission errors also differed. Unlike other linear models, which resulted in more errors of omission (underestimating tree numbers) than of commission, the logarithmic model, detected similar numbers of omission and commission errors. The other two empirical functions: simple linear B, and quadratic linear, had similar RMSE, R^2 and correlation coefficients.

In contrast, the simple linear A model (arbitrary function introduced by (Plowright, 2020). resulted in the lowest RMSE, and highest R^2 and correlation coefficient. Consequently, the simple linear A model was used to generate the window-size function for tree-top point detection in the CHM, and the minimum height of tree-top points was set to 1.0 m.

4.4 Tree-crown boundaries detected by *watershed* algorithm

4.4.1 The best setting of minimum crown-boundary height

Since the setting for detecting tree-top points was selected using the simple linear A model, the detected tree-top points were used as markers in watershed algorithms to detect tree-crown boundaries. Figures 4.6 & 4.7 present the effect of minimum tree-crown boundary height on detection of canopy cover.

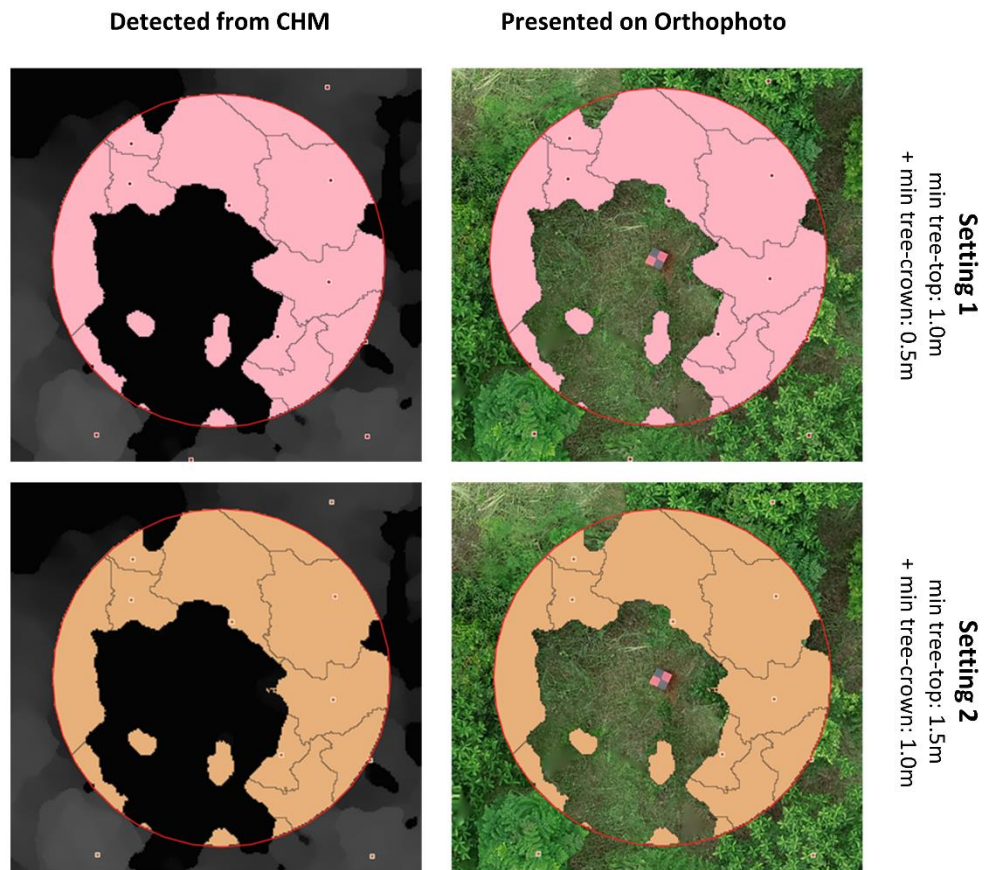


Figure 4.6 Example result of detected tree-crown boundaries comprising canopy cover, with different minimum crown boundary heights (0.5 m, and 1.0 m from top to down)

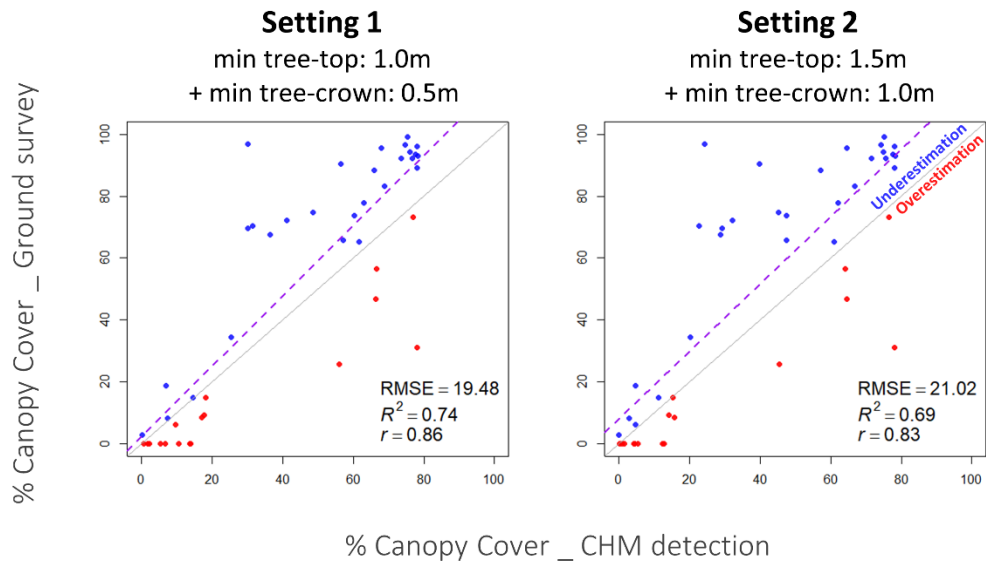


Figure 4.7 Comparison of setting, for delineating tree-crown boundaries by *watershed* algorithm, with different minimum crown boundary heights

The per cent canopy cover was highly correlated in both settings (Setting 1: $R^2 = 0.74$, and $r = 0.85$, Setting 2: $R^2 = 0.69$, $r = 0.83$) (Figure 4.7), but as the Setting1 was more correlated with smaller RMSE (19 %), it was selected for the analysis.

4.5 Correlation between the variables from ground and UAV surveys

4.5.1 Tree stocking-density

Tree stocking-density, recorded during ground surveys, was correlated weakly with the number of tree-top points, detected on the CHM ($R^2 = 0.12$, $r = 0.35$) (Figure 4.8 Left). Consequently, actual tree stocking-density could not be determined accurately from UAV-derived data. This was because small trees, obscured by tall tree-crowns, were counted in the ground survey, but not detected from above. Thus, an additional predictor variable, i.e., per cent canopy cover in each sample plot, was applied using a multiple regression model. Predictor variables in a multiple regression model, should not be strongly inter-correlated and should be correlated with the dependent variable. As two the predictor variables (i.e., tree stocking-density and per cent canopy cover from the CHM) and one dependent variable (i.e., tree stocking-density from ground-survey) satisfy this condition, tree stocking-density was estimated, by a multiple regression model, from the two variables derived from the CHM. Adjusted tree stocking-density, from the CHM, was highly correlated ($R^2 = 0.71$, $r = 0.84$) with the tree stocking-density recorded during ground surveys. And the root mean square error (RMSE) was 493 trees per hectare, which is about 4 trees per plot (5 m-radius circular plot) (Figure 4.8 Right).

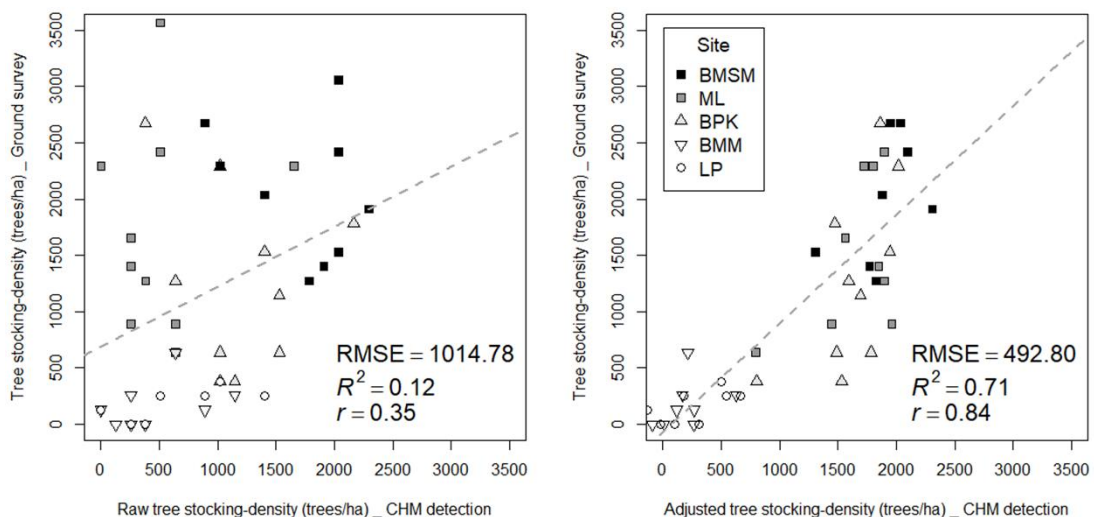


Figure 4.8 Scatter plots of tree stocking-density. (Left) Tree stocking-density from CHM, (Right) adjusted tree stocking-density from multiple regression model derived from tree stocking-density and per cent canopy cover both from the CHM.

4.5.2 Tree height

Tree height variables, derived from the CHM, were weakly correlated with the same measured in ground surveys (max, mean and median tree height in each circular sample plot) (Figure 4.9). Highest correlation between UAV-derived and ground data was achieved for max tree height ($R^2 = 0.51$, $r = 0.71$). However, tallest tree per plot is a poor representation of overall tree height, since tallest trees are outliers. Therefore, their use is likely to overestimate tree height at the site level. Mean tree height reduced the influence of outliers, despite weak correlation ($r = 0.56$) and low R^2 (0.31), and was a better measure than median height ($R^2 = 0.23$, $r = 0.48$). Furthermore, RMSE of mean height was lower (3.3 m) than for maximum (4.1 m) and median height (3.5 m).

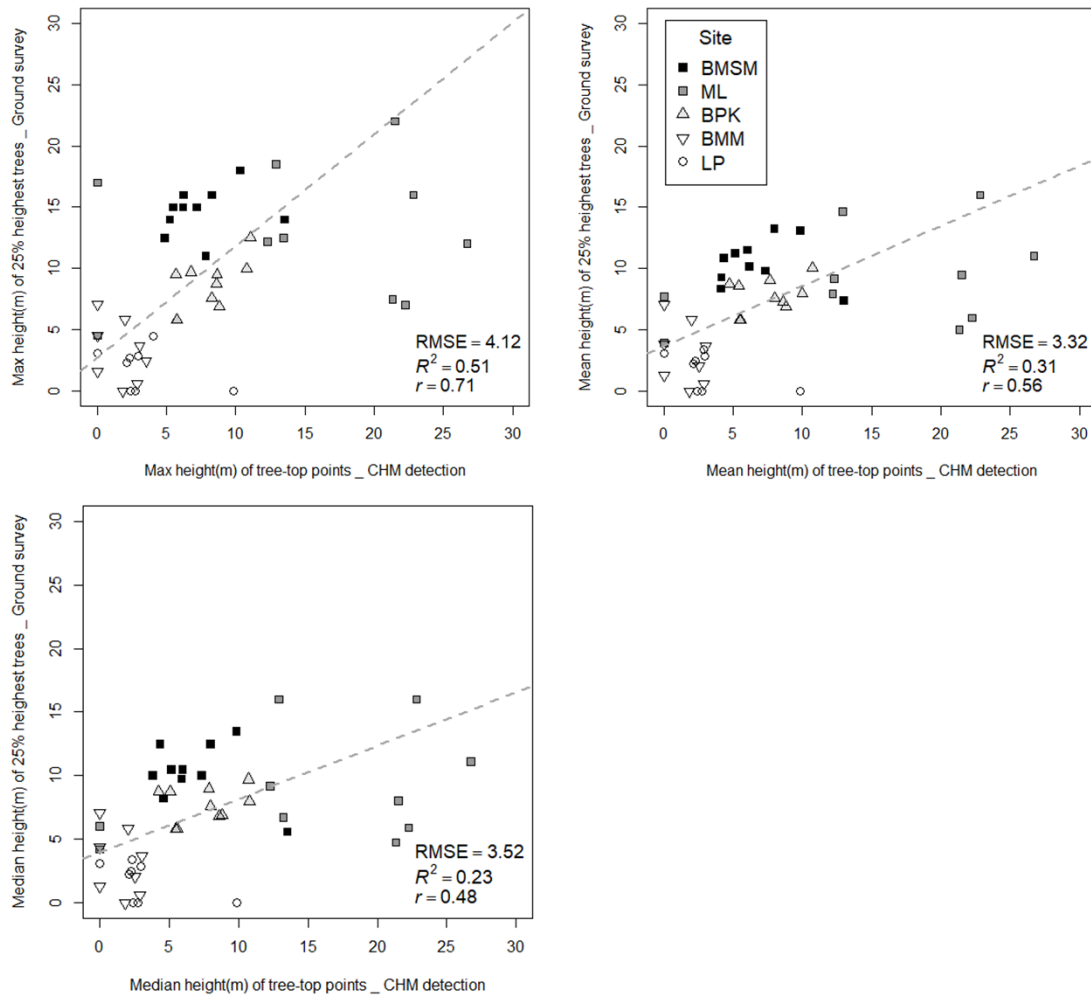


Figure 4.9 Scatter plots of tree height descriptive statistic values. (Left) Max height, (Right) mean height, (lower) median height.

4.5.3 Per cent canopy cover, ground vegetation, and exposed soil + rock

Relative cover of the three ground-cover elements (canopy cover, ground vegetation, and exposed soil + rock), detected from UAV-derived data, were all highly correlated with ground-survey data. Per cent canopy cover was the most highly correlated ($R^2 = 0.82$, $r = 0.91$), followed by ground vegetation ($R^2 = 0.71$, $r = 0.84$) and exposed soil + rock ($R^2 = 0.56$, $r = 0.75$) (Figure 4.10).

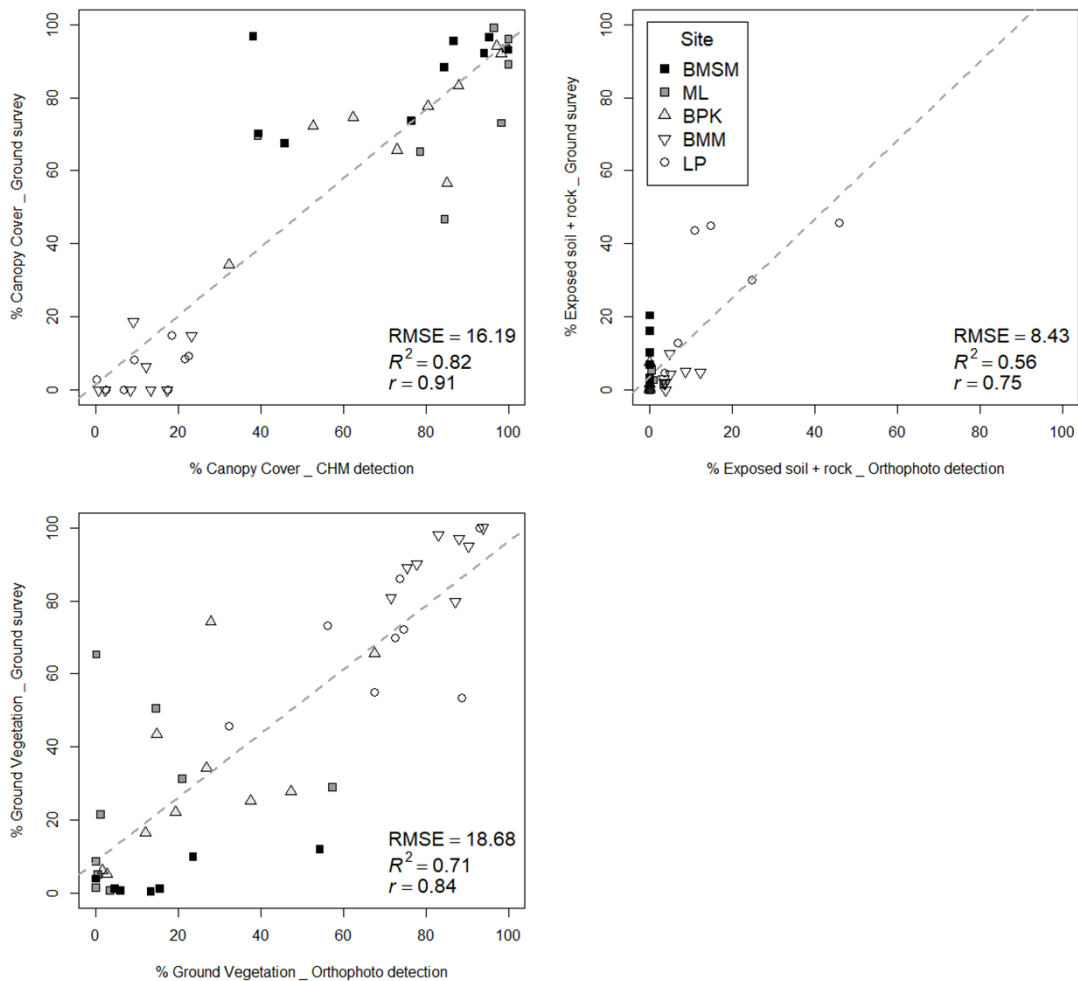


Figure 4.10 Scatter plots of per cent of three ground-elements. (Left) per cent canopy cover, (Right) per cent ground vegetation, (Lower) per cent exposed soil + rock.

4.5.4 Aboveground Carbon Density (ACD)

CHM-derived ACD was not correlated with ACD calculated from ground survey data ($R^2 = 0.24$, $r = 0.49$) (Figure 4.11 Left). Adding another predictor variable, tree stocking-density, to create a multiple linear regression model, increased the correlation ($R^2 = 0.45$, $r = 0.67$) and reduced RMSE (8.86 MgC/ha) (Figure 4.11 Right). However, overestimation was evident for the more degraded sites, e.g., LP and BMM.

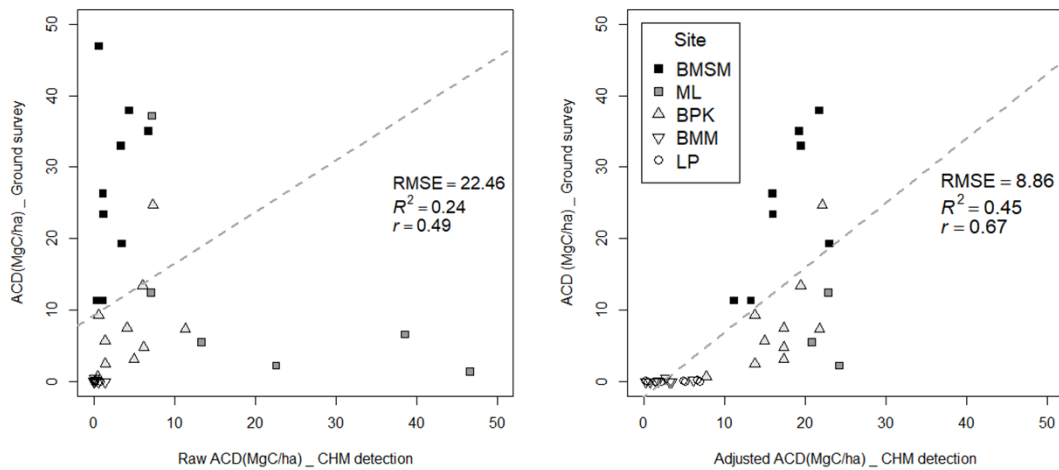


Figure 4.11 Scatter plots of ACD. (Left) ACD from CHM, (Right) Adjusted ACD from multiple regression model with ACD and tree stocking-density from CHM.

4.6 Estimated measurements of overall sites

Figure 4.12 presents comparisons of tree stocking-density estimates, based on data from the circular sample plots and from UAV imagery across each entire plot (all standardized to number of trees per hectare).

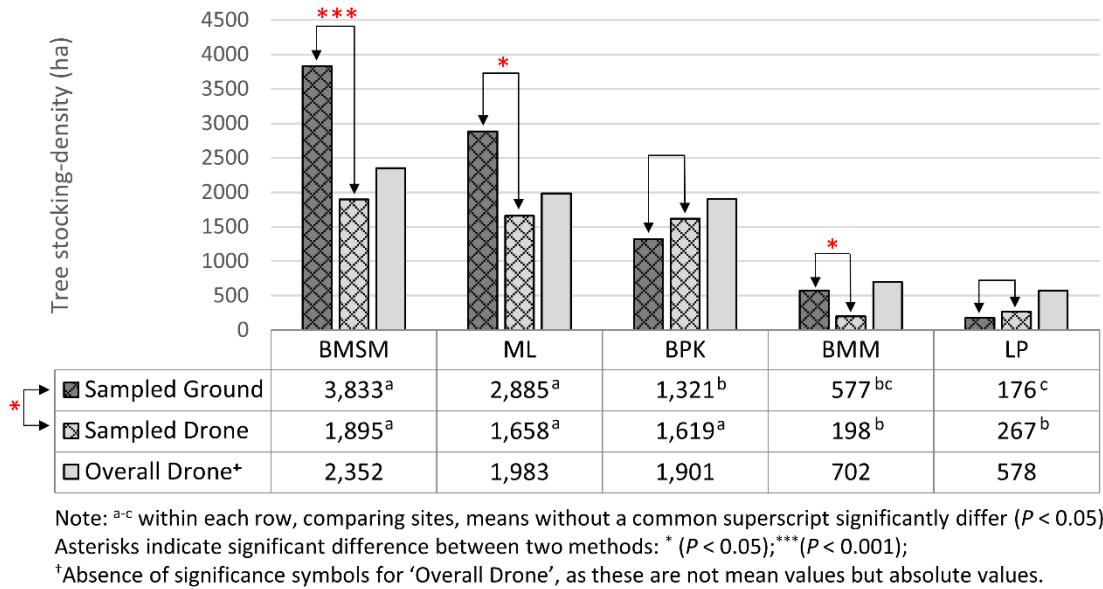
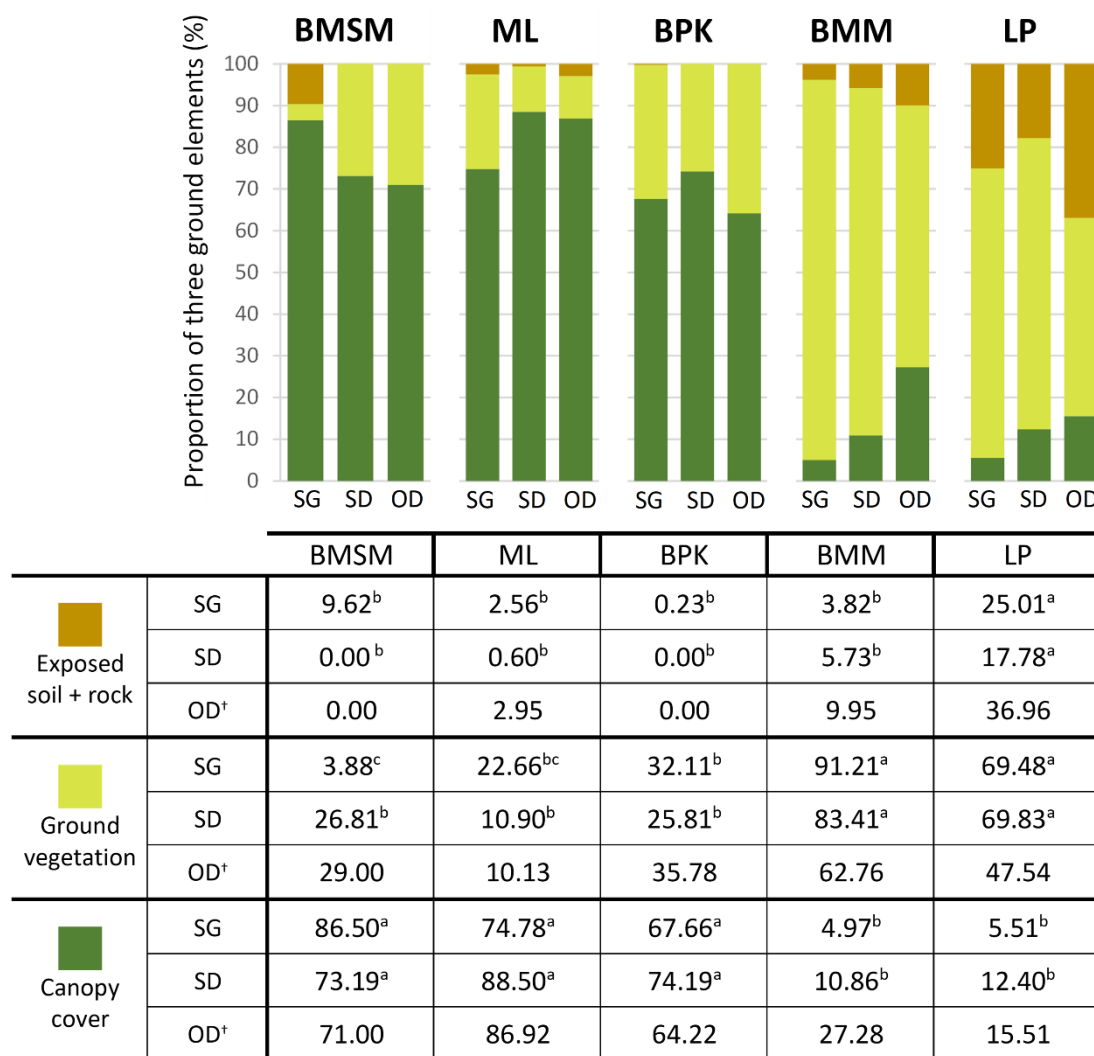


Figure 4.12 Mean stocking-density estimates from sample plots: i) sampled ground survey (dark grey with pattern), ii) sampled UAV survey (light grey with pattern), and iii) overall-detected UAV survey (each whole site, light grey with no pattern). Stocking-density from UAV surveys were estimated by multiple regression model.

In the least degraded sites (BMSM and ML), where stocking-densities were high, UAV surveys substantially underestimated stocking-density (by 50.6 % and 42.5 % respectively for the sample-based estimates compared to the sampled ground survey). This was because the crowns of tall trees obscured those of small trees, when viewed from above. Even use of the multiple regression model, which combined tree-top points with canopy cover, was not enough to estimate the number of hidden trees.

In contrast, in the BPK site, use of UAV imagery for sample plots over-estimated stocking-density (22.6 %), probably because fewer small trees were recorded in ground surveys at this site (see Figure 4.14), whilst dense canopy cover (74.9 % Figure 4.13), in the multiple regression model, contributed to a prediction of higher stocking.

Similarly, tree stocking-density was overestimated in LP site—the limestone quarry planted with trees one year previously. Canopy cover was not high enough (12.40 %) to obscure many smaller trees, but allowed estimation of hidden trees by the model. The histogram (Figure 4.14) shows about 90 % of trees were in the smallest size bin (1 ~ 3 m), and very few trees were in the second smallest size class (3 ~ 5 m)—not enough to obscure small trees.



Note: where, SG: Sampled ground survey; SD: Sampled Drone survey; OD: Overall Drone survey;

^{a-c} within each row, comparing sites, means without a common superscript significantly differ ($P < 0.05$);

[†]Absence of significance symbols for 'Overall Drone (OD)', as these are not mean values but absolute values.

Figure 4.13 Per cent three ground elements, averaged from sample plots: i) sampled ground survey, ii) sampled UAV survey, and iii) overall-detected UAV survey (each whole site).

In contrast, at the BMM site, even though large trees were not dominant, the CHM underestimated numbers of trees (by 65.69 %). This may have been due to dense cover of tall weeds (83.41 %—highest weed cover among the five sites). Many of the small trees, found beneath the weeds in the ground survey, were not detected in the CHM. Seventy-nine per cent of trees were in the smallest size class (1-3 m) (Figure 4.14). Another issue at BMM was that tree stocking-density and per cent canopy cover were substantially underestimated from sampled drone survey (SD), extrapolated from the sample circular plots, compared with results from overall drone (OD), collected across the entire site, by 71.79 and 60.19 % respectively. This may have been due to non-representativeness of the randomly positioned sample plots, which excluded most of the few very large trees that were present on the study site. Such trees, of course were included in the overall site survey by UAV.



ลิขสิทธิ์มหาวิทยาลัยเชียงใหม่
Copyright© by Chiang Mai University
All rights reserved

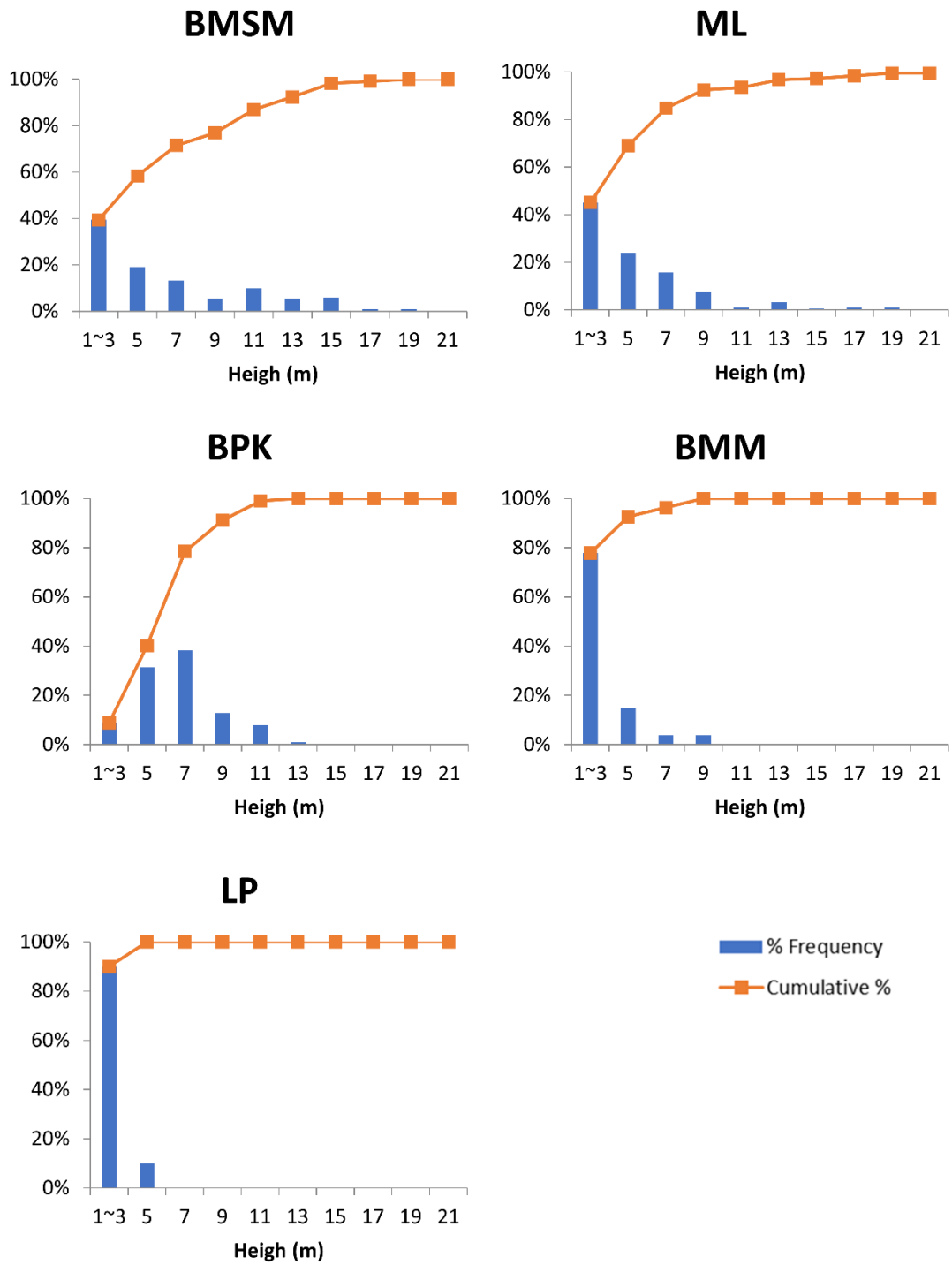


Figure 4.14 Per cent frequency of tree size class from ground surveys in sample plots for each site

4.7 Forest-Degradation Index (FDI)

4.7.1 Selected criteria to be integrated into the index

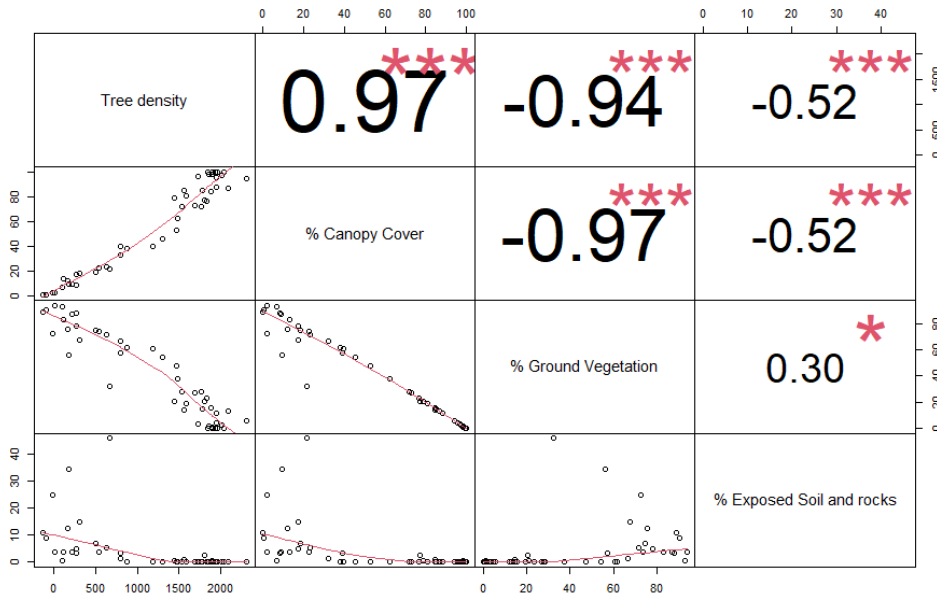
Of the six variables examined, only four were highly correlated between ground surveys and UAV imagery (over sample plots) ($r \geq 0.70$, Table 4.4). Consequently, tree stocking-density, per cent canopy cover, per cent ground vegetative and per cent exposed soil + rock were initially considered for inclusion in the FDI.

Table 4.4 R-Squared and correlation coefficients with reference (ground surveyed data), highly correlated coefficients are in bold

Variables	R squared	Correlation coefficient (r)
Tree stocking-density	0.71	0.84
% Canopy cover	0.82	0.91
Mean of height	0.31	0.56
% Ground vegetative	0.71	0.84
% Exposed soil + rock	0.56	0.75
Aboveground carbon density (ACD)	0.45	0.67

The four remaining variables were then examined for intercorrelation, to prevent over-weighting of related factors in the overall FDI. Each of the 4 variables was correlated with the other 3 (Figure 4.15). High correlation was found for three pairs of the pairwise correlations, i.e., tree stocking-density and per cent canopy cover ($r = 0.97$); tree stocking-density and per cent ground vegetation ($r = -0.94$); and per cent canopy cover and per cent ground vegetation ($r = -0.97$). Per cent canopy cover was screened out, because it was already used as a predictor variable for estimating tree stocking-density in the multiple regression model. However, per cent ground vegetation was not screened out, because it was negatively correlated with the other variables.

Consequently, three variables were selected as criteria for inclusion in the FDI: tree stocking-density, per cent ground vegetation, and per cent exposed soil + rock.



Note: Numbers are correlation coefficients. Size of fonts is directly proportional with level of correlations. Asterisks indicate significant difference between two methods: * ($P < 0.05$); *** ($P < 0.001$).

Figure 4.15 Intercorrelations among the four variables that were closely correlated between UAV and ground surveys

4.7.2 Weighting each criterion using the AHP method

Nine experts (in the field of forest ecology and restoration) performed pairwise comparison among the criteria, generating 9 pairwise matrices (PCMs). Of these only 4 responses achieved acceptable consistency ratios (CR) of lower than 0.1 (10 %). Geometric means within the 4 acceptable PCMs were then determined (PCM_{total}). From this matrix, the comparative weights of each criterion (w_1, w_2, w_3) were calculated, whose sum is equal to 1.

$$PCM_{total} = \begin{bmatrix} a_{11} & a_{12} & a_{13} \\ a_{21} & a_{22} & a_{23} \\ a_{31} & a_{32} & a_{33} \end{bmatrix} = \begin{bmatrix} 1 & 0.144 & 0.170 \\ 6.964 & 1 & 1.189 \\ 5.886 & 0.841 & 1 \end{bmatrix}$$

$$w_1 = 0.072, \quad w_2 = 0.504, \quad w_3 = 0.424$$

Where,

Criterion 1: tree stocking-density,

Criterion 2: per cent ground vegetation,

Criterion 3: per cent exposed soil + rock.

4.7.3 Data normalization and resultant FDI

Table 4.5 Data min-max normalization

Selected Three Criteria		1	2	3
		Tree stocking-density per hectare (TD)	Per cent Ground Vegetation (VEG)	Per cent Exposed Soil + Rock (SOIL)
weight (w_i)		0.072	0.504	0.424
Max degraded		577.62	62.76	36.96
Min degraded		2352.14	10.13	0.00
SITE	BMSM	2352.14 (0.00)	29.00 (0.36)	0.00 (0.00)
	ML	1982.95 (0.21)	10.13 (0.00)	2.95 (0.08)
	BPK	1901.05 (0.25)	35.78 (0.49)	0.00 (0.00)
	BMM	701.67 (0.93)	62.76 (1.00)	9.95 (0.27)
	LP	577.62 (1.00)	47.54 (0.71)	36.96 (1.00)

Note: Numbers are the measured value of each criterion in each site, and numbers in brackets are normalized scores. Numbers rounded to up or down nearest 0.01.

Minimum and maximum scores of each criterion were determined (Table 4.5), based on the scores from the sites at various stages of degradation and were used for normalizing the measured scores (Table 4.5). The normalized scores were aggregated into the FDI by weighted linear combination (WLC), resulting in equation 4.1.

$$\begin{aligned}
 FDI &= 10 \times \left\{ \begin{aligned} &\left(\frac{TD - 2,352.14}{577.62 - 2,352.14} \right) \times 0.072 \\ &+ \left(\frac{VEG - 10.13}{62.76 - 10.13} \right) \times 0.504 \\ &+ \left(\frac{SOIL - 0.00}{36.96 - 0.00} \right) \times 0.424 \end{aligned} \right\} \\
 &\rightarrow 10 \times \left\{ \begin{aligned} &- (TD - 2,352.14) \times 0.000041 \\ &+ (VEG - 10.13) \times 0.009568 \\ &+ (SOIL - 0.00) \times 0.011478 \end{aligned} \right\} \\
 &\rightarrow 10 \times (-0.000041 \cdot TD + 0.009568 \cdot VEG + 0.011478 \cdot SOIL - 0.001206) \\
 \therefore FDI &= -0.00041 \cdot TD + 0.09568 \cdot VEG + 0.11478 \cdot SOIL + 0.01206 \quad (\text{eq 4.1})
 \end{aligned}$$

Finally, the FDI of each site was computed in Table 4.6 and compared with the originally assigned degradation stage of each site (Stage 1-5). The FDI scale (0-10) was divided into 5 equal intervals (each interval of 2 units) corresponding with the 5 FDI categories of degradation (I-V) illustrated in figure 4.1.

Table 4.6 Calculated FDI and comparison between five stages and FDI categories

Five Stages of degradation from ground surveys.	SITE	Forest-Degradation Index (FDI)	FDI Category (I ~ V)
Stage 1	BMSM	1.81	I (0.00 ~1.99)
Stage 3	ML	0.49	I (0.00 ~1.99)
Stage 3	BPK	2.64	II (2.00 ~ 3.99)
Stage 3	BMM	6.85	IV (6.00 ~7.99)
Stage 5	LP	8.54	V (8.00 ~10.00)

The FDI placed BMSM and LP at the least (Category-I) and the most degraded classes (Category-V), respectively, as originally assigned (Stage-1 and Stage-5). However, it moved ML to Category-I degradation, from its original assignment, Stage-3; with an FDI even lower than that of BMSM (Stage-1).

The reason why ML was assigned to Stage-3 during the ground survey was because tree stocking-density, estimated from the circular plots (2,884 tree/ha (Figure 4.12)), was slightly below the tipping point, at which tree planting is considered necessary to complement ANR (3,100 trees/ha (Figure 4.1, Table 2.1)), even though mean stocking-density did not differ significantly between ML and BMSM. The same is also true of per cent three ground elements (in the ground survey). This contrasts with the UAV imagery which estimated that per cent ground vegetation cover at BMSM was more than double that at ML (Figure 4.13)—a criterion which the AHP weighted most heavily (0.504) in the FDI—resulting in a higher FDI for BMSM. The ground surveys determined this result is understandable, considering that restoration at ML was initiated just two years after BMSM. Furthermore, ML retained several large remnant trees from the original forest at the start of restoration, whereas the BMSM plot was being restored from cleared agricultural land (Figure 4.16).



Figure 4.16 (Top) BMSM re-planting day in 2012: small previously planted trees which have survived from fire two years previously (see Table 3.1); (Down) ML planting day in 2014: remnant enrichment planting amongst scattered remnant mature trees.

Another interesting comparison is that between BPK and BMM which the FDI separated as Category-II and Category-IV respectively, whereas the ground survey data classify both of them together into Stage-3. Ground survey data placed BPK into Stage-3 because its tree stocking-density (1,321 trees/ha, Figure 4.12) was below 3,100 trees/ha, the tipping point between Stage-2 and Stage-3 degradation (Table 2.1). Furthermore, the ground survey data placed the BMM into Stage-3 because its soil condition did not limit establishment of tree seedlings, the tipping point between Stage-3 and Stage-4

degradation (Table 2.1, Figure 4.1). However, since the FDI was not limited by rigid tipping point and aggregated ranges of criteria, it was more able to separate two sites. Significant difference of tree stocking-density between two sites were also visible during ground survey (Figure 4.17).



Figure 4.17 (Top) Ground survey in BPK: large and dense trees; (Down) Ground survey in BMM: dense weed, low tree stocking-density but no exposed soil + rock.

4.8 Limitations and challenges

4.8.1 Weather, time of day and seasonality

Phantom 4 pro drone used in this project is not water-proof and therefore it is inadvisable to fly during rain due to the risk of short-circuiting in the motors. Several flights during this study were aborted due to on-coming rain. Furthermore, this UAV cannot be flown if wind speed exceeds 24km/h and even below this wind speed, flying UAVs against wind drains the battery power and shorten mission time, and thus limiting the area covered. So, continuous attention on weather condition is required when operating UAVs in the field. Therefore, development of water-proof UAVs with longer battery time will be required if UAVs play a role in forest restoration (Elliott et al., 2020). UAV image quality is greatly affected by the time of day and weather (Figure 4.18). high elevation sites are frequently shrouded in thick mist. Furthermore, strong sunlight causes high contrast (see Figure 4.18 Center). In particular, SfM software has difficulties distinguishing objects in dark shadows. Similarly, low solar angle, usually in the late afternoon, creates long shadows across sites. Therefore, it is recommended to fly in the middle of the day when the shadows are minimal (Elliott et al., 2020).



Figure 4.18 Examples of different quality of UAV-derived RGB images from various weather condition in ML site (1,290 m a.s.l.). (Left) cloud interrupted condition, 13:42 PM, 4th September, 2020, (Center) high contrast from strong sunlight, 14:16 PM, 26th October, 2020, (Right) comparatively stable light contrast without obstacles, 11:30 AM, 9th November, 2020.

The two most significant seasonal effects related to color of the vegetation and tree phenology. In the dry season, weeds turn brown and appear similar to exposed soil; in the rainy season, they are green and appear similar to tree-crowns. Trees also undergo seasonal changes in appearance. Particularly, deciduous trees, which may be completely bare in the dry season, are totally green in the rainy season. However, because the algorithm distinguishes trees from weeds by height (not color), the optimal season to fly is just after the end of rainy season when both trees and weeds are green, and rain is less likely to disrupt flight.

4.8.2 Absence of ground control points (GCPs)

Ground control points (GCPs) are marked points on the ground, recognizable from above, whose precise coordinates are measured by GPS receivers with enhanced precision, e.g., Real-Time Kinematic (RTK) or Post-Processing Kinematic (PPK) GPS receivers. GCPs are used as thumbtacks for geo-referencing UAV data to achieve high degree i) global accuracy, corresponding to the actual coordinate system and ii) local accuracy for measurements in DEMs and orthophotos (Coveney & Roberts, 2017; DroneDeploy, 2017; Sanz-Ablanedo et al., 2018).

However, in this study, GCPs could not be used because of highly dense canopy cover in some study sites (i.e., BMSM and ML), where suitable position for setting GCPs could not be determined. Another reason was the expensive cost for RTK or PPK GPS receivers (e.g., DJI D-RTK 2 High Precision GNSS Mobile Station, priced about 3,600 USD).

Therefore, the stadia method was applied instead, to conform sample plots on the processed DEMs and orthophotos to the actual coordinate system (global accuracy) (see. 4.2.3 Accuracy of positioning circular plots using stadia method). However, absence of GCPs still affected the local accuracy of measurements, especially of tree height in CHMs. It may have contributed to the low accuracy in estimating mean tree heights (Figure 4.9) and ACD (Figure 4.11) (which were calculated from *absolute* height values in CHMs). In contrast, tree stocking-density and per cent canopy cover, derived from *comparative* heights in CHMs were determined with higher accuracy. Zahawi *et al.* (2015) compared non-GPS CHM, generated from point clouds without geo-referencing,

and GPS CHM, geo-referenced with differential GPS elevation, collected on the ground; both methods without GCPs. Geo-referencing improved accuracy of canopy height measurements ($R^2 = 0.94$) and AGB ($R^2 = 0.75$), compared with non-GPS CHM (canopy height, $R^2 = 0.61$; AGB, $R^2 = 0.68$) in dense forest. Swinfield *et al.*, (2019) reported that the application of GCPs enhanced correlation between LiDAR- and SfM-derived data for height (from $R^2 = 0.51$ to 0.67) and ACD (from $R^2 = 0.53$ to 0.68). Therefore, it is recommended that future studies that depend on absolute height values in CHMs should at least apply geo-referencing using elevation data from an advanced GPS receiver (differential GPS), although use of GCPs, with precise coordinates measured by RTK or PPK, is optimal.

4.8.3 Limited visibility of understory in UAV imagery

One of the biggest challenges using SfM for surveying forests, is the fact that large tree-crowns obscure those of understory trees often. In contrast, LiDAR can, to a certain extent, penetrate the upper canopies to produce point clouds of underlying objects. (e.g., ground, small trees and shrubs, tree trunks, etc.) (Figure 4.19).

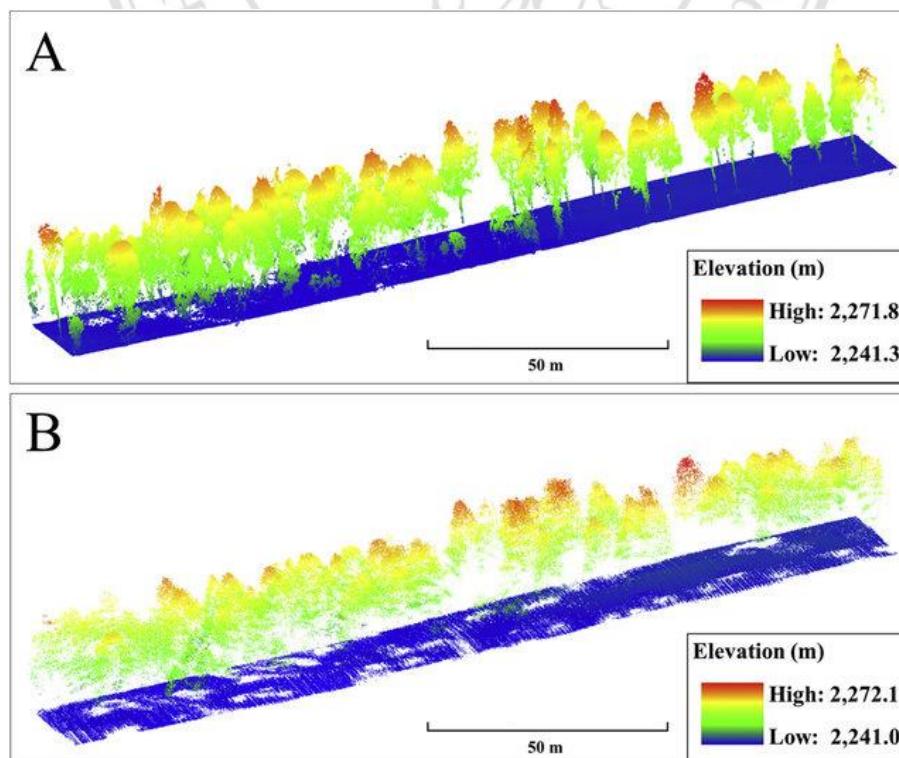


Figure 4.19 Examples of UAV derived point clouds in the same forest by (A) LiDAR and (B) SfM point cloud (adopted from Sankey *et al.*, 2017)

Despite this limitation of RGB photographs and SfM, this study used RGB photogrammetry with a consumer-grade UAV, due to its relative availability and affordability to local restoration practitioners. Furthermore, to minimize this limitation, multiple regression models were applied to estimate tree stocking-density, by adding per cent canopy cover as a predictor variable, with the expectation that a higher canopy cover would predict greater numbers of obscured small trees. Although this approach generally improved prediction of numbers of understory trees (Figure 4.8), it did tend to underestimate tree numbers where upper canopy cover was high and overestimated it where upper canopy cover was low.

4.8.4 Non-inclusion of landscape criteria

The present study focused only on site-factors, however landscape-wide factors also influence forest degradation. For example, Elliott *et al.*, (2013) divided the critical thresholds, that determine degradation levels, into two categories: site thresholds and landscape thresholds (Table 2.1). Their site critical thresholds were: weed cover, natural regenerants, and soil exposure (all included in present study.). Landscape-critical thresholds were: i) remnant forest within seed-dispersal distance, ii) populations of seed-dispersing animals and iii) fire risk (not included in present study).

Two environmental attributes in landscape (i.e., remnant forest and fire risks) can be detected using spaceborne data with ancillary data. For example, the amount and distance of remnant forest, likely to act as a source of seed rain reaching restoration sites, can be calculated from satellite images. Rapinel *et al.*, (2014) used satellite images with thematic ancillary data to classify non-, artificial-, and natural- vegetation. Furthermore, various attributes, related to the risk of forest fire, can be estimated from satellite images and be integrated. Adab *et al.*, (2013) generated indices of fire risk, combining variables of vegetation, topography, and impact from human activities, detected from satellite images.

Automated techniques for detecting viable populations of animal seed-dispersal in the landscape include i) camera traps, ii) thermal cameras on UAVs, and iii) bio acoustic monitoring in conjunction with CHMs. Conventional camera traps are static, limited to take picture at single viewpoint. Thermal cameras on UAVs cannot detect animals

beneath dense forests. Since birds are the most abundant seed-dispersers during forest restoration, the recent development of combining bio-acoustic monitoring—understanding population and behavior of animals from triangulating bird songs—with CHMs is promising. Wilson et al., (2021) used an array of microphones to map bird abundance on CHMs across boreal forest in Canada (Figure 4.20).

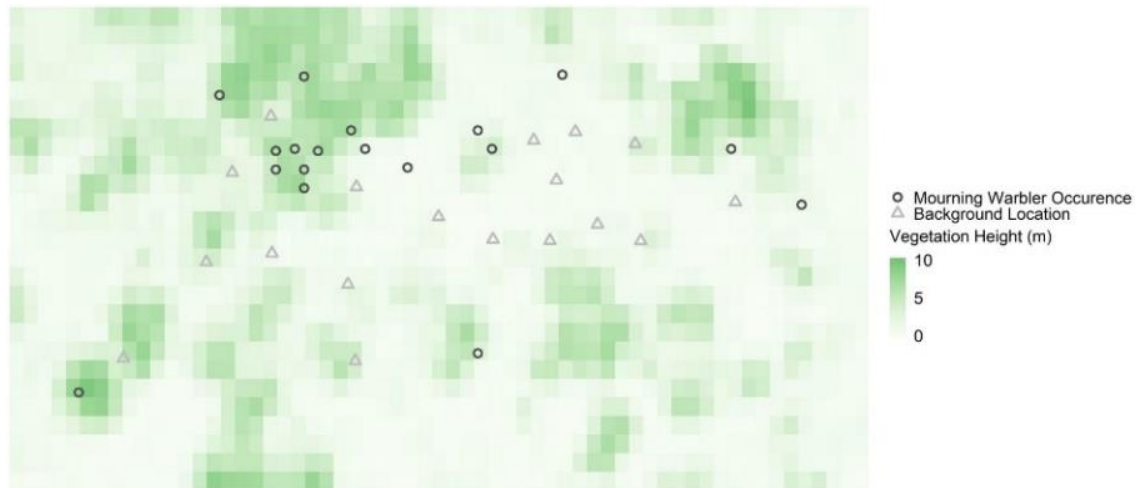


Figure 4.20 UAV-derived CHM marked with mourning warblers' occurrence and background location (absence) (adopted from Wilson et al., 2021)

Whereas, the examples above show that it is feasible to add landscape criteria to improve the accuracy of FDIs, the cost of doing so, in terms of time, labor, and equipment needed, must also be taken into consideration.

4.8.5 Application of the FDI in more or less degraded sites

The sites, used to develop the FDI, represented a wide range of degradation states. The most degraded site was a limestone-quarry (LP), although not totally bare substrate. The least degraded sites were advanced restoration (BMSM and ML; 8 and 6 years after tree-planting), but not yet totally recovered. Therefore, the FDI should be applied with caution if used on sites that are more degraded than the former or less degraded than the latter, as it would deliver FDI values of <1 or >10 respectively. To prevent such anomalies additional sites at the extreme limits of the degradation spectrum would be needed to recalibrate the index. In addition, adding sites to fill gaps within the spectrum (in this study Stage-2 and 4 or Category-III (Table 4.6)) may help to develop a more precise FDI.

4.8.6 Labor, time and costs for UAV-derived FDI

Qualitatively, labor, time, and costs for UAV-derived FDI are compared with ground surveys for assessing forest-degradation stages in Table 4.7. One of the apparent barriers for applying UAVs is the initial cost for purchasing set of gadgets and recruiting technicians or developing capacity of current personnel. However, if organizations have long term plans for applying UAVs, these initial costs are spread over many projects. Another issue of is complicated data processing. This could be overcome in the future by developing automated platform.

Table 4.7 Consumption comparison between ground survey and UAV-derived FDI

Cost type		Ground Survey	UAV-derived FDI
		<i>per each project (approximately 0.5 – 3.0 hectare)</i>	
Setup	Training	- Simple technique - Short training	- High-end technique - Period of training
	Gadgets	- Cheaper - ex) tape measure, laser range finder	- Expensive - ex) craft, controller, tablet or mobile device, extra batteries
Data acquisition (Field)	Time	- A whole daytime	- Few hours
	Labor (Salary, food)	- 3 - 4 teams × 2 - 4 members - More expense	- 1 team × 3 members - Less expense
	Weather limitation	- Less sensitive - Affecting collectors' safety by severely bad weather, - ex) Heavy rain and storm	- More sensitive - Affecting gadgets' applicability by slightly bad weather, - ex) Light rain, fog, and strong wind.
Data processing (Lab)	Technique	- Simple software - ex) spreadsheet (MS excel)	- Advanced software - ex) WebODM, Image-J, and QGIS, etc.

CHAPTER 5

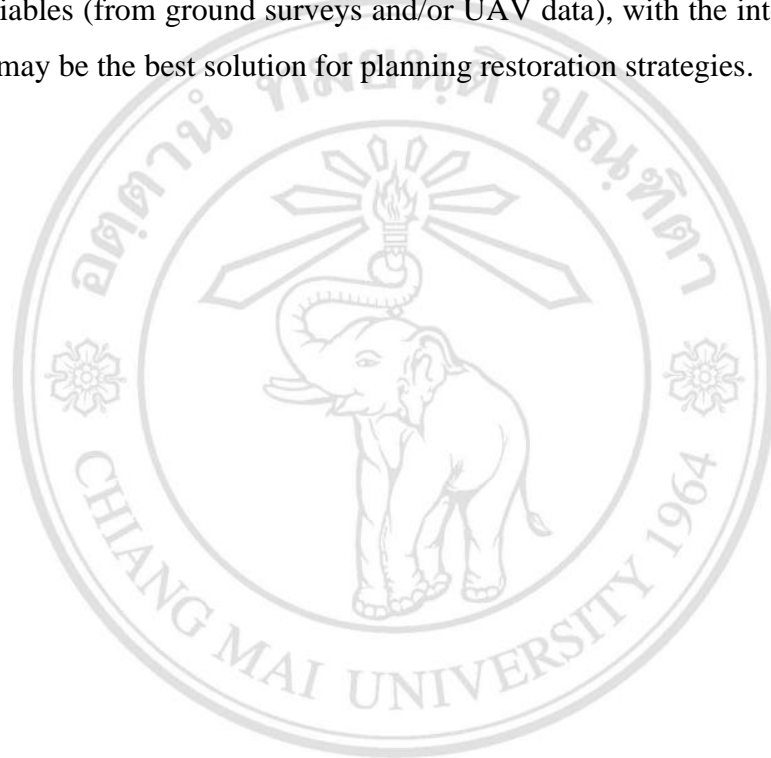
Conclusion

This project was a first attempt to develop an index of forest degradation based on UAV-derived data. It aimed to find *practical* and *accurate* solutions using UAVs, to replace conventional time-consuming and labor-intensive ground surveys, to help guide restoration projects. The study specifically focused on the development of affordable photo-grammetric techniques, using RGB photography and open-source software, rather than more expensive options (e.g., LiDAR, and hyperspectral data). The first objective was to detect correlations between UAV-derived data, and ground surveyed data. This was achieved for four out of the six variables tested; tree stocking-density, per cent canopy cover, per cent ground vegetation and per cent exposed soil + rock.

The second objective was to develop a forest-degradation index (FDI), based on such correlations. This was achieved with three additional procedures: i) removal of intercorrelated variables, ii) normalizing the measured values, iii) weighting each criterion. The result was an FDI ranging from 0 to 10, which ranked the study sites in logical order, from the least to the most degraded, and quantified degradation levels fairly intuitively.

However, the FDI, developed in this study, could not be used to determine the fine details of restorative interventions (e.g., planning number of trees, to be planted), which were better determined directly from single variables, sometimes from the ground survey and sometimes from UAV-derived data. Furthermore, it would be dubious to use the FDI to determine restoration strategy (e.g., no-intervention, protection, assisted natural regeneration, framework species method, maximum-diverse species method, and nurse plantation methods), since it is not yet precise enough. This may have been due to fundamental differences between FDIs and discrete degradation stages. FDIs integrate several criteria into a single number, which is easily understood. However, it can also

obscure the distinctions (tipping points) between degradation stages, which have conventionally been used to determine restoration strategies. This may help to explain why the FDI degradation categories, in this study, did not match the conventional degradation stages (1-5). Also contributing to the explanation may be i) the division of the FDI into 5 arbitrary categories (five equal divisions of 2) and ii) the exclusion of landscape criteria. Addressing these issues will be essential for the development of more workable FDIs in the future. Until these issues are resolved, a hybrid system, combining individual variables (from ground surveys and/or UAV data), with the integrated UAV-derived FDIs may be the best solution for planning restoration strategies.



ลิขสิทธิ์มหาวิทยาลัยเชียงใหม่
Copyright© by Chiang Mai University
All rights reserved

REFERENCES

- Adab, H., Kanniah, K. D., & Solaimani, K. (2013). Modeling forest fire risk in the northeast of Iran using remote sensing and GIS techniques. *Natural Hazards*, 65(3), 1723–1743. <https://doi.org/10.1007/s11069-012-0450-8>
- Adesoye, P., & Akinwunmi, A. A. (2016). Tree Slenderness Coefficient and Percent Canopy Cover in Oban Group Forest , Nigeria Tree Slenderness Coefficient and Percent Canopy Cover in Oban. *Journal of Natural Sciences Research*, 6(4)(January), 9–17.
- AFR100 Governance. (2017). *Terms of Reference for AFR100 Governance Bodies*.
- Alonzo, M., Andersen, H. E., Morton, D. C., & Cook, B. D. (2018). Quantifying boreal forest structure and composition using UAV structure from motion. *Forests*, 9(3), 1–15. <https://doi.org/10.3390/f9030119>
- Ananda, J., & Herath, G. (2009). A critical review of multi-criteria decision making methods with special reference to forest management and planning. *Ecological Economics*, 68(10), 2535–2548. <https://doi.org/10.1016/j.ecolecon.2009.05.010>
- APEC Economic Leaders. (2007). *Sydney APEC Leaders' Declaration on Climate Change, Energy Security and Clean Development*. https://www.apec.org/Meeting-Papers/Leaders-Declarations/2007/2007_aelm/aelm_climatechange
- Baena, S., Moat, J., Whaley, O., & Boyd, D. S. (2017). Identifying species from the air: UAVs and the very high resolution challenge for plant conservation. *PLoS ONE*, 12(11), 1–21. <https://doi.org/10.1371/journal.pone.0188714>
- Bahamóndez, C., Martin, M., Müller-Using, S., Rojas, Y., & Vergara, G. (2009). Case studies on measuring and assessing forest degradation: an operational approach to forest degradation. In *Forest Resources Assessment Working Paper 158*. FAO. <http://www.fao.org/docrep/012/k7177e/k7177e00.pdf>.

- Bahamondez, C., & Thompson, I. D. (2016). Determining forest degradation, ecosystem state and resilience using a standard stand stocking measurement diagram: Theory into practice. *Forestry*, 89(3), 290–300. <https://doi.org/10.1093/forestry/cpv052>
- Benton, A. R. T., & Taetz, P. J. (1991). *Elements of Plane Surveying*. McGraw-Hill Inter.
- Beucher, S., & Meyer, F. (1993). The Morphological Approach to Segmentation: The Watershed Transformation. In *Mathematical morphology in image processing* (pp. 433–481). <https://doi.org/10.3969/j.issn.1000-8152.2001.04.002>
- Brinker, R. C., & Wolf, P. R. (1984). *Elementary surveying* (7th ed.). Harper & Row.
- Camarretta, N., Harrison, P. A., Bailey, T., Potts, B., Lucieer, A., Davidson, N., & Hunt, M. (2019). Monitoring forest structure to guide adaptive management of forest restoration: a review of remote sensing approaches. *New Forests*, 51(4), 573–596. <https://doi.org/10.1007/s11056-019-09754-5>
- Caughlin, T. T., Rifai, S. W., Graves, S. J., Asner, G. P., & Bohlman, S. A. (2016). Integrating LiDAR-derived tree height and Landsat satellite reflectance to estimate forest regrowth in a tropical agricultural landscape. *Remote Sensing in Ecology and Conservation*, 2(4), 190–203. <https://doi.org/10.1002/rse2.33>
- CBD. (2010). *Quick guide to the Aichi Biodiversity Targets 15. Ecosystems restored and resilience enhanced*. <https://www.cbd.int/nbsap/training/quick-guides/>
- Coveney, S., & Roberts, K. (2017). Lightweight UAV digital elevation models and orthoimagery for environmental applications: data accuracy evaluation and potential for river flood risk modelling. *International Journal of Remote Sensing*, 38(8–10), 3159–3180. <https://doi.org/10.1080/01431161.2017.1292074>
- Da Ponte, E., Mack, B., Wohlfart, C., Rodas, O., Fleckenstein, M., Oppelt, N., Dech, S., & Kuenzer, C. (2017). Assessing forest cover dynamics and forest perception in the Atlantic Forest of Paraguay, combining remote sensing and household level data. *Forests*, 8(10), 1–21. <https://doi.org/10.3390/f8100389>

- Dave, R., Saint-Laurent, C., Murray, L., Antunes Daldegan, G., Brouwer, R., de Mattos Scaramuzza, C. A., Raes, L., Simonit, S., Catapan, M., García Contreras, G., Ndoli, A., Karangwa, C., Perera, N., Hingorani, S., & Pearson, T. (2019). Second Bonn Challenge progress report: application of the Barometer in 2018. In *Second Bonn Challenge progress report: application of the Barometer in 2018*. IUCN. <https://doi.org/10.2305/iucn.ch.2019.06.en>
- De Almeida, D. R. A., Almeyda Zambrano, A. M., Broadbent, E. N., Wendt, A. L., Foster, P., Wilkinson, B. E., Salk, C., Papa, D. d. A., Stark, S. C., & Valbuena, R. (2020). Detecting successional changes in tropical forest structure using gatereye drone-borne lidar. *Biotropica*, 52, 1155–1167. <https://doi.org/https://doi.org/10.1111/btp.12814>
- De Castro, M., & Urios, V. (2016). A critical review of multi-criteria decision making in protected areas. *Economia Agraria y Recursos Naturales*, 16(2), 89–109. <https://doi.org/10.7201/earn.2016.02.04>
- DroneDeploy. (2017). *When To Use Ground Control Points: How To Decide If Your Drone Mapping Project Needs GCPs*. <https://medium.com/aerial-acuity/when-to-use-ground-control-points-2d404d9f5b15>
- Elliott, S. D., Blakesley, D., & Hardwick, K. (2013). *Restoring Tropical Forests: a practical guide*. Royal Botanic Gardens, Kew.
- Elliott, S., Gale, G., & Robertson, M. (Eds.). (2020). *Automated Forest Restoration: Could Robots Revive Rain Forests?* FORRU-CMU. <https://www.forru.org/library/0000099?t%5B0%5D=41&page=1>
- Etten, J. Van, Sumner, M., Cheng, J., Baston, D., Bevan, A., Bivand, R., Busetto, L., Canty, M., Fasoli, B., Forrest, D., Golicher, D., Gray, J., Greenberg, J. A., Hiemstra, P., Karney, C., Mattiuzzi, M., Mosher, S., & Wueest, R. (2020). *Package ‘ raster ’ R topics documented :*
- FAO. (2011). Assessing forest degradation: Towards the development of globally applicable guidelines. In *Forest Resources Assessment*. <https://doi.org/10.1023/B:VEGE.0000029381.63336.20>

- FAO. (2019). *Forest futures - Sustainable pathways for forests, landscapes and people in the Asia-Pacific region*.
- FAO. (2002). *Expert Meeting on Harmonizing forest-related definitions for use by various stakeholders. January, 193*.
http://www.fao.org/documents/show_cdr.asp?url_file=/DOCREP/005/Y4171E/Y4171E36.htm
- FAO, & APFNet. (2018). Regional Strategy and Action plan for the Forest and Landscape Restoration in Asia-Pacific. In *FAO & APFNet*.
- FAO Regional Office for Asia and the Pacific. (2005). *Helping Forests Take Cover On forest protection, increasing forest cover and future approaches to reforesting degraded tropical landscapes in Asia and the Pacific* (S. A. and P. B. D. V. Poopathy (Ed.)). <http://www.fao.org/3/ae945e/ae945e00.htm>
- Figueira, J., Greco, S., & Ehrogott, M. (2005). *Multiple Criteria Decision Analysis: State of the Art Surveys* (S. Greco (Ed.); 1st ed.). Springer.
<https://doi.org/https://doi.org/10.1007/b100605>
- Fisher, A. (2013). Cloud and cloud-shadow detection in SPOT5 HRG imagery with automated morphological feature extraction. *Remote Sensing*, 6(1), 776–800.
<https://doi.org/10.3390/rs6010776>
- Fujimoto, A., Haga, C., Matsui, T., Machimura, T., Hayashi, K., Sugita, S., & Takagi, H. (2019). An end to end process development for UAV-SfM based forest monitoring: Individual tree detection, species classification and carbon dynamics simulation. *Forests*, 10(8), 1–27. <https://doi.org/10.3390/f10080680>
- Getzin, S., Wiegand, K., & Schöning, I. (2012). Assessing biodiversity in forests using very high-resolution images and unmanned aerial vehicles. *Methods in Ecology and Evolution*, 3(2), 397–404. <https://doi.org/10.1111/j.2041-210X.2011.00158.x>
- Ginrich, S. (1967). Measuring and Evaluating Stocking and Stand Density in Upland Hardwood Forests in the Central States. *Forest Science*, 13(1), 38–53.
<https://doi.org/10.1093/forestscience/13.1.38>

- Goepel, K. D. (2018). Implementation of an Online Software Tool for the Analytic Hierarchy Process (AHP-OS). *International Journal of the Analytic Hierarchy Process*, 10(3), 469–487. <https://doi.org/10.13033/ijahp.v10i3.590>
- Hansen, M. C., Potapov, P. V., Goetz, S. J., Turubanova, S., Tyukavina, A., Krylov, A., Kommareddy, A., & Egorov, A. (2016). Mapping tree height distributions in Sub-Saharan Africa using Landsat 7 and 8 data. *Remote Sensing of Environment*, 185, 221–232. <https://doi.org/10.1016/j.rse.2016.02.023>
- IPCC. (2003). *Definitions and Methodological Options to Inventory Emissions from Direct Human-induced Degradation of Forests and Devegetation of Other Vegetation Types* (K. T. and F. W. Jim Penman, Michael Gytarsky, Taka Hiraishi, Thelma Krug, Dina Kruger, Riitta Pipatti, Leandro Buendia, Kyoko Miwa, Todd Ngara (Ed.)). IPCC.
- ITTO. (2002). *ITTO guidelines for the restoration, management and rehabilitation of degraded and secondary tropical forests* (Issue ITTO Policy Development Series No.13).
- IUCN. (2017). The Bonn Challenge: Catalysing Leadership in Latin America. In *IUCN Forest Brief* (Issue 14). IUCN.
- Jucker, T., Asner, G. P., Dalponte, M., Brodrick, P. G., Philipson, C. D., Vaughn, N. R., Arn Teh, Y., Brelsford, C., Burslem, D. F. R. P., Deere, N. J., Ewers, R. M., Kvasnica, J., Lewis, S. L., Malhi, Y., Milne, S., Nilus, R., Pfeifer, M., Phillips, O. L., Qie, L., ... Coomes, D. A. (2018). Estimating aboveground carbon density and its uncertainty in Borneo's structurally complex tropical forests using airborne laser scanning. *Biogeosciences*, 15(12), 3811–3830. <https://doi.org/10.5194/bg-15-3811-2018>
- Khokthong, W., Zemp, D. C., Irawan, B., Sundawati, L., Kreft, H., & Hölscher, D. (2019). Drone-Based Assessment of Canopy Cover for Analyzing Tree Mortality in an Oil Palm Agroforest. *Frontiers in Forests and Global Change*, 2(April), 1–10. <https://doi.org/10.3389/ffgc.2019.00012>

- Lewis, S. L., Wheeler, C. E., Mitchard, E. T. A., & Koch, A. (2019). Restoring natural forests is the best way to remove atmospheric carbon. *Nature*, 568(7750), 25–28. <https://doi.org/10.1038/d41586-019-01026-8>
- Miranda, A., Catalán, G., Altamirano, A., & Cavieres, M. (2020). Automating site assessments using data from UAVs. In G. & M. R. (Eds) Elliott S., G (Ed.), *Automated Forest Restoration: Could Robots Revive Rain Forests?* (pp. 64–73). Chiang Mai University. <https://www.forru.org/library/0000149>
- Modica, G., Merlino, A., Solano, F., & Mercurio, R. (2015). An index for the assessment of degraded mediterranean forest ecosystems. *Forest Systems*, 24(3). <https://doi.org/10.5424/fs/2015243-07855>
- Mutwiri, F. K., Odera, P. A., & Kinyanjui, M. J. (2017). Estimation of Tree Height and Forest Biomass Using Airborne LiDAR Data: A Case Study of Londiani Forest Block in the Mau Complex, Kenya. *Open Journal of Forestry*, 07(02), 255–269. <https://doi.org/10.4236/ojf.2017.72016>
- NYDF Assessment Partners. (2019). *Protecting and Restoring Forests : A Story of Large Commitments. New York Declaration on Forests Five-Year Assessment Report. September*, 94. forestdeclaration.org
- Plowright, A. (2020). *Canopy analysis in R using Forest Tools*. <https://cran.r-project.org/web/packages/ForestTools/vignettes/treetopAnalysis.html>
- Plowright, A., & Roussel, J.-R. (2020). *ForestTools: Analyzing Remotely Sensed Forest Data. R package version 0.2.1*. <https://cran.r-project.org/package=ForestTools>
- Pothong, T., Elliott, S., Chairuang Sri, S., Chanthorn, W., Shannon, D. P., & Wangpakapattanawong, P. (2021). New allometric equations for quantifying tree biomass and carbon sequestration in seasonally dry secondary forest in northern Thailand. *New Forests*, 0123456789. <https://doi.org/10.1007/s11056-021-09844-3>
- Rapinel, S., Clément, B., Magnanon, S., Sellin, V., & Hubert-Moy, L. (2014). Identification and mapping of natural vegetation on a coastal site using a Worldview-2 satellite image. *Journal of Environmental Management*, 144, 236–246. <https://doi.org/10.1016/j.jenvman.2014.05.027>

- Riihimäki, H., Luoto, M., & Heiskanen, J. (2019). Estimating fractional cover of tundra vegetation at multiple scales using unmanned aerial systems and optical satellite data. *Remote Sensing of Environment*, 224(January), 119–132.
<https://doi.org/10.1016/j.rse.2019.01.030>
- Roger, A., Rowlingson, B., Sumner, M., & Hijmans, R. (2020). *Package 'rgdal' R topics documented* :
- Saaty, R. W. (1987). The analytic hierarchy process-what it is and how it is used. *Mathematical Modelling*, 9(3–5), 161–176. [https://doi.org/10.1016/0270-0255\(87\)90473-8](https://doi.org/10.1016/0270-0255(87)90473-8)
- Saaty, T. L. (2003). Decision-making with the AHP: Why is the principal eigenvector necessary. *European Journal of Operational Research*, 145(1), 85–91.
[https://doi.org/10.1016/S0377-2217\(02\)00227-8](https://doi.org/10.1016/S0377-2217(02)00227-8)
- Saaty, T. L., & Shang, J. S. (2011). An innovative orders-of-magnitude approach to AHP-based multi-criteria decision making: Prioritizing divergent intangible humane acts. *European Journal of Operational Research*, 214(3), 703–715.
<https://doi.org/10.1016/j.ejor.2011.05.019>
- Sankey, T., Donager, J., McVay, J., & Sankey, J. B. (2017). UAV lidar and hyperspectral fusion for forest monitoring in the southwestern USA. *Remote Sensing of Environment*, 195(November), 30–43.
<https://doi.org/10.1016/j.rse.2017.04.007>
- Sanz-Ablanedo, E., Chandler, J. H., Rodríguez-Pérez, J. R., & Ordóñez, C. (2018). Accuracy of Unmanned Aerial Vehicle (UAV) and SfM photogrammetry survey as a function of the number and location of ground control points used. *Remote Sensing*, 10(10). <https://doi.org/10.3390/rs10101606>
- Sasaki, N., Asner, G. P., Knorr, W., Durst, P. B., Priyadi, H. R., & Putz, F. E. (2011). Approaches to classifying and restoring degraded tropical forests for the anticipated REDD+ climate change mitigation mechanism. *IForest*, 4(JANUARY), 1–6. <https://doi.org/10.3832/ifor0556-004>

- SCBD: Secretariat of the Convention on Biological Diversity. (2002). *Review of the status and trends of, and major threats to, the forest biological diversity (CBD Technical Series no. 7)*. SCBD.
- Shimabukuro, Y. E., Beuchle, R., Grecchi, R. C., & Achard, F. (2014). Assessment of forest degradation in Brazilian Amazon due to selective logging and fires using time series of fraction images derived from Landsat ETM+ images. *Remote Sensing Letters*, 5(9), 773–782. <https://doi.org/10.1080/2150704X.2014.967880>
- Simula, M. (2009). Towards defining forest degradation: comparative analysis of existing definitions. In *Forest Resources Assessment Programme working Paper 154* (FAO, p. 62). http://www.ardot.fi/Documents_2/Degradationdefinitions.pdf
- Stockman, G., & Shapiro, L. G. (2001). *Computer Vision*. Prentice Hall.
- Swinfield, T., Lindsell, J. A., Williams, J. V., Harrison, R. D., Agustiono, Habibi, Elva, G., Schönlieb, C. B., & Coomes, D. A. (2019). Accurate Measurement of Tropical Forest Canopy Heights and Aboveground Carbon Using Structure From Motion. *Remote Sensing*, 11(928). <https://doi.org/10.3390/rs11080928>
- Thomas, E., Jalonon, R., Loo, J., & Bozzano, M. (2015). Avoiding failure in forest restoration: The importance of genetically diverse and site-matched germplasm. *Unasylva*, 66(245), 29–36.
- Thompson, I. D., Guariguata, M. R., Okabe, K., Bahamondez, C., Nasi, R., Heymell, V., & Sabogal, C. (2013). An operational framework for defining and monitoring forest degradation. *Ecology and Society*, 18(2). <https://doi.org/10.5751/es-05443-180220>
- Ullman, S. (1979). The Interpretation of Structure From Motion. *Royal Society of London*, 405–426. <https://doi.org/10.7551/mitpress/3877.003.0009>
- UN Climate Summit. (2014). *New York Declaration on Forests: Declaration and Action Agenda*.
- UNEP, & FAO. (2019). *The United Nations Decade on Ecosystem Restoration*.

- UNEP, & FAO. (2020). The UN Decade on Ecosystem Restoration 2021-2030. In *UNEP/FAO Factsheet*.
- UNFCCC. (2008). *Report of the Conference of the Parties on its thirteenth session, held in Bali from 3 to 15 December 2007*. <https://unfccc.int/documents/5079>
- Vásquez-Grandón, A., Donoso, P. J., & Gerding, V. (2018). Forest degradation: When is a forest degraded? *Forests*, 9(11). <https://doi.org/10.3390/f9110726>
- Wilson, S. J., Hedley, R. W., Rahman, M. M., & Bayne, E. M. (2021). Use of an unmanned aerial vehicle and sound localization to determine bird microhabitat. *Journal of Unmanned Vehicle Systems*, 9(1), 59–66. <https://doi.org/10.1139/juvs-2020-0021>
- Zahawi, R. A., Dandois, J. P., Holl, K. D., Nadwodny, D., Reid, J. L., & Ellis, E. C. (2015). Using lightweight unmanned aerial vehicles to monitor tropical forest recovery. *Biological Conservation*, 186, 287–295. <https://doi.org/10.1016/j.biocon.2015.03.031>
- Zhai, D. L., Xu, J. C., Dai, Z. C., Cannon, C. H., & Grumbine, R. E. (2014). Increasing tree cover while losing diverse natural forests in tropical Hainan, China. *Regional Environmental Change*, 14(2), 611–621. <https://doi.org/10.1007/s10113-013-0512-9>
- Zhuravleva, I., Turubanova, S., Potapov, P., Hansen, M., Tyukavina, A., Minnemeyer, S., Laporte, N., Goetz, S., Verbelen, F., & Thies, C. (2013). Satellite-based primary forest degradation assessment in the Democratic Republic of the Congo, 2000-2010. *Environmental Research Letters*, 8(2). <https://doi.org/10.1088/1748-9326/8/2/024034>

APPENDIX A

Experts' evaluation of weighting drone-derived indicators for Forest-Degradation Index

Kyuho Lee (Environmental Science Program, Chiang Mai University)

This research is developing a **Forest Degradation Index**, using values of various variable that can be derived from the drone-images. Some variables may be more important at determine degree of forest degradation than others. So, I would value your expert opinion on how much weight to assign to each of the drone-derived variables. Thank you for participation in the survey.

The variables are:

Indicator 1. Tree Density.

Number of trees per hectare (taller than 2m)

Indicator 2. % Crown Cover

Percentage of the entire site covered by tree crowns

Indicator 3. Mean height of trees

Mean height of trees across the entire site (taller than 2 m)

Indicator 4. % Exposed soil

Percentage of the entire site showing exposed soil and/or rocks (detected by color threshold of pixels in photographs)

Indicator 5. % Ground vegetation and weeds

Percentage of the entire site covered by ground vegetation and weeds (detected by color threshold of pixels in photographs)

Indicator 6. Derived Aboveground Carbon Density (MgC/ha)

Estimated aboveground carbon density per hectare, calculated by allometric equations from mean height of trees and %Crown cover

Instructions

- For each of the following pairs of variables, please select the one you consider to be more sensitive to changes in level of forest degradation i.e. the one that would change the most if the site became more or less degraded.
- Please select only one variable in each pair (each row)
- If you find it impossible to decide, or both variables are equally sensitive to changes in forest degradation level, please tick "Equal 1"
- If you decide one variable is more sensitive than the other one please indicate the degree of sensitivity on a scale of 2 (slightly more sensitive) to 9 (extremely more sensitive)
- ***If you are unsure of any other matters concerning this assessment, please contact Kyuho Lee(paulestlee@gmail.com).***

<Evaluation Form>

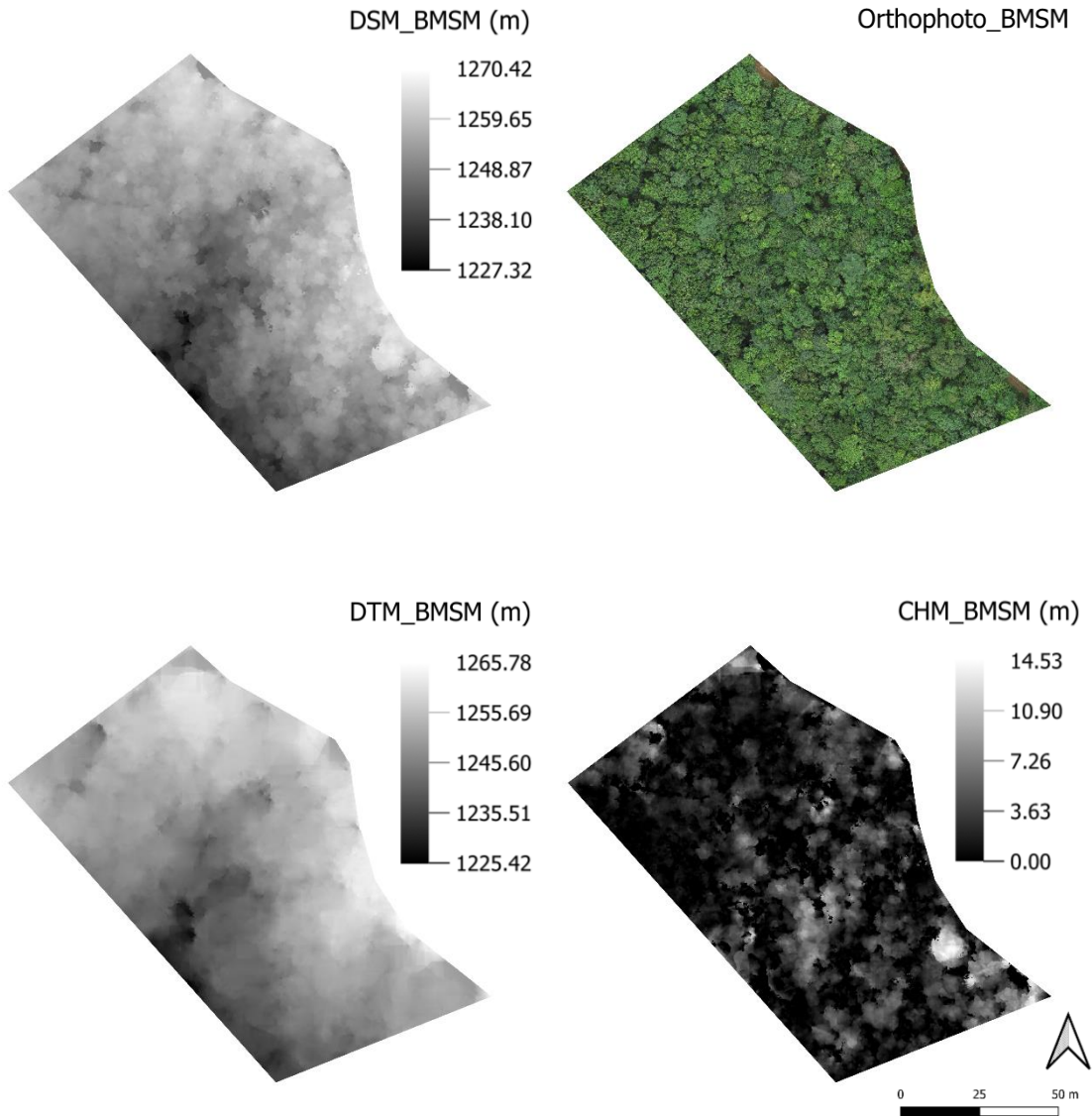
Date		Name	
------	--	------	--

<p style="text-align: center;">A VS B</p> <p style="text-align: center;">Please tick only one in each pair Or no tick for answering 'Equal 1'</p>		Equal	The selected Indicator is							
			Slightly more sensitive						Very much more sensitive	
		1	2	3	4	5	6	7	8	9
<input type="checkbox"/>	Tree Density (Number of trees/ ha)	<input type="checkbox"/>	% Crown Cover in the overall site.	Select one of the answers. Click and Drop down this box →						
<input type="checkbox"/>	Tree Density (Number of trees/ ha)	<input type="checkbox"/>	Mean height of trees in the overall site.	Select one of the answers. Click and Drop down this box →						
<input type="checkbox"/>	Tree Density (Number of trees/ ha)	<input type="checkbox"/>	% Exposed soil in the overall site.	Select one of the answers. Click and Drop down this box →						
<input type="checkbox"/>	Tree Density (Number of trees/ ha)	<input type="checkbox"/>	% Weed in the overall site.	Select one of the answers. Click and Drop down this box →						
<input type="checkbox"/>	Tree Density (Number of trees/ ha)	<input type="checkbox"/>	Derived Aboveground Carbon Density (MgC/ha)	Select one of the answers. Click and Drop down this box →						
<input type="checkbox"/>	% Crown Cover in the overall site.	<input type="checkbox"/>	Mean height of trees in the overall site.	Select one of the answers. Click and Drop down this box →						
<input type="checkbox"/>	% Crown Cover in the overall site.	<input type="checkbox"/>	% Exposed soil in the overall site.	Select one of the answers. Click and Drop down this box →						
<input type="checkbox"/>	% Crown Cover in the overall site.	<input type="checkbox"/>	% Weed in the overall site.	Select one of the answers. Click and Drop down this box →						
<input type="checkbox"/>	% Crown Cover in the overall site.	<input type="checkbox"/>	Derived Aboveground Carbon Density (MgC/ha)	Select one of the answers. Click and Drop down this box →						
<input type="checkbox"/>	Mean height of trees in the overall site.	<input type="checkbox"/>	% Exposed soil in the overall site.	Select one of the answers. Click and Drop down this box →						
<input type="checkbox"/>	Mean height of trees in the overall site.	<input type="checkbox"/>	% Weed in the overall site.	Select one of the answers. Click and Drop down this box → Can not decide/ Both are Equal (1) 2: Slightly more sensitive 3 4 5 6 7 8 9: Very much more sensitive						
<input type="checkbox"/>	Mean height of trees in the overall site.	<input type="checkbox"/>	Derived Aboveground Carbon Density (MgC/ha)	Select one of the answers. Click and Drop down this box → Can not decide/ Both are Equal (1) 2: Slightly more sensitive 3 4 5 6 7 8 9: Very much more sensitive						
<input type="checkbox"/>	% Exposed soil in the overall site.	<input type="checkbox"/>	% Weed in the overall site.	Select one of the answers. Click and Drop down this box → Can not decide/ Both are Equal (1) 2: Slightly more sensitive 3 4 5 6 7 8 9: Very much more sensitive						
<input type="checkbox"/>	% Exposed soil in the overall site.	<input type="checkbox"/>	Derived Aboveground Carbon Density (MgC/ha)	Select one of the answers. Click and Drop down this box → Can not decide/ Both are Equal (1) 2: Slightly more sensitive 3 4 5 6 7 8 9: Very much more sensitive						
<input type="checkbox"/>	% Weed in the overall site.	<input type="checkbox"/>	Derived Aboveground Carbon Density (MgC/ha)	Select one of the answers. Click and Drop down this box → Can not decide/ Both are Equal (1) 2: Slightly more sensitive 3 4 5 6 7 8 9: Very much more sensitive						

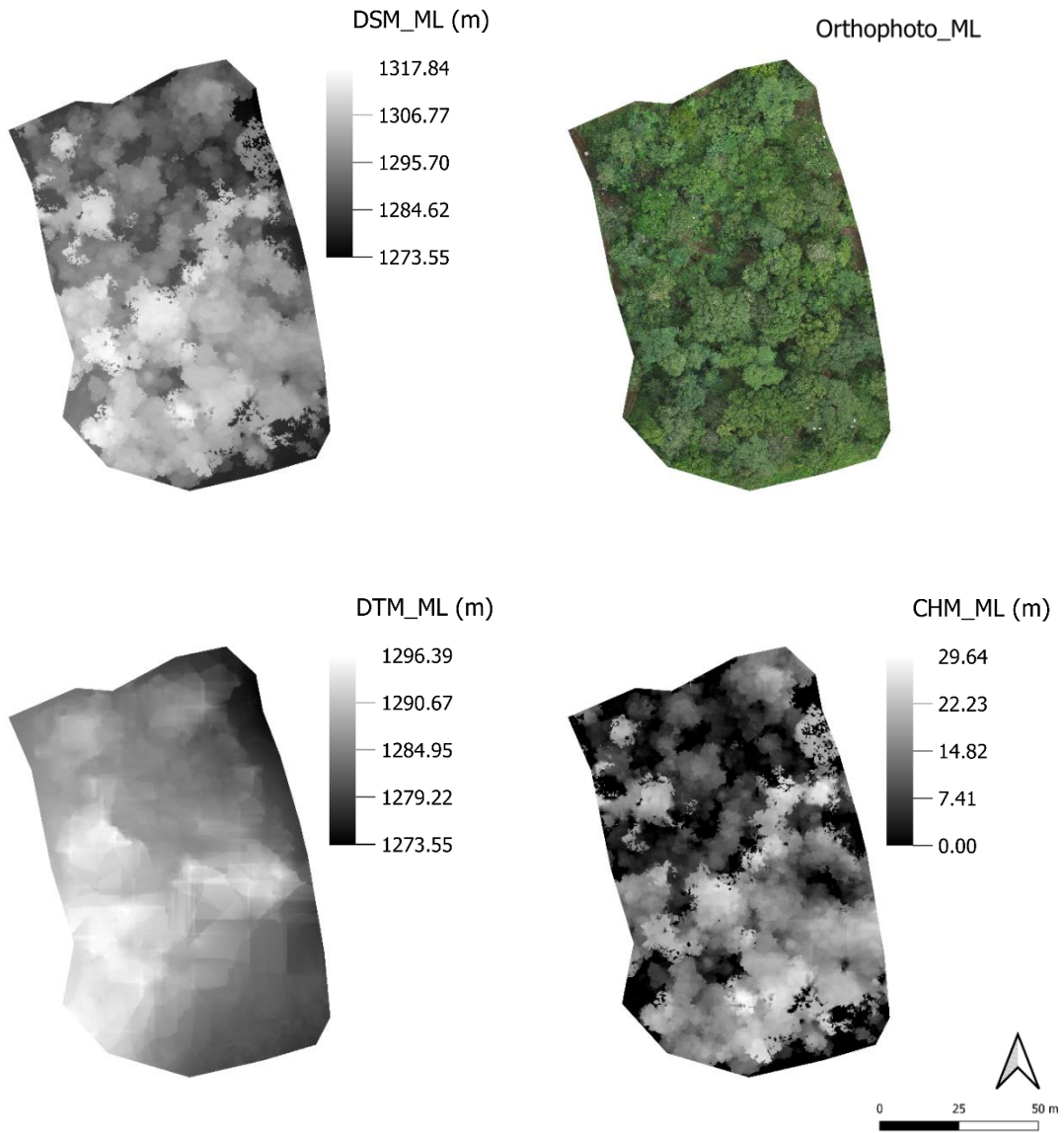
APPENDIX B

Orthophotos presented with DEMs (i.e., DSM, DTM, and CHM)

1. BMSM

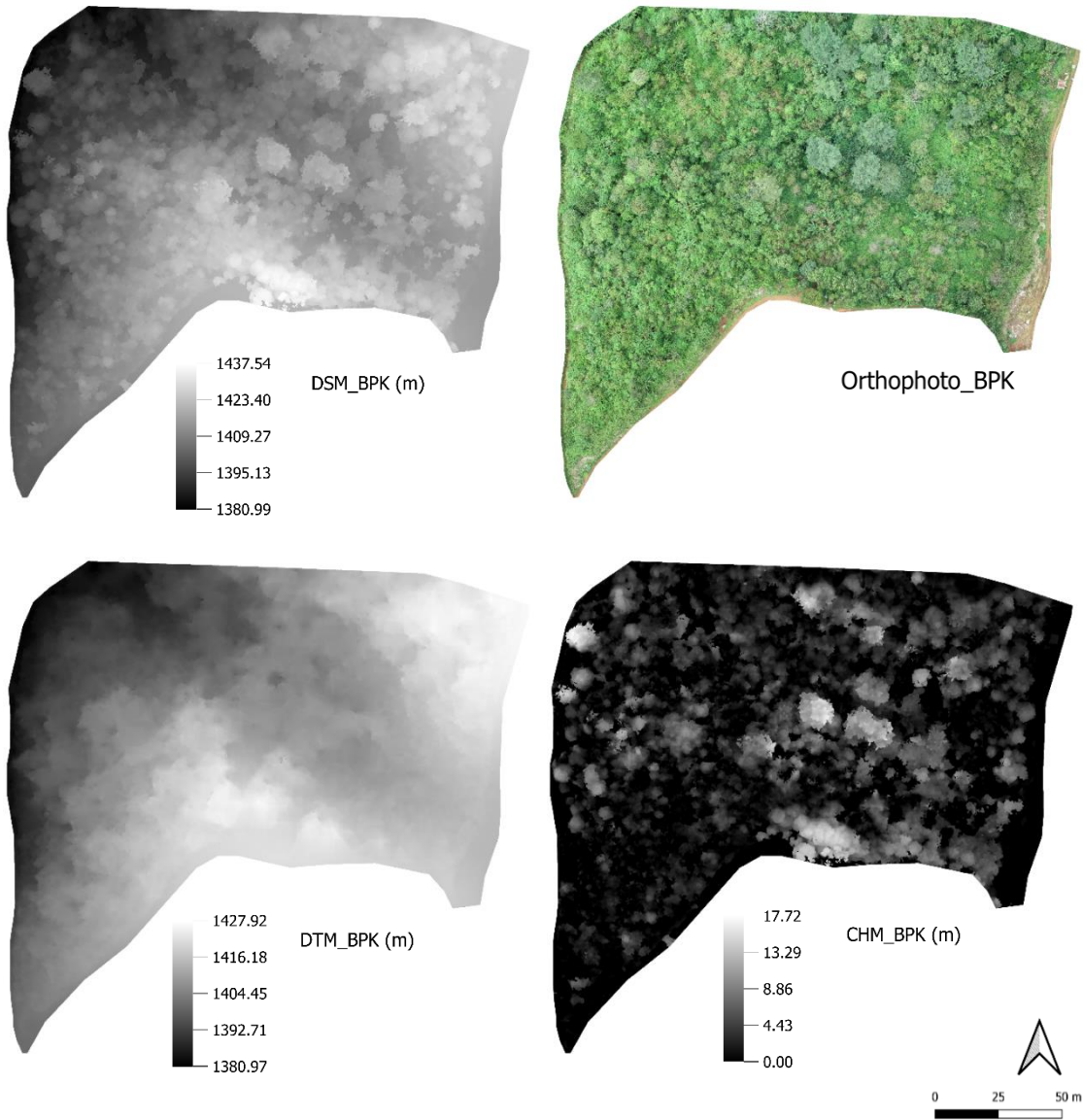


2. ML



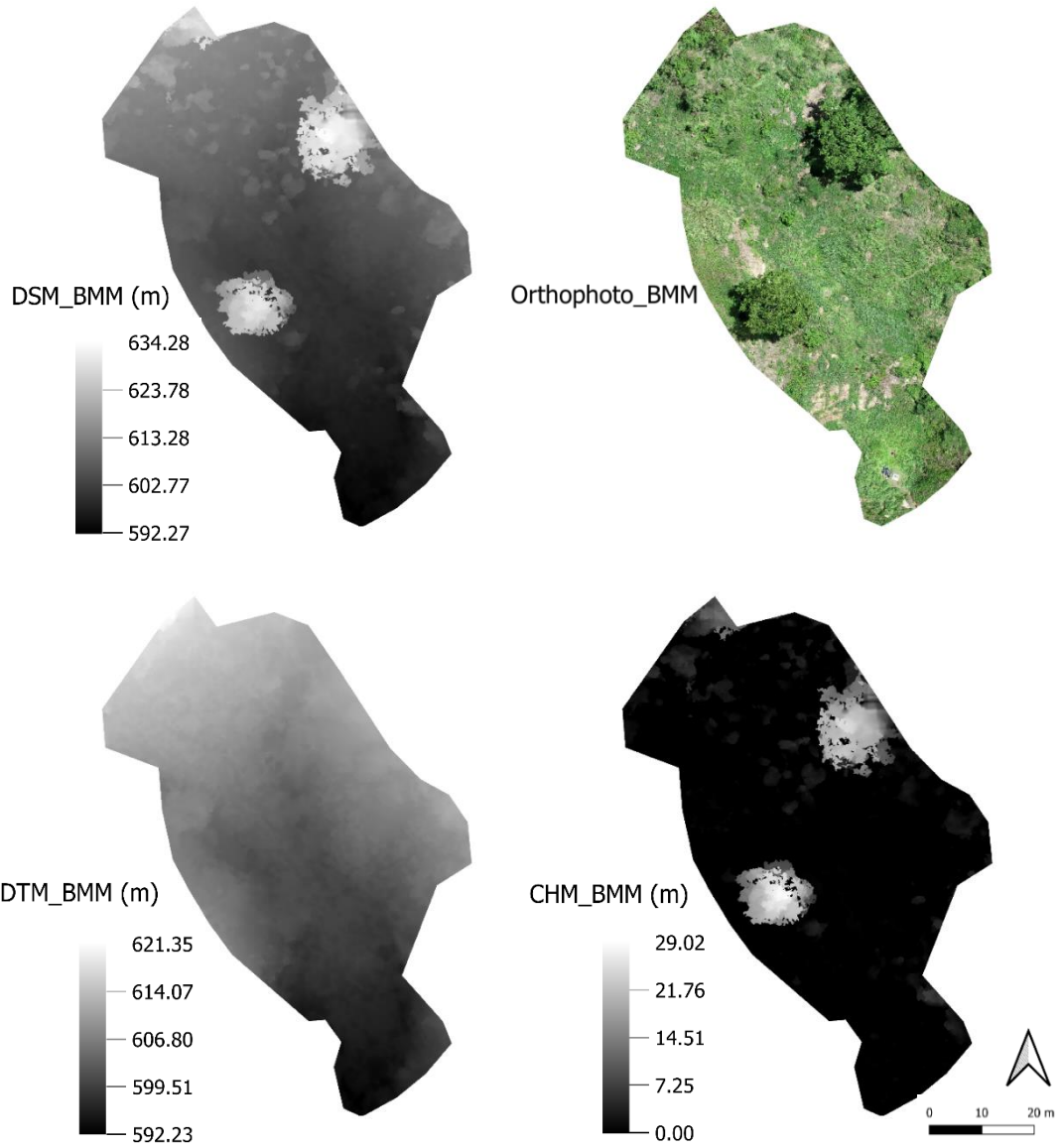
All rights reserved

3. BPK



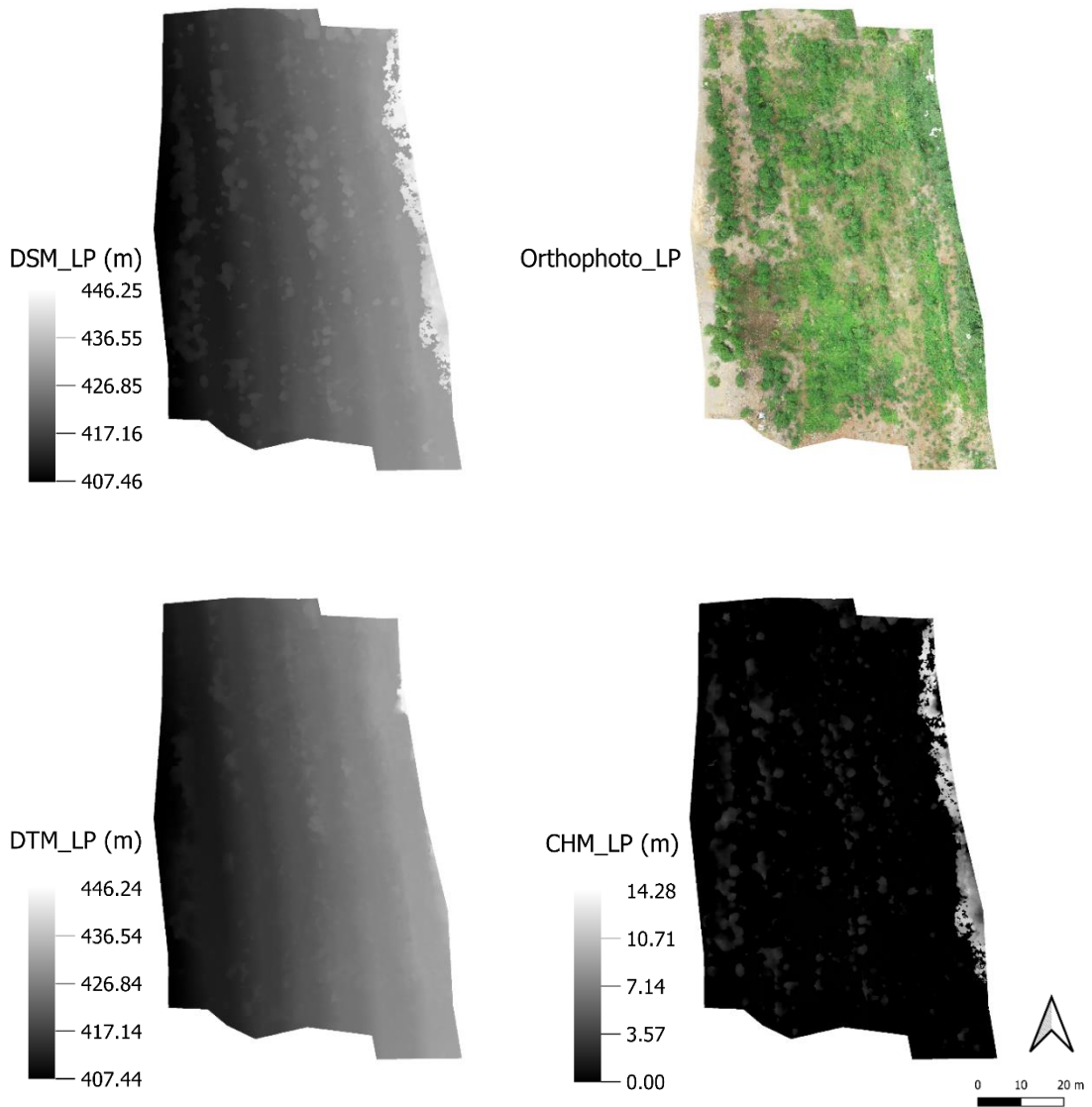
All rights reserved

4. BMM



All rights reserved

5. LP

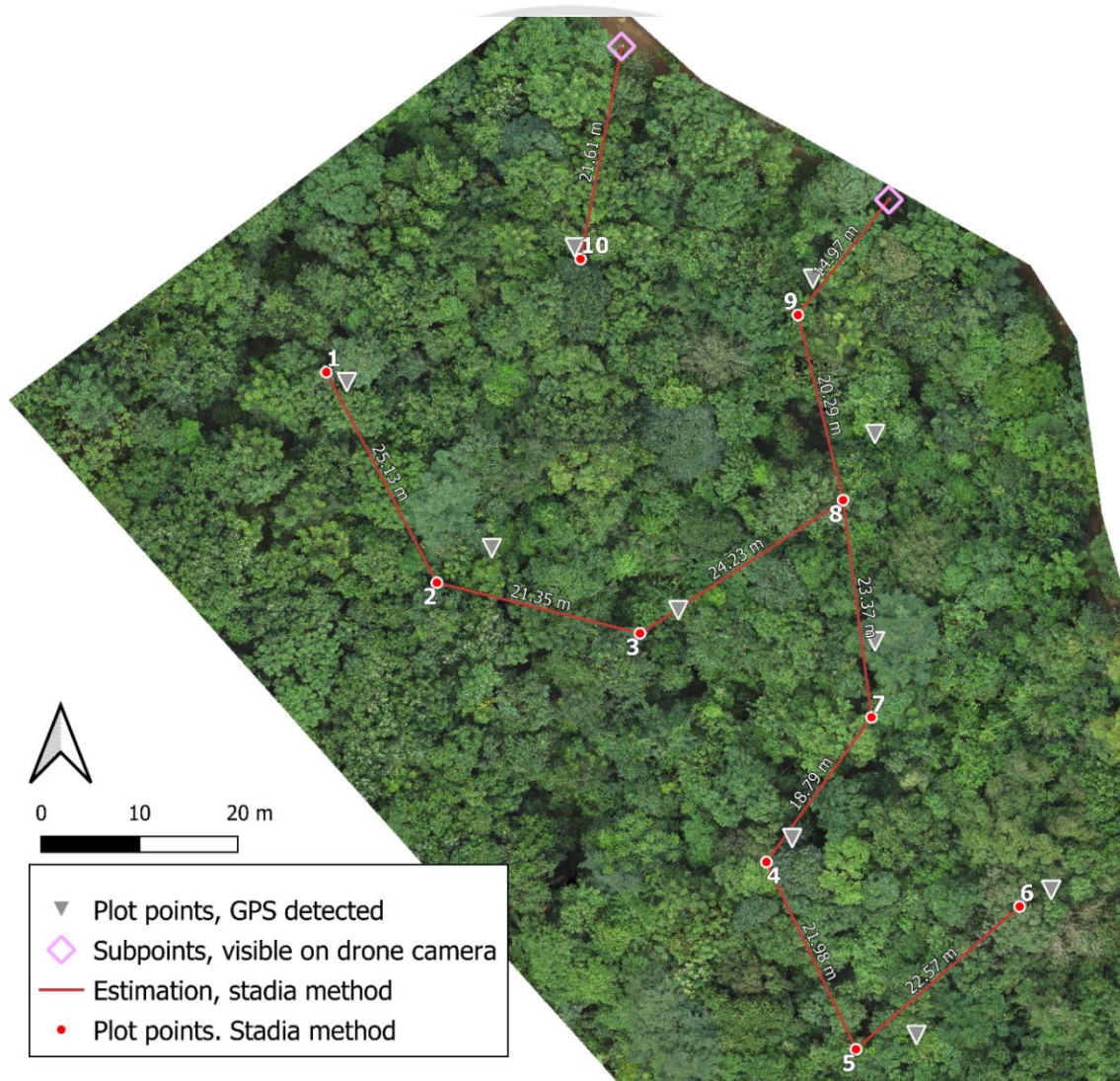


All rights reserved

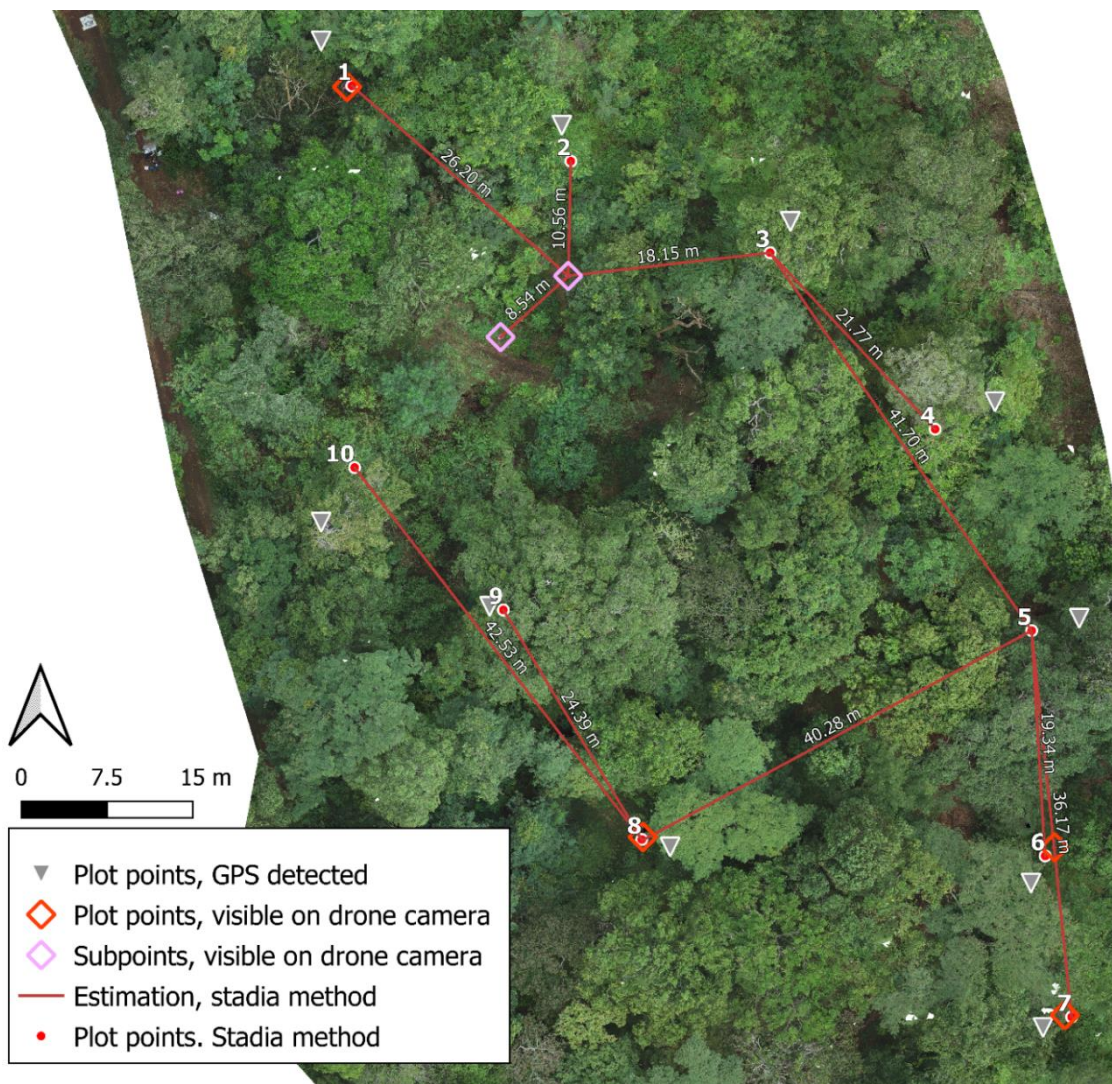
APPENDIX C

Estimating plot points using stadia method and comparisons with GPS detected points in orthophotos

1. BMSM

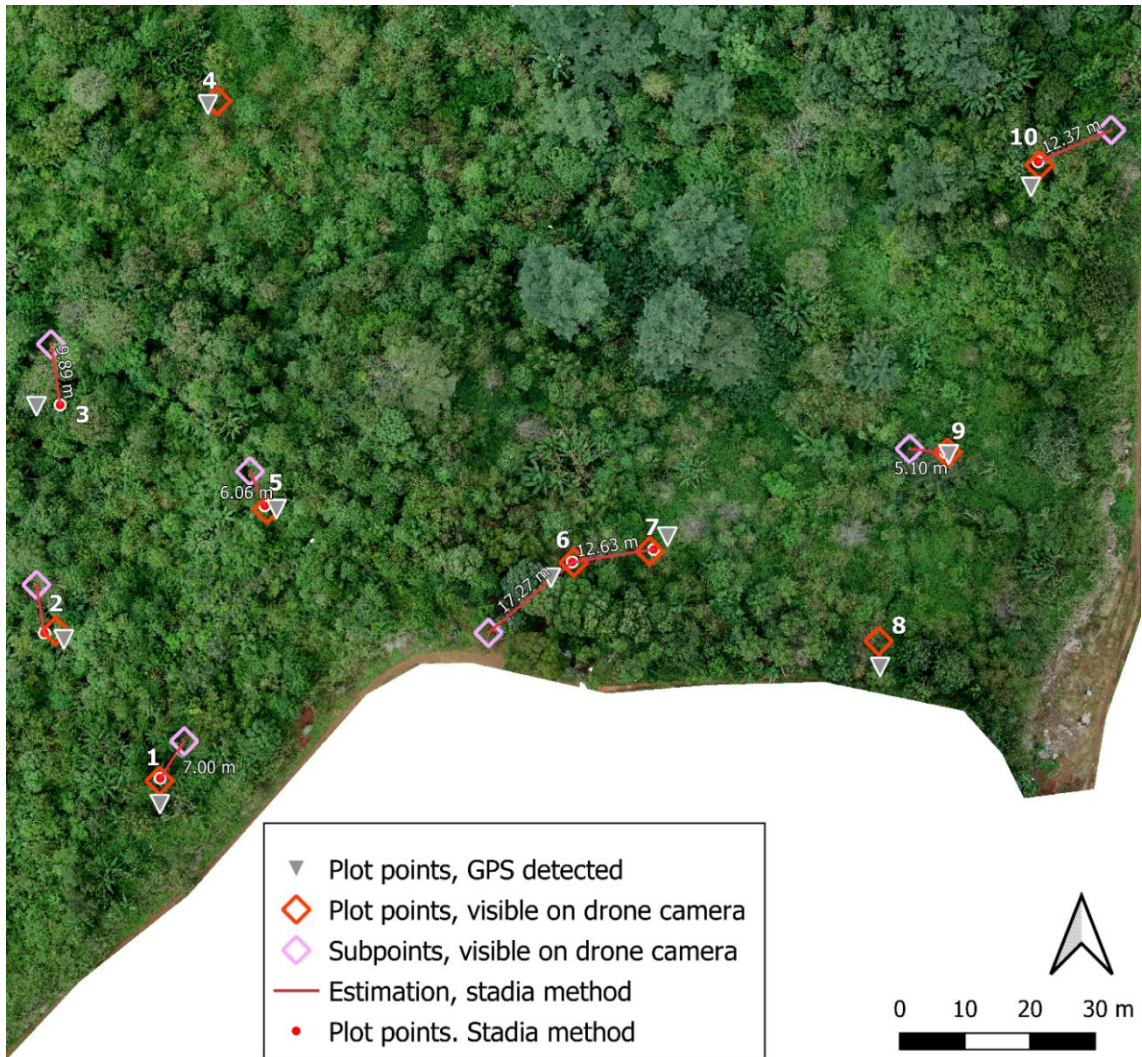


2. ML



Copyright© by Chiang Mai University
All rights reserved

3. BPK



Copyright© by Chiang Mai University
All rights reserved

CURRICULUM VITAE

Author's Name Mr. Kyuho Lee

Date/Year of Birth May 23, 1991

Place of Birth Incheon, Republic of Korea (KR)

Education 2017. Bachelor of Agriculture, Major in Forestry & Environmental Resources, Chungnam National University (CNU), Daejeon, KR.

Scholarship 2019 - 2021. CMU Presidential Scholarship, Chiang Mai University.

Experience Aug 2018 - Jun 2019. Researcher at Korea Program on International Agriculture (KOPIA) – Cambodia Center, Phnom Penh, Cambodia.

Jan 2017 - May 2018. Researcher at Forest Resources Taxonomy Lab of CNU, Daejeon, KR.

Aug - Dec 2016. Research assistant at Korea Protected Area Forum (KPAF) and MAB National Committee of the Republic of Korea in Korea National Park Service (KNPS), Seoul, KR.

Jan 2015 - Feb 2016. Manager in Vision English Learning Center, Bacolod city, the Philippines.

Others Jun - Jul 2016. Voluntary Interpreter for Korea National Park Friendship Program (KNPFP) of KNPS, Seoul (HQ) & Sokcho (Seoraksan National Park), KR.

2013 - 2014. President of International Forestry Students' Association (IFSA) Local Committee – CNU.